CMS

# Measurement and QCD analysis of double-differential inclusive jet cross sections in proton-proton collisions at $\sqrt{s} = 13\,\text{TeV}$

The CMS Collaboration*

## Abstract

A measurement of the inclusive jet production in proton-proton collisions at the LHC at $\sqrt{s} = 13\,\text{TeV}$ is presented. The double-differential cross sections are measured as a function of the jet transverse momentum $p_T$ and the absolute jet rapidity $|y|$. The anti-$k_T$ clustering algorithm is used with distance parameter of 0.4 (0.7) in a phase space region with jet $p_T$ from 97 GeV up to 3.1 TeV and $|y| < 2.0$. Data collected with the CMS detector are used, corresponding to an integrated luminosity of $36.3\,\text{fb}^{-1}$ ($33.5\,\text{fb}^{-1}$). The measurement is used in a comprehensive QCD analysis at next-to-next-to-leading order, which results in significant improvement in the accuracy of the parton distributions in the proton. Simultaneously, the value of the strong coupling constant at the Z boson mass is extracted as $\alpha_S(m_Z) = 0.1170 \pm 0.0019$. For the first time, these data are used in a standard model effective field theory analysis at next-to-leading order, where parton distributions and the QCD parameters are extracted simultaneously with imposed constraints on the Wilson coefficient $c_1$ of 4-quark contact interactions.

*See Appendix C for the list of collaboration members

# 1  Introduction

Quantum chromodynamics (QCD) is the theory describing strong interactions among partons (quarks and gluons), the fundamental constituents of hadrons. In high-energy proton-proton (pp) collisions, partons from both colliding protons interact, producing energetic collimated sprays of hadrons (jets) in the final state. Inclusive jet production in $p + p \rightarrow jet + X$, consisting of events with at least one jet, is a key process to test QCD predictions at the highest achievable energy scales. At the CERN LHC, inclusive jet production in pp collisions has been extensively measured by both the ATLAS and CMS Collaborations at several centre-of-mass energies $\sqrt{s}$. The present status of the measurements with corresponding integrated luminosities is summarised in Table 1; the earlier 7 TeV measurements [1–3] with lower integrated luminosities are omitted. In Ref. [4], the first data collected by the CMS Collaboration at 13 TeV were analysed.

Table 1: Recent measurements of inclusive jet production, performed by the ATLAS and CMS Collaborations at different $\sqrt{s}$, with the corresponding integrated luminosities.

| $\sqrt{s}$ | ATLAS | CMS |
|---|---|---|
| 2.76 TeV | $0.0002\,\text{fb}^{-1}$ [5] | $0.0054\,\text{fb}^{-1}$ [6] |
| 7 TeV | $4.5\,\text{fb}^{-1}$ [7] | $5.0\,\text{fb}^{-1}$ [8, 9] |
| 8 TeV | $20\,\text{fb}^{-1}$ [10] | $20\,\text{fb}^{-1}$ [11] |
| 13 TeV | $3.2\,\text{fb}^{-1}$ [12] | $0.071\,\text{fb}^{-1}$ [4] |

These measurements were compared with fixed-order predictions in perturbative QCD (pQCD) at next-to-leading order (NLO). Predictions at next-to-leading-logarithmic order (NLL) [13] and at next-to-next-to-leading order (NNLO) are available [14, 15] and describe the LHC data [12] well using the transverse momentum $p_\text{T}$ of an individual jet as the renormalisation and factorisation scales.

Inclusive jet production at high momenta probes the proton structure in the kinematic range of high fraction $x$ of the proton momentum carried by the parton. In particular, it is directly sensitive to the gluon distribution in the proton at high $x$. Measurements of the inclusive jet cross sections provide additional constraints on the parton distribution functions (PDFs) and the value of the strong coupling constant $\alpha_\text{S}$, as demonstrated e.g. in previous CMS publications [11, 16].

In this paper, the data collected by the CMS experiment in 2016, corresponding to an integrated luminosity of up to $36.3\,\text{fb}^{-1}$, are analysed. The measurement of the double-differential inclusive jet cross sections is presented as a function of the jet $p_\text{T}$ and jet rapidity $|y|$. The jets are clustered with the anti-$k_\text{T}$ jet algorithm [17], as implemented in the FASTJET package [18]. Two jet distance parameters, $R = 0.4$ and $0.7$, are used:

- $R = 0.4$ is a default in most recent analyses both in ATLAS and CMS at 13 TeV.
- $R = 0.7$ is chosen for most of QCD analyses using jet measurements because the effects of out-of-cone radiation are smaller. In particular, this value is used in the analogous analysis [11] with CMS data at 8 TeV.

The size of the nonperturbative (NP) corrections as a function of $R$ is discussed in Ref. [19]. Experimentally, the impact of the jet radius on the inclusive jet cross sections is studied by the CMS Collaboration in Ref. [20].

The impact of the present measurements on the proton PDFs is illustrated in a QCD analy-

sis, where the measured double-differential cross sections of inclusive jet production are used together with data from deep inelastic scattering (DIS) at HERA [21]. In addition, the CMS measurements [22] of normalised triple-differential top quark-antiquark ($t\bar{t}$) production cross sections are used, which provide additional sensitivities to the gluon distribution, $\alpha_S$, and the top quark mass $m_t$.

Furthermore, the effect of beyond the standard model (BSM) particle exchanges between the quarks is studied, using the model of contact interactions (CI) [23, 24], added to the standard model (SM) process via effective couplings. The earlier searches for CI by the CMS Collaboration were performed using inclusive jet [25] and dijet [26–28] production. In those analyses, fixed values for the Wilson coefficients were assumed and the limits on the scale of the new interactions were set based on a comparison of data to the SM+CI prediction. However, the PDFs used in the SM prediction are derived assuming the validity of the SM at high jet $p_T$, where the effects of new physics are expected to be most pronounced. Consequently, the BSM effects might be absorbed into PDFs and the interpretation of high-$p_T$ jet data may be biased. In the present analysis, the CI Wilson coefficient $c_1$ is a free parameter in the effective field theory (EFT)-improved SM (SMEFT) fit and is extracted simultaneously with the PDFs. The scenarios investigated correspond to purely left-handed, vector- and axial vector-like CI.

The paper is organised as follows. In Section 2, a brief description of the detector is given. In Section 3, the measurement of the double-differential cross sections is detailed. Theoretical predictions are explained in Section 4. Experimental and theoretical cross sections are compared in Section 5. Finally, the QCD interpretation is given in Section 6. The paper is summarised in Section 7.

## 2   The CMS detector

The central feature of the CMS apparatus is a superconducting solenoid of 6 m internal diameter, providing a magnetic field of 3.8 T. Within the solenoid volume are a silicon pixel and strip tracker, a lead tungstate crystal electromagnetic calorimeter (ECAL), and a brass and scintillator hadron calorimeter (HCAL), each composed of a barrel and two endcap sections. Forward calorimeters extend the pseudorapidity $\eta$ coverage provided by the barrel and endcap detectors. Muons are detected in gas-ionisation chambers embedded in the steel flux-return yoke outside the solenoid.

The ECAL consists of 75 848 lead tungstate crystals, which provide coverage in $|\eta| < 1.48$ in the barrel region and $1.48 < |\eta| < 3.00$ in two endcap regions. Preshower detectors consisting of two planes of silicon sensors interleaved with a total of $3X_0$ of lead are located in front of each ECAL endcap detector.

In the region $|\eta| < 1.74$, the HCAL cells have widths of 0.087 in $\eta$ and 0.087 in azimuth ($\phi$). In the $\eta$-$\phi$ plane, and for $|\eta| < 1.48$, the HCAL cells map on to 5×5 arrays of ECAL crystals to form calorimeter towers projecting radially outwards from close to the nominal interaction point. For $|\eta| > 1.74$, the coverage of the towers increases progressively to a maximum of 0.174 in $\Delta\eta$ and $\Delta\phi$. Within each tower, the energy deposits in ECAL and HCAL cells are summed to define the calorimeter tower energies.

The reconstructed vertex with the largest value of summed physics-object $p_T^2$ is taken to be the primary pp interaction vertex.

The particle-flow (PF) algorithm [29] reconstructs and identifies each individual particle in an event, with an optimised combination of information from the various elements of the CMS

detector. The energy of charged hadrons is determined from a combination of their momentum measured in the tracker and the matching ECAL and HCAL energy deposits, corrected for zero-suppression effects and for the response function of the calorimeters to hadronic showers. Finally, the energy of neutral hadrons is obtained from the corresponding corrected ECAL and HCAL energies. Jets are reconstructed offline from PF objects using the anti-$k_T$ algorithm [17, 18] with $R$ of 0.4 and 0.7.

Jet momentum is the vector sum of all PF candidate momenta in the jet, and is determined from simulation to be, on average, within 5–10% of the true momentum over the entire $p_T$ spectrum and detector acceptance. Additional pp interactions within the same or nearby bunch crossings (pileup) can contribute additional tracks and calorimetric energy depositions that increase the detector-level jet momentum. To mitigate this effect, tracks identified as originating from pileup vertices are discarded and an offset correction is applied to correct for remaining contributions. Jet energy corrections are derived from simulation studies so the average measured response of jets becomes identical to that of particle-level jets. In situ measurements of the momentum balance in dijet, photon+jet, Z +jet, and multijet events are used to determine any residual differences between the jet energy scale (JES) in data and in simulation, and appropriate corrections are derived [30]. Additional selection criteria are applied to each jet to remove jets potentially affected by instrumental effects or reconstruction failures [31].

The missing transverse momentum vector $\vec{p}_T^{\text{miss}}$ is computed as the negative vector $p_T$ sum of all the PF candidates in an event, and its magnitude is denoted as $p_T^{\text{miss}}$ [32]. The $\vec{p}_T^{\text{miss}}$ is modified to account for corrections to the energy scale of the reconstructed objects in the event. Anomalous high-$p_T^{\text{miss}}$ events can be due to a variety of reconstruction failures, detector malfunctions, or noncollisions backgrounds. Such events are rejected by event filters that are designed to identify more than 85–90% of the spurious high-$p_T^{\text{miss}}$ events with a mistagging rate less than 0.1%.

Events of interest are selected online using a two-tiered trigger system [33]. The first level, composed of custom hardware processors, uses information from the calorimeters and muon detectors to select events at a rate of up to 100 kHz within a latency of less than 4 $\mu$s [34]. The second level, known as the high-level trigger (HLT), consists of a farm of processors running a version of the full event reconstruction software optimised for fast processing, and reduces the event rate to around 1 kHz before data storage.

During the 2016 data taking, a gradual shift in the timing of the inputs of the ECAL first-level trigger in the region $|\eta| > 2.0$, referred to as prefiring, caused a specific trigger inefficiency. For events containing a jet with $p_T$ larger than $\approx$100 GeV in the region $2.5 < |\eta| < 3.0$, the efficiency loss is $\approx$10–20%, depending on $p_T$, $\eta$, and data taking period. Correction factors were computed from data and applied to the acceptance evaluated by simulation.

A more detailed description of the CMS detector, together with a definition of the coordinate system used and the relevant kinematic variables, can be found in Ref. [35].

## 3 Data analysis

The inclusive jet double-differential cross section, as a function of the individual jet $p_T$ and $y$ is defined as follows:

$$\frac{\mathrm{d}^2\sigma}{\mathrm{d}p_T\,\mathrm{d}y} = \frac{1}{\mathcal{L}}\frac{N_{\text{jets}}^{\text{eff}}}{\Delta p_T\,\Delta y}, \tag{1}$$

where $\mathcal{L}$ corresponds to the integrated luminosity, $\Delta p_T$ ($\Delta y$) to the bin width of the jet $p_T$ ($y$), and $N_{\text{jets}}^{\text{eff}}$ to the effective number of jets per bin estimated at the particle level, i.e. after corrections for detector effects. The binning scheme coincides with the one chosen in former publications [4, 8, 9, 11].

The details of the data and simulation are described in the following: the selection of the events and jets (Section 3.1), the triggers (Section 3.2), the calibrations (Section 3.3), corrections for efficiencies, misidentification, and migrations due to the limited resolution of the detector (Section 3.4), and the experimental uncertainties (Section 3.5).

## 3.1 Event selection

The data samples recorded in 2016 correspond to an integrated luminosity of $36.3\,\text{fb}^{-1}$ ($33.5\,\text{fb}^{-1}$) for events with jets clustered with $R = 0.4$ (0.7) [36]. Triggers for the larger jet distance parameter were activated after $2.8\,\text{fb}^{-1}$ of data had been taken, which explains the difference in the integrated luminosities.

The detector response in simulations is modelled with GEANT4 [37]. The simulations in Table 2 include a simulation of the pileup produced with PYTHIA 8+CUETP8M1, which correspond to the pileup conditions in the data.

The primary vertex (PV) must satisfy $|z_{\text{PV}}| < 24\,\text{cm}$ and $\rho_{\text{PV}} < 2\,\text{cm}$, where $z_{\text{PV}}$ ($\rho_{\text{PV}}$) corresponds to the longitudinal (radial) distance from the nominal interaction point. Event filters mentioned in Section 2 are applied to reduce the noise from the detector.

In addition, the jets must satisfy quality criteria based on the jet constituents to remove the effect of detector noise, and must be reconstructed within $|y| < 2.5$, corresponding to the tracker acceptance. Jets reconstructed in regions of the detector corresponding to defective zones in the calorimeters are excluded from the measurement and recovered later in the unfolding procedure; the effect is of the order of a percent and is uniform as a function of $p_T$.

Table 2: Description of the simulations used in the analysis.

| generator | PDF | matrix element | tune |
|---|---|---|---|
| PYTHIA 8 (230) [38] | NNPDF 2.3 [39] | LO $2 \to 2$ | CUETP8M1 [40] |
| MADGRAPH5_aMC@NLO (2.4.3) [41, 42] | NNPDF 2.3 [39] | LO $2 \to 2, 3, 4$ | CUETP8M1 [40] |
| HERWIG++ (2.7.1) [43] | CTEQ6L1 [44] | LO $2 \to 2$ | CUETHppS1 [40] |

## 3.2 Triggers

The prescaled single-jet triggers are used, requiring at least one jet in the event with jet $p_T^{\text{HLT}}$ larger than a certain threshold. All triggers are prescaled, except the one with the highest threshold, and correspond to different effective integrated luminosities. Two different series of triggers are used for each value of the $R$ parameter, shown in Tables 3-4. The jets are weighted event by event in contrast to previous measurements [4, 8, 9, 11] of inclusive jet production by the CMS Collaboration, where the whole contribution of each trigger is normalised with respect to its effective luminosity. This makes a difference, especially in terms of smoothness of the spectrum even after unfolding, since the trigger rate is nonlinear as a function of the instantaneous luminosity and the JES corrections generally vary with time and with pileup conditions.

An event is considered for the measurement only if the leading jet reconstructed with the offline PF algorithm is matched to an HLT jet. The data contain events selected with a combination

of triggers in different, exclusive intervals of the leading jet $p_T$. The edges of each interval are determined in such a way that the corresponding trigger has an efficiency above 99.5% in all $p_T$ and $|y|$ bins. The efficiency of each trigger is determined from the data set recorded by the next single-jet trigger (with lower but closest threshold), except for the most inclusive trigger. To determine the region of efficiency of the most inclusive trigger and to cross-check the efficiencies obtained for the other triggers, a tag-and-probe method is applied to dijet topologies, which counts the leading and subleading offline PF jets that can be matched to HLT jets. The measured spectrum is corrected for the residual trigger inefficiency as a function of $p_T$ and $|y|$. Finally, to control possible steps in the distribution caused by passing the trigger thresholds, the spectrum is fitted in $|y|$ regions using a truncated Taylor expansion with Chebyshev polynomials of the first kind as basis [45]; the $\chi^2 / N_{dof}$ (where dof is degree of freedom) is compatible or close to one within statistical uncertainties.

The additional trigger inefficiency due to the prefiring effect, mentioned in Section 2, is corrected event by event in the data before the unfolding procedure, using maps of prefiring probability in $2.0 < |\eta| < 3.0$ as a function of $p_T$ and $\eta$. The total event weight is obtained as the product of the nonprefiring probability of all jets. The resulting effect is typically 2% for the spectrum at $|y| < 2.0$.

Table 3: The HLT ranges and effective integrated luminosities used in the jet cross section measurement for $R = 0.4$. The first (second) row shows the $p_T$ threshold for the HLT (offline PF) reconstruction; the third row corresponds to the effective luminosity of each trigger $\mathcal{L}$.

| $p_T^{HLT}$ (GeV) | 40 | 60 | 80 | 140 | 200 | 260 | 320 | 400 | 450 |
|---|---|---|---|---|---|---|---|---|---|
| $p_T^{PF}$ (GeV) | 74–97 | 97–133 | 133–196 | 196–272 | 272–362 | 362–430 | 430–548 | 548–592 | >592 |
| $\mathcal{L}$ (pb$^{-1}$) | 0.267 | 0.726 | 2.76 | 24.2 | 103 | 594 | 1770 | 5190 | 36300 |

Table 4: The HLT ranges and effective integrated luminosities used in the jet cross section measurement for $R = 0.7$. The first (second) row shows the $p_T$ threshold for the HLT (offline PF) reconstruction; the third row corresponds to the effective luminosity of each trigger $\mathcal{L}$.

| $p_T^{HLT}$ (GeV) | 40 | 60 | 80 | 140 | 200 | 260 | 320 | 400 | 450 |
|---|---|---|---|---|---|---|---|---|---|
| $p_T^{PF}$ (GeV) | 74–97 | 97–114 | 114–196 | 196–272 | 272–330 | 330–395 | 395–507 | 507–592 | >592 |
| $\mathcal{L}$ (pb$^{-1}$) | 0.0497 | 0.328 | 1.00 | 10.1 | 85.8 | 518 | 1526 | 4590 | 33500 |

## 3.3 Calibration

The JES corrections are applied according to the standard CMS procedure [30]. An additional smoothing procedure is applied to the JES corrections (originally parameterised with linear splines in bins of $p_T$) to ensure and preserve the smoothness of the cross sections using the same fit method described in Section 3.2.

The detector-level $p_T$ ($p_T^{rec}$) is rescaled such that the jet energy resolution (JER) in the simulated samples matches the JER in the data; this procedure is also known as JER smearing. A matching between the particle- and detector-level jets is performed for each event. The particle-level jets are ordered by decreasing $p_T$. Each particle-level jet is matched to the highest-$p_T$ detector-level jet present in a cone with $\Delta R = 0.2$ (0.35) for jets clustered with $R = 0.4$ (0.7); a particle-level jet may be matched to only one detector-level jet. The response is fitted from matched jets using a double Crystal-Ball function [46, 47] to account for the presence of non-Gaussian tails. The width of the resolution is extracted and fitted as a function of $p_T^{rec}$, in bins of $\eta$ and the variable $\rho$ defined in Ref. [48]. A modified NSC function is used, where the second term in Eq. (8.10) of

Ref. [30] is extended by $p_T^d$ with $d$ being an additional fit parameter. The $p_T^{rec}$ is then rescaled as a function of the response with a scale factor; if no matching can be performed in the Gaussian core of the double Crystal-Ball function, the response is estimated with a Gaussian of width obtained from the modified NSC function.

The simulation of the pileup also includes the signal, but with a lower event count. To avoid double-counting and ensure a good statistical precision over the whole phase space, events with a hard scatter from the pileup simulation and events with anomalously large weights are discarded from the simulated samples. To ensure correct normalisation, the remaining events are reweighted to restore the originally generated spectrum. Finally, the pileup profile used in the simulation is corrected to match that in data.

### 3.4 Correction for detector effects

The measured detector-level distribution is unfolded to the particle level using corrections derived from the simulated events.

Sequentially, corrections for the background, migrations and inefficiencies are applied. To estimate the different effects, the same matching algorithm as described in the context of the JER smearing is used. Successfully matched jets, both in the Gaussian core and in the tails of the response, are used to estimate the response matrix, whereas unmatched jets at the particle (detector) level are used to estimate the inefficiencies (background). The background contribution is at 1–2%-level at low $p_T$ and is negligible at medium at high $p_T$, while the maximum inefficiency reaches 2–5% at low and high $p_T$.

Various types of backgrounds and inefficiencies are considered: the migrations in/out of the phase space, and the unmatched jets that correspond to either pileup or objects wrongly identified as jets by the reconstruction algorithm.

The probability matrix (PM), shown in Fig. 1 for jets clustered with $R = 0.7$, is obtained by normalising the response matrix row by row. It contains the probability for a given particle-level jet to be reconstructed as a given detector-level jet. Assuming a PM **A** and the sum of the backgrounds **b**, both obtained from the simulation, and given a measured detector-level distribution **y**, the particle-level distribution **x** is determined by minimising the following objective function:

$$\chi^2 = \min_{\mathbf{x}} \left[ (\mathbf{Ax} - \mathbf{y} - \mathbf{b})^{\mathsf{T}} \mathbf{V}^{-1} (\mathbf{Ax} - \mathbf{y} - \mathbf{b}) \right], \tag{2}$$

where **V** is the covariance matrix of the detector-level data describing the statistical uncertainties associated with the data (including correlations), as well as with the backgrounds. The detector-level distribution has twice the number of bins as in the particle-level distribution. The matrix condition number of the PM, i.e. the ratio of the highest and lowest eigenvalues, is close to 4, assuring that the PM is not ill-conditioned; therefore no additional regularisation is applied. The whole procedure is performed with the TUNFOLD package [49], version 17.9.

Finally, the residual inefficiencies are obtained from the rate of particle-level jets that cannot be matched to any detector-level jets passing the event selection, and corrected bin-by-bin on the particle-level distribution **x**.

### 3.5 Uncertainties

The measurement is affected by systematic and statistical uncertainties. The contributions of the various uncertainties are shown in Fig. 2, where the coloured band indicates the bin-to-bin fully correlated uncertainties and the vertical error bars indicate the uncorrelated uncertainties.
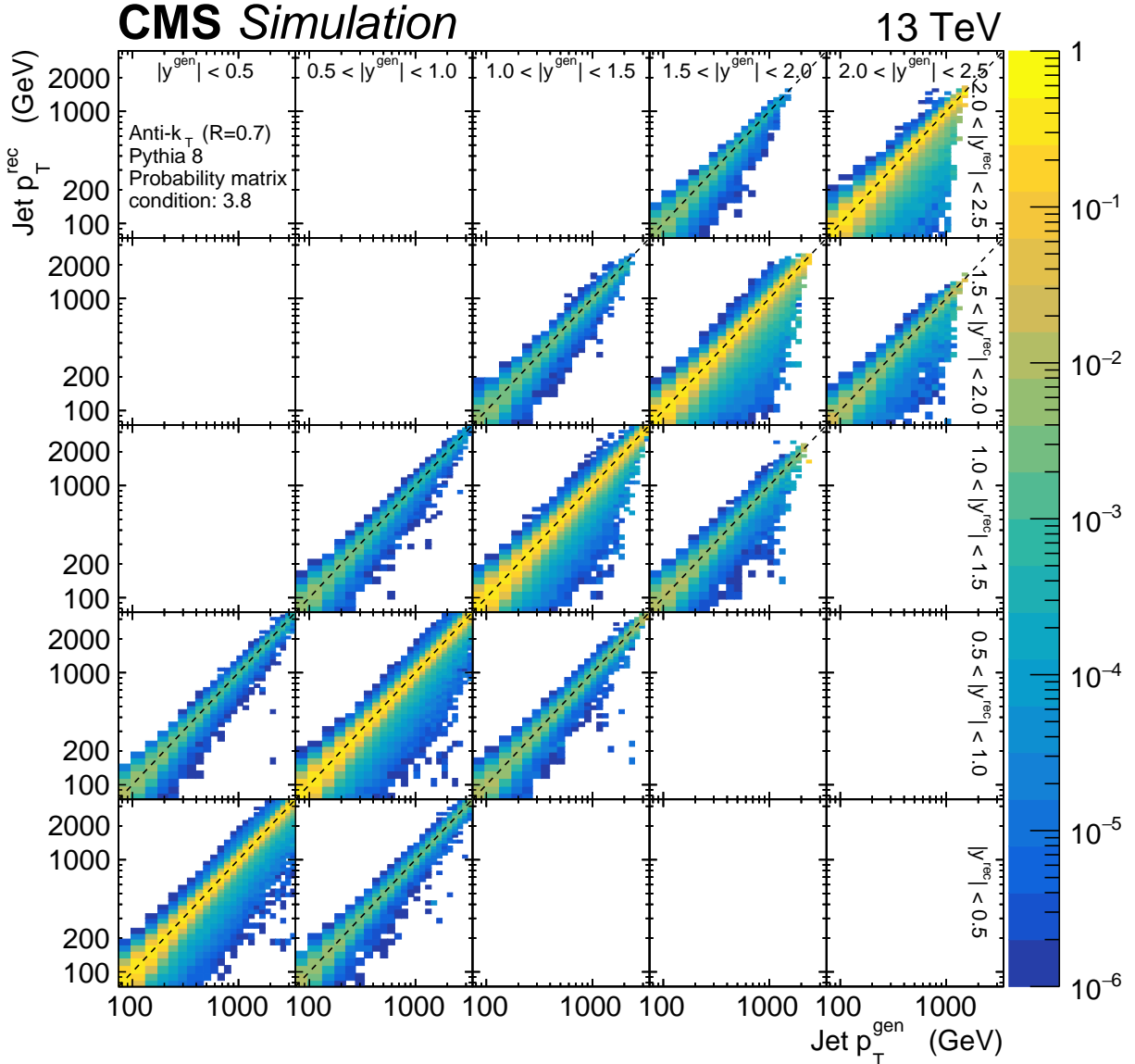
Figure 1: The probability matrix, estimated with a simulated sample based on PYTHIA 8, for jets clustered using the anti-$k_T$ algorithm with $R = 0.7$. The horizontal (vertical) axis corresponds to jets at the particle (detector) level. The global $5 \times 5$ structure corresponds to the bins of rapidity $y$ of the jets, indicated by the labels in the uppermost row and rightmost column; the horizontal and vertical axes of each cell correspond to the transverse momentum $p_T$ of the jets. The colour range covers a range from $10^{-6}$ to 1 and the rows are normalised to unity, indicating the probability for a particle-level jet generated with values of $p_T^{gen}$ and $|y|^{gen}$ to be reconstructed at the detector level with values of $p_T^{rec}$ and $|y|^{rec}$. Migrations outside of the phase space are not included; migrations across rapidity bins only occur among adjacent rapidity bins. The dashed lines indicate the diagonal bins in each rapidity cell.

The bin-to-bin fully correlated uncertainties are determined as follows:

- Variations of the JES corrections and of the prefiring correction are applied to the data at the detector level and are mapped to the particle level by repeating the unfolding procedure. The JES uncertainties are the dominant uncertainties in this measurement.

- Systematic effects related to the JER and to the pileup profile correction are varied in the simulated sample and propagated to the particle level by repeating the unfolding procedure.

- The normalisation of the estimates of the inefficiencies and backgrounds, obtained from the Monte Carlo (MC) simulation, are varied separately within a conservative estimate of 5%, covering a potential model dependence in migrations in the phase space and an impact from the matching algorithm in the unfolding procedure.

- The model dependence in the unfolding for $p_\mathrm{T}$ and $|y|$ is assessed by a model uncertainty derived as the difference between the nominal cross section obtained with the original PYTHIA 8 simulation and a modified version in which the inclusive jet spectrum is corrected to match the data. The modified version is obtained by applying a smooth correction as a function of the $p_\mathrm{T}$, $y$, and jet multiplicity. The effect is strongest for $|y| > 1.5$, where PYTHIA 8 does not describe the data well. Alternatively to PYTHIA 8, MADGRAPH5_aMC@NLO simulation is used and agrees well with the PYTHIA 8 results.

- A fully correlated 1.2% uncertainty in the integrated luminosity calibration is applied to the nominal variation of the unfolded spectrum [36].

Bin-to-bin fluctuations in the systematic variations are removed by applying a smoothing procedure based on Chebyshev polynomials following the method described in Section 3.2.

Uncorrelated and partly correlated uncertainties among $p_\mathrm{T}$ and $y$ bins arise from various origins:

- The inclusive jet measurement is based on multiple jets recorded in each event. This is the dominant contribution to the uncorrelated uncertainties shown in Fig. 2.

- An additional uncorrelated systematic uncertainty of 0.2% is added before the unfolding to account for differences in alternative methods of determining the trigger efficiency.

- Statistical fluctuations in the simulated distributions.

After unfolding, the different sources are no longer distinguished from one another; in addition, the unfolding procedure introduces anti-correlations among directly neighbouring bins. The correlation matrix after the unfolding is shown in Fig. 3.

## 4   Theoretical predictions

In the following, the fixed-order pQCD predictions, the electroweak (EW) corrections, and the NP corrections are described.

### 4.1   Fixed-order predictions

Fixed-order pQCD predictions for the inclusive jet production are available at NLO and NNLO accuracy, obtained using the NLOJet++ [50, 51] and NNLOJET (rev5918) [14, 15, 52] programs, with NLO calculations implemented in FASTNLO [53]. The calculations are performed for five
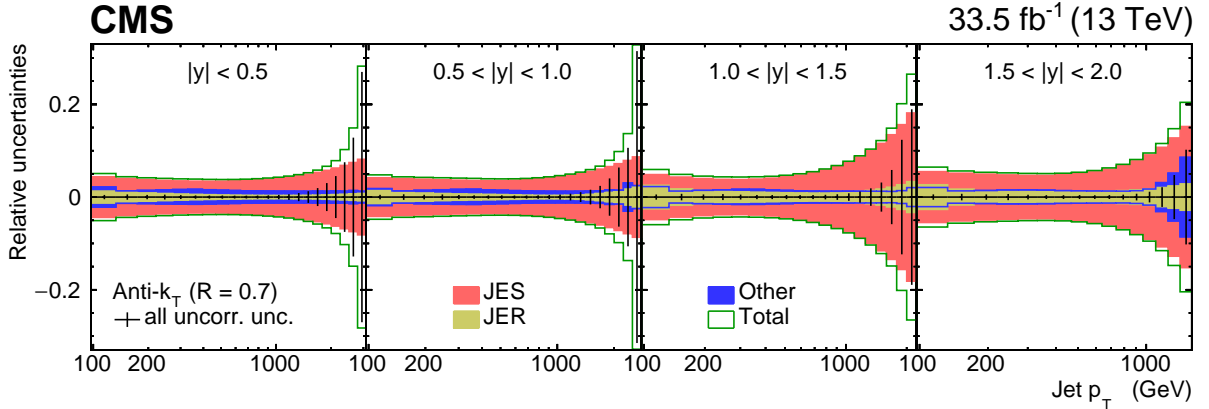
Figure 2: Relative uncertainties in the double-differential cross section, as functions of jet transverse momentum ($x$ axis) and rapidity (cells), for jets clustered using the anti-$k_T$ algorithm with $R = 0.7$. The systematic uncertainties are shown in different, noncumulative colour bands: the red bands correspond to JES uncertainties, the yellow bands to the JER uncertainties, and the blue bands to all other sources, including the integrated luminosity uncertainty, the model uncertainty, uncertainties in the migrations in and out of the phase space, and uncertainties in various inefficiencies and backgrounds. The vertical error bars include the statistical uncertainties from the data and from the PYTHIA 8 simulated sample used for the unfolding, as well as the binwise systematic uncertainties, all summed in quadrature. The total uncertainty, shown in green, includes all systematic and statistical uncertainties summed in quadrature.

active massless quark flavours. The renormalisation ($\mu_r$) and factorisation ($\mu_f$) scales are set to the individual jet $p_T$. Alternative prediction using $\mu_r$ and $\mu_f$ set to the scalar sum of the parton $p_T$ ($H_T$ parton) is used for comparison. In Ref. [15] the individual jet $p_T$ was found to be a better choice for the scale than the transverse momentum of the leading-jet $p_T^{max}$. Furthermore in Refs. [54–56] it was discussed that NNLO calculations with jet distance parameter of the anti-$k_T$ clustering algorithm $R = 0.7$ are more stable than those with $R = 0.4$.

To estimate possible uncertainty due to missing higher-order contributions, the scales are varied independently by a factor of 2 up and down, avoiding cases with $\mu_f/\mu_r = 4^{\pm 1}$. The largest deviation of the cross section from the result obtained with the central scale choice is used as an estimate of the scale uncertainty. In general, the scale uncertainties for $R = 0.7$ are larger than for $R = 0.4$.

In the QCD predictions at NLO and NNLO, the proton structure is described by several alternative PDF sets: CT14 [57], NNPDF 3.1 [58], MMHT2014 [59], ABMP 16 [60], and HERA-PDF 2.0 [21], obtained at NLO or NNLO, respectively, and each using their default value of $\alpha_S(m_Z)$.

The NLO QCD prediction is improved to NLO+NLL accuracy with a simultaneous jet radius and threshold resummation $k$-factor for each bin $i$:

$$k_i^{\text{NLO+NLL}} = \frac{\sigma_i^{\text{NLO}} - \sigma_{\text{sing.},i}^{\text{NLO}} + \sigma_i^{\text{NLL}}}{\sigma_i^{\text{NLO}}}, \tag{3}$$

where the singular NLO terms $\sigma_{\text{sing.}}^{\text{NLO}}$ and the resummed contributions $\sigma^{\text{NLL}}$ are obtained using the NLL-JET calculation, provided by the authors of Ref. [13]. Following their approach, the $\sigma^{\text{NLO}}$ for the resummation factor is computed using the modified Ellis Kunszt Soper (MEKS) code version 1.0 [61], and choosing the renormalisation and factorisation scales $\mu_r = \mu_f = p_T^{max}$.
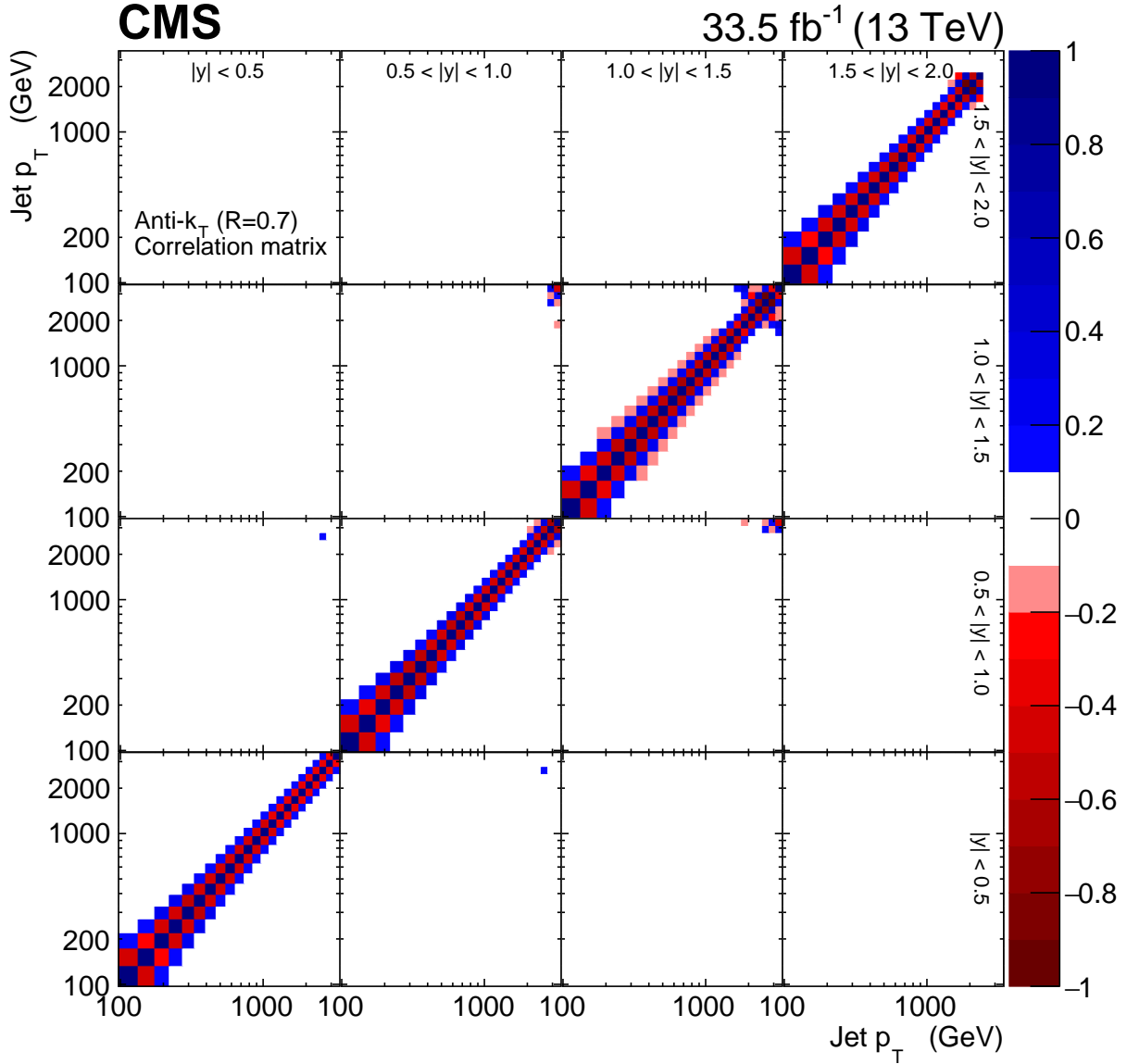
Figure 3: The correlation matrix at the particle level, for jets clustered using the anti-$k_T$ algorithm with $R = 0.7$. It contains contributions from the data and from the PYTHIA 8 sample used to perform the unfolding. The global $4 \times 4$ structure corresponds to the bins of rapidity $y$ of the jets, indicated by the labels in the uppermost row and rightmost column; the horizontal and vertical axes of each cell correspond to the transverse momentum $p_T$ of the jets. The colour range covers a range from $-1$ to $1$ and indicates correlations in blue shades and anti-correlations in red shades, except for values between $-0.1$ and $0.1$. Correlations across rapidity bins reach significant values mostly at the edges of the $p_T$ range.
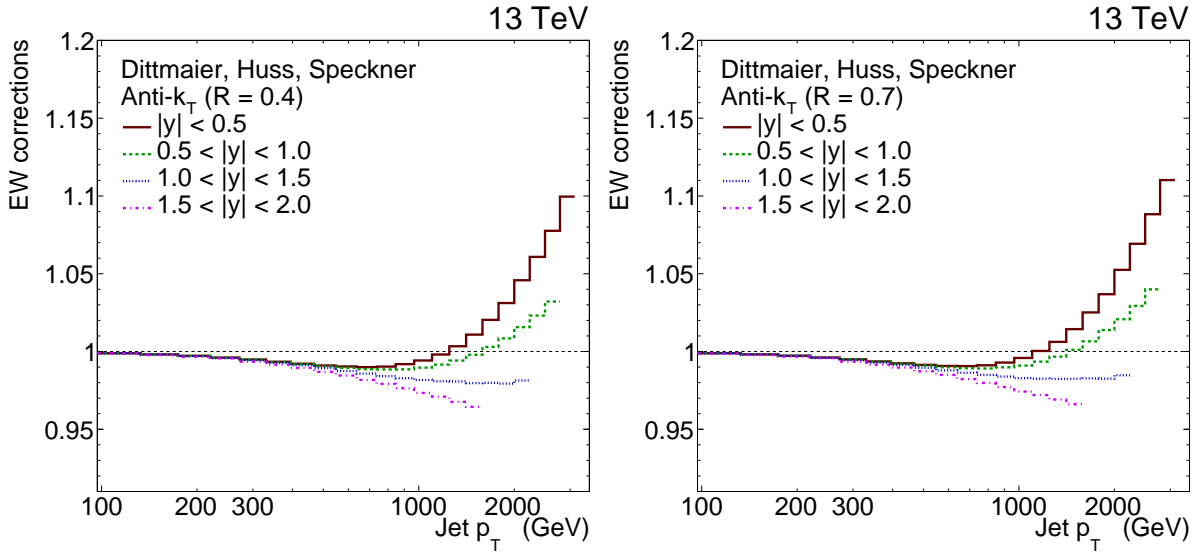
Figure 4: The EW corrections for inclusive jet cross sections, as reported in Ref. [62]. The values for jets clustered using the anti-$k_T$ algorithm with $R = 0.4$ (0.7) are shown on the left (right); each curve corresponds to a rapidity bin.

## 4.2 Electroweak corrections

The EW effects, which arise from the virtual exchange of the massive W and Z gauge bosons are calculated to NLO accuracy [62] and are applied to the fixed-order QCD predictions. In the high-$p_T$ region, these EW effects grow to 11%, as illustrated in Fig. 4. No uncertainty associated with these corrections is available yet.

The contribution of real production of EW boson production in association with jets is estimated at NLO using MCFM [63–65] program to be at most at percent level which is negligible for the present analysis.

## 4.3 Nonperturbative corrections

The NP corrections are defined for each bin $i$ as

$$\mathrm{NP}_i = \frac{\sigma_i^{\mathrm{MC}}(\mathrm{PS\ \&\ MPI\ \&\ HAD})}{\sigma_i^{\mathrm{MC}}(\mathrm{PS})}, \tag{4}$$

where PS stands for parton shower, HAD for hadronisation, and MPI for multiparton interaction. The NP factors correct for the hadronisation and the MPI effects that are not included in the fixed-order pQCD predictions. At low $p_T$, the NP corrections are dominated by MPI, which increases the radiation in the jet cone by a constant offset. This is especially important for $R = 0.7$. On the other hand, hadronisation plays a role at smaller $R$. The effects of perturbative radiation are partially considered in the higher-order predictions; for this reason the PS simulation is included in both the numerator and the denominator. It is stronger for smaller $R$, where out-of-cone radiation plays a larger role, which NLL corrections can account for.

To define final NP corrections, PYTHIA 8 CP1 tune [66] and HERWIG++ EE5C tune [40] are fitted with a smooth function $a_0 + a_1 / p_T^{a_2}$. The correction is obtained from the resulting envelope with the central value taken in the middle of the envelope and the uncertainties from its edges.

The NP corrections defined in Eq. (4) are shown in Fig. 5. The corrections are larger for $R = 0.7$ than for $R = 0.4$, since a larger cone size includes more effects from the underlying event.
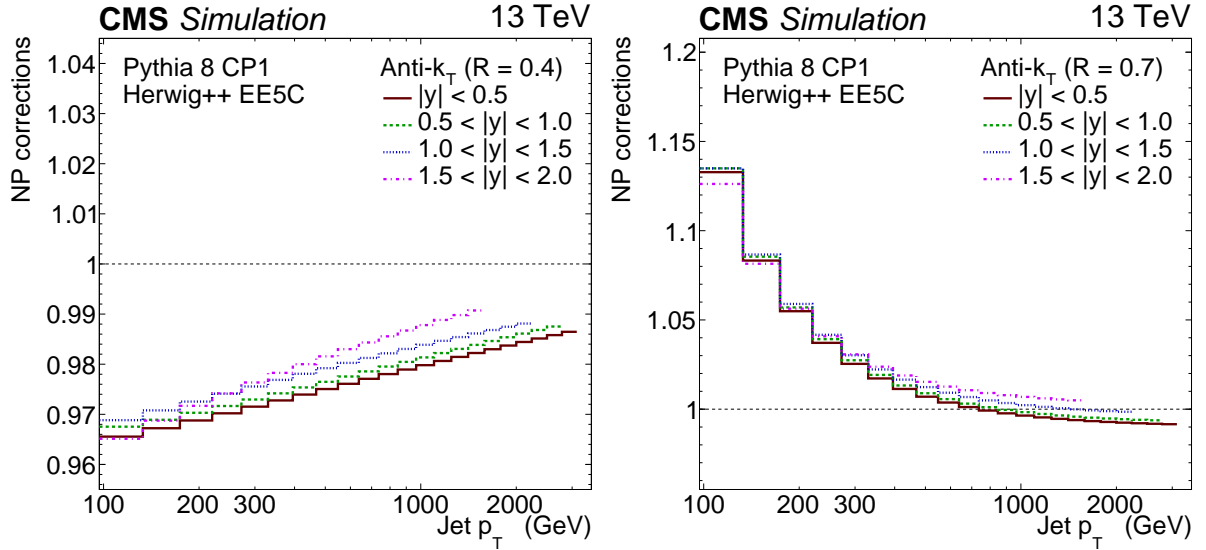
Figure 5: The values for NP corrections for inclusive jet cross sections. The values for jets with $R = 0.4$ (0.7) are shown on the left (right); each curve corresponds to a rapidity bin. The values correspond to the average of the corrections obtained with PYTHIA 8 and with HERWIG++.

# 5 Results

In Fig. 6, the inclusive jet cross sections are presented as functions of the jet $p_T$ and $|y|$ for $R = 0.4$ and 0.7. The cross sections are shown for four absolute rapidity intervals: $|y| < 0.5$, $0.5 < |y| < 1.0$, $1.0 < |y| < 1.5$, and $1.5 < |y| < 2.0$ with jet $p_T > 97$ GeV. The data are compared with fixed-order NNLO QCD predictions using CT14 PDF, corrected for NP and EW effects. The data cover a wide range of the jet $p_T$ from 97 GeV up to 3.1 TeV.

In Fig. 7 (Fig. 8), the ratios of the measured cross sections to the NNLO QCD predictions using different scale choices and to the NLO+NLL predictions with various PDFs sets are shown for jets with $R = 0.4$ (0.7). In general at high $p_T$, smaller (higher) cross sections are predicted than experimentally measured for the central (forward) rapidities. The theoretical uncertainties are larger at high $p_T$ and are dominated by the PDF uncertainties. The scale uncertainties are significantly smaller at NNLO as compared to NLO+NLL. The prediction using jet $p_T$ as renormalisation and factorisation scale results in a harder $p_T$ spectrum than in case of scale set to $H_T$ parton. The NLO+NLL calculations predict harder $p_T$ spectrum than the NNLO calculations. All predictions describe the data well within the experimental and theory uncertainties.

The CT14, NNPDF 3.1, and MMHT 2014 PDF sets include CMS and ATLAS measurements of inclusive jet cross sections at 7 TeV, whereas ABMP 16 does not include LHC jet measurements and HERAPDF 2.0 is based only on the HERA DIS data. Predictions obtained with these PDFs are similar at low $p_T$, although significant differences at high $p_T$ are observed. These differences arise from differences in the gluon distribution at high $x$ in the available PDFs and point to high sensitivity of the present measurement to the proton PDFs.

Additional comparisons to theoretical predictions are available in Appendix A.
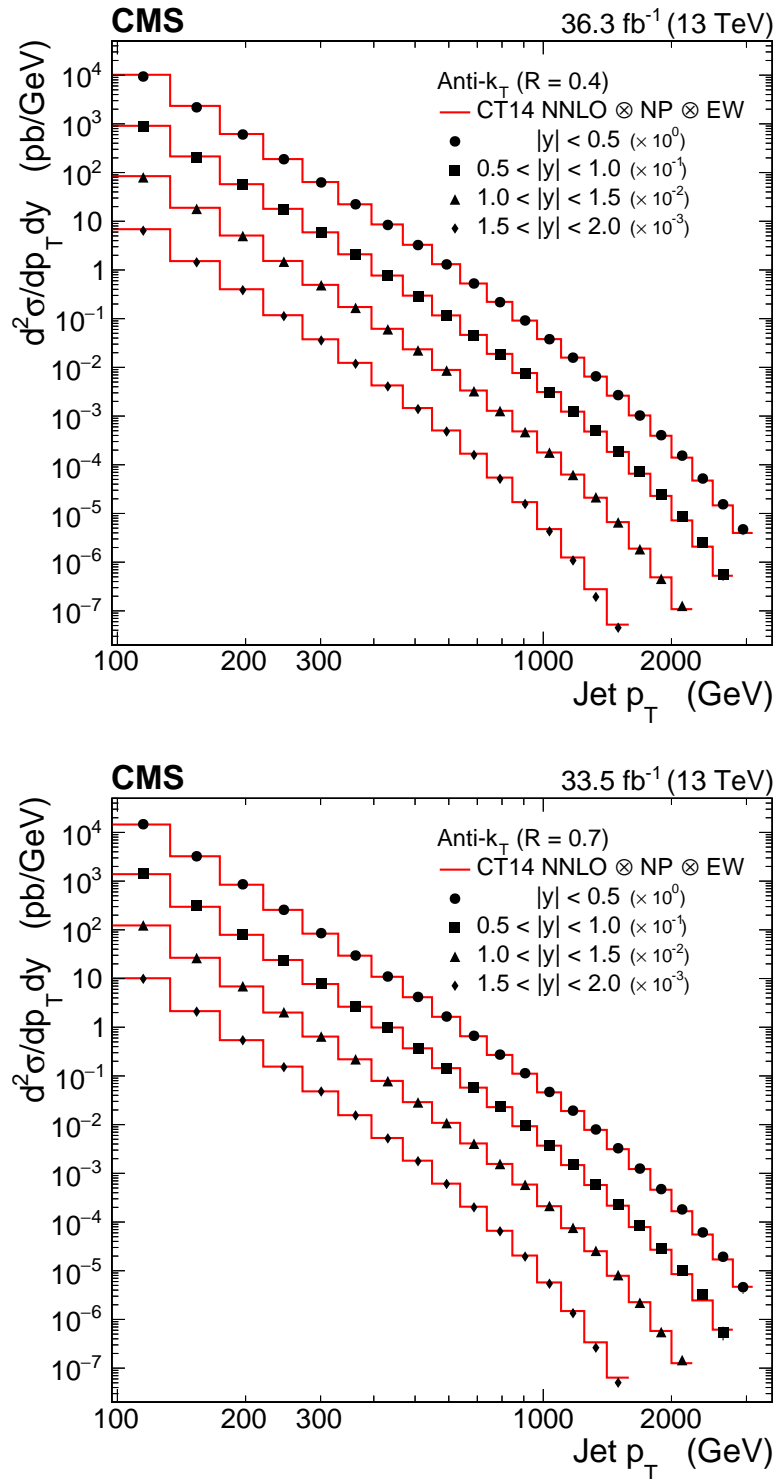
Figure 6: The inclusive jet production cross sections as a function of the jet transverse momentum $p_T$ measured in intervals of the absolute rapidity $|y|$. The cross section obtained for jets clustered using the anti-$k_T$ algorithm with $R = 0.4$ (0.7) is shown on the upper (lower) plot. The results in different $|y|$ intervals are scaled by a constant factor for presentation purpose. The data in different $|y|$ intervals are shown by markers of different style. The statistical uncertainties are too small to be visible; the systematic uncertainties are not shown. The measurements are compared with fixed-order NNLO QCD predictions (solid line) using CT14nnlo PDF and corrected for EW and NP effects.
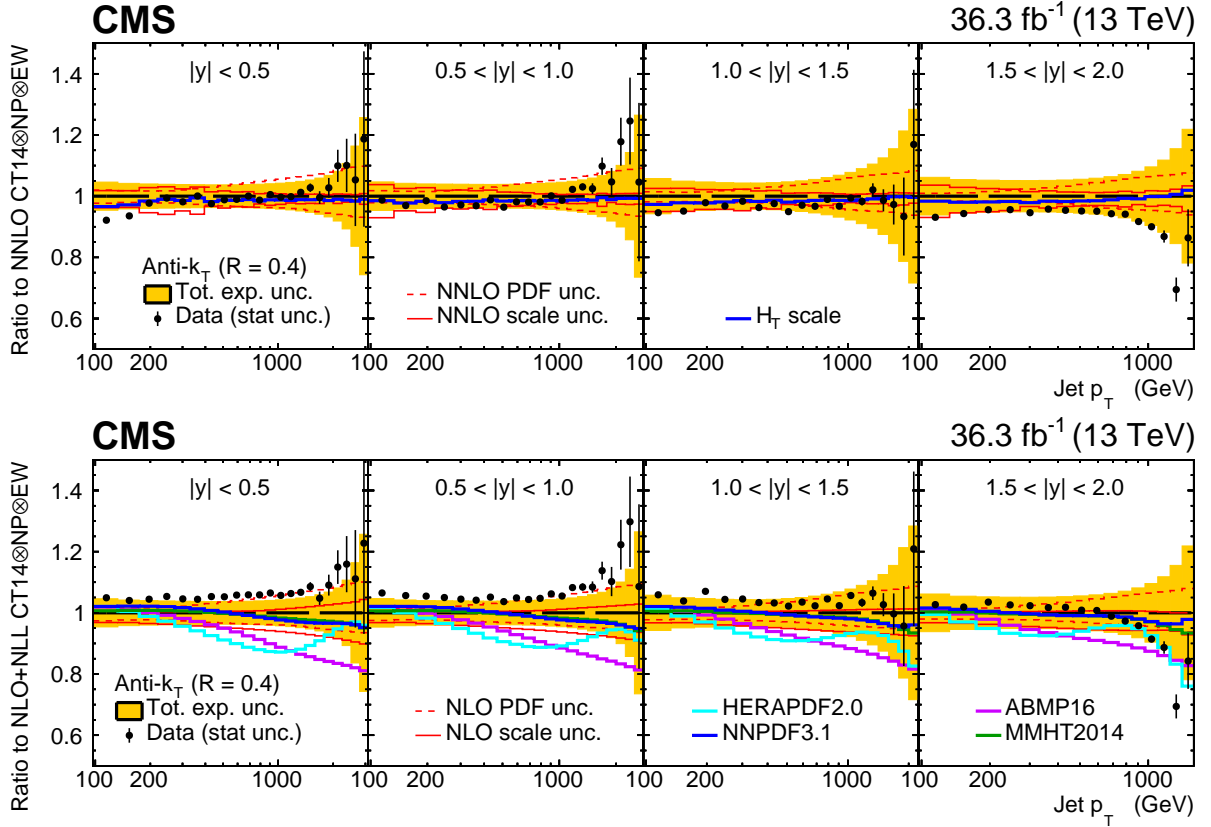
Figure 7: The double-differential cross section of inclusive jet production, as a function of $p_T$ and $|y|$, for jets clustered using the anti-$k_T$ algorithm with $R = 0.4$, presented as ratios to the QCD predictions. The data points are shown by filled circles, with statistic uncertainties shown by vertical error bars, while the total experimental uncertainty is centred at one and is presented by the orange band. In the upper panel, the data are divided by the NNLO prediction, corrected for NP and EW effects, using CT14nnlo PDF and with renormalisation and factorisation scales jet $p_T$ and, alternatively $H_T$ (blue solid line). In the lower panel, the data are shown as ratio to NLO+NLL prediction, calculated with CT14nlo PDF, and corrected for NP and EW effects. The scale (PDF) uncertainties are shown by red solid (dashed) lines. NLO+NLL predictions obtained with alternative PDF sets are displayed in different colours as a ratio to the central prediction using CT14nlo.
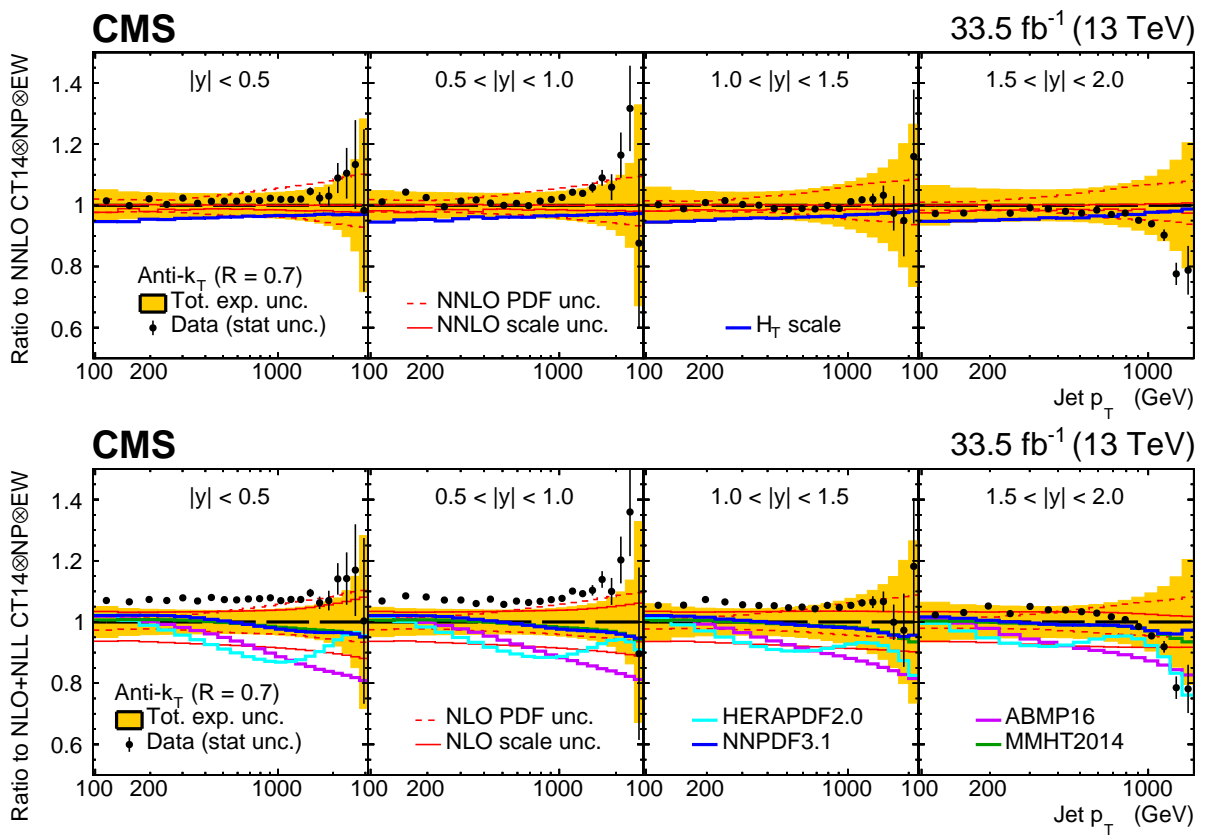
Figure 8: The double-differential cross section of inclusive jet production, as a function of $p_T$ and $|y|$, for jets clustered using the anti-$k_T$ algorithm with $R = 0.7$, presented as ratios to the QCD predictions. The notations are identical to those of Fig. 7.

# 6 The QCD analysis

The sensitivity of the presented measurement of the inclusive jet production to the proton PDFs and to the value of the strong coupling constant at the mass of the Z boson $\alpha_S(m_Z)$ is investigated in a comprehensive QCD analysis. The jet cross section for $R = 0.7$ is used because of reduced out-of-cone radiation and a better description of the measurement by the pQCD predictions. The QCD analysis is performed either assuming only the standard model or applying effective corrections to the QCD calculation of the inclusive jet production to include 4-quark contact interactions.

## 6.1 Data sets used

In this QCD analysis, the double-differential inclusive jet production cross section with $R = 0.7$ is used together with the charged- and neutral-current DIS cross sections of HERA [21]. In addition, the normalised triple-differential $t\bar{t}$ cross section [22] from CMS is used. As demonstrated in Ref. [22], the top quark pole mass $m_t^{\text{pole}}$, the gluon distribution, and the value of $\alpha_S(m_Z)$ are closely correlated in the triple-differential $t\bar{t}$ production cross section, thus providing additional sensitivity to the gluon distribution and to $\alpha_S(m_Z)$. Combining this data, the proton PDFs and the values of $\alpha_S(m_Z)$ and of $m_t^{\text{pole}}$ are extracted simultaneously. Although the inclusive jet production has no sensitivity to the value of $m_t^{\text{pole}}$, the strong constraints it has on the gluon distribution and on the value of $\alpha_S(m_Z)$ are reflected in the improved value and uncertainty in $m_t^{\text{pole}}$, since both $t\bar{t}$ and inclusive jet production cross sections are used in the fit.

For the QCD analysis, the open-source framework XFITTER [67–69] version 2.2.1, extended to SMEFT prediction, is used. The DGLAP [70–75] evolution is implemented using QCDNUM [76] version 17-01/14. The analysis is performed at NLO or NNLO, depending on the physics case, as described in the following. The correlations of the experimental statistics and systematic uncertainties in each individual data set are included. The HERA DIS measurements and the CMS data are treated as uncorrelated. In the CMS $t\bar{t}$ and jet measurements, the common systematic sources associated with the JES uncertainties are taken as 100% correlated.

## 6.2 Theoretical calculations used in QCD analysis

The SM theoretical predictions for the inclusive jet production cross section at NLO and NNLO are obtained as described in Section 4.1 and are corrected for NP and EW effects. The NNLO calculation is approximated by $k$-factors, obtained as a ratio of fixed-order NNLO to NLO calculations using CT14nnlo PDF in each bin in $p_T$ and $|y|$. These are applied to the NLOJet++ prediction interfaced to XFITTER using fast-grid techniques of FASTNLO [53]. In a similar way, the NLO prediction is improved to NLO+NLL as explained in Section 4. The QCD prediction for the normalised triple-differential cross section of the $t\bar{t}$ production is available only at NLO and is described in detail in Ref. [22].

The renormalisation and factorisation scales are set to the four-momentum transfer $Q$ for the DIS data and to the individual jet $p_T$ for inclusive jet cross section measurements. Following Ref. [22], in the case of $t\bar{t}$ production, the scales are set to $\mu_r = \mu_f = \frac{1}{2}\sum_i m_{Ti}$. The sum over $i$ covers the final-state partons t, $\bar{t}$, and at most three light partons in a $t\bar{t} + 2$ jets scenario. The transverse mass $m_{Ti} \equiv \sqrt{m_i^2 + p_{Ti}^2}$ is computed using the mass $m_i$ and transverse momentum $p_{Ti}$ of the partons [22].

The QCD analysis at NLO is extended into a SMEFT study by adding dimension-6 operators

for colour-charged fermions to the SM Lagrangian $\mathcal{L}_{SM}$ [23, 24], so that

$$\mathcal{L}_{SMEFT} = \mathcal{L}_{SM} + \frac{2\pi}{\Lambda^2} \sum_{n \in \{1,3,5\}} c_n O_n. \tag{5}$$

Here, the $c_n$ are Wilson coefficients and $\Lambda$ is the scale of new physics. For the 4-quark CI, the nonrenormalisable operators $O_n$ are

$$O_1 = \delta_{ij}\delta_{kl} \left( \sum_{c=1}^{3} \overline{q}_{Lci} \gamma_\mu q_{Lcj} \sum_{d=1}^{3} \overline{q}_{Ldk} \gamma^\mu q_{Ldl} \right), \tag{6}$$

$$O_3 = \delta_{ij}\delta_{kl} \left( \sum_{c=1}^{3} \overline{q}_{Lci} \gamma_\mu q_{Lcj} \sum_{d=1}^{3} \overline{q}_{Rdk} \gamma^\mu q_{Rdl} \right), \tag{7}$$

$$O_5 = \delta_{ij}\delta_{kl} \left( \sum_{c=1}^{3} \overline{q}_{Rci} \gamma_\mu q_{Rcj} \sum_{d=1}^{3} \overline{q}_{Rdk} \gamma^\mu q_{Rdl} \right), \tag{8}$$

where the sums in $c$ and $d$ run over generations, whereas $i, j, k, l$ are colour indices. The $L$ and $R$ subscripts denote the handedness of the quarks. The operators in Eqs. (6)–(8) correspond to having integrated out a colour-singlet BSM exchange between two quark lines. The colour-singlet exchanges are dominant in quark compositeness [77] or $Z'$ models [78]. The operators commonly denoted $O_2$, $O_4$ and $O_6$ in literature involve a product of Gell-Mann matrices in place of $\delta_{ij}\delta_{kl}$ and cause colour-octet; they are not considered here.

The CI studied in the SMEFT fits is either purely left-handed, vector-like, or axial vector-like. The only free Wilson coefficient is $c_1$, which multiplies the operator $O_1$ in Eq. (5). The coefficients $c_3$ and $c_5$ are determined from $c_1$ in accordance with how the quark-line handedness may change in the interaction. In the left-handed singlet model there are CI only between two left-handed lines, and hence $c_3 = c_5 = 0$. Vector-like and axial vector-like exchanges allow interactions also between right-handed quarks, giving $c_5 = c_1$ in both cases. For interactions between quark lines of different handedness, the vector-like exchange implies $c_3 = 2c_1$, whereas the axial vector-like model has $c_3 = -2c_1$. Further details of the theoretical model are given in Ref. [23].

In the QCD analysis, the SMEFT prediction for the double-differential cross section of the inclusive jet production reads

$$\sigma^{SMEFT} = \sigma^{NLO}_{FASTNLO} k^{NLO+NLL} \, EW \, NP + CI, \tag{9}$$

where $k^{NLO+NLL}$ is given in Eq. (3) and EW and NP are explained in Sections 4.2-4.3; the CI term is computed at NLO using the CIJET software [24] interfaced to XFITTER.

## 6.3 The general QCD analysis strategy and PDF uncertainties

The procedure for determining the PDFs follows the approach of HERAPDF [21, 79]. The contributions of charm and beauty quarks are treated in the Thorne–Roberts [80–82] variable-flavour number scheme at NLO. The values of heavy quark masses are set to $m_c = 1.47\,\text{GeV}$ and $m_b = 4.5\,\text{GeV}$. The $m_t^{pole}$ and $\alpha_S(m_Z)$ are free parameters in the PDF fits. The DIS data are restricted to high $Q^2$ by setting $Q^2_{min} = 7.5\,\text{GeV}^2$.

The parameterised PDFs are the gluon distribution $xg(x)$, the valence quark distributions $xu_v(x)$, and $xd_v(x)$, as well as $x\overline{U}(x)$ for the up- and $x\overline{D}(x)$ for the down-type antiquark distributions. At the starting scale of QCD evolution $Q^2_0 = 1.9\,\text{GeV}^2$, the general form of the

parameterisation for a PDF f is

$$xf(x) = A_f x^{B_f}(1 - x)^{C_f}(1 + D_f x + E_f x^2), \tag{10}$$

with the normalisation parameters $A_{u_v}$, $A_{d_v}$, and $A_g$ determined from QCD sum rules. The small-$x$ behaviour of the PDFs is driven by the $B$ parameters, whereas the $C$ parameters are responsible for the shape of the distribution as $x \to 1$.

The relations $x\overline{U}(x) = x\overline{u}(x)$ and $x\overline{D}(x) = x\overline{d}(x) + x\overline{s}(x)$ are assumed, with $x\overline{u}(x)$, $x\overline{d}(x)$, and $x\overline{s}(x)$ being the distributions for the up, down, and strange antiquarks, respectively. The sea quark distribution is defined as $x\Sigma(x) = 2 \cdot x\overline{u}(x) + x\overline{d}(x) + x\overline{s}(x)$. Further constraints $B_{\overline{U}} = B_{\overline{D}}$ and $A_{\overline{U}} = A_{\overline{D}}(1 - f_s)$ are imposed, so that the $x\overline{u}$ and $x\overline{d}$ distributions have the same normalisation as $x \to 0$. Here $f_s = \overline{s}/(\overline{d} + \overline{s})$ is the strangeness fraction, fixed to $f_s = 0.4$ as in the HERAPDF2.0 analysis [21].

The $D_f$ and $E_f$ parameters probe the sensitivity of the results to the specific selected functional form. In general, the parameterisation is obtained by first setting all $D$ and $E$ parameters to zero and then including them in the fit, one at a time. The improvement in the $\chi^2$ of a fit is monitored and the procedure is stopped when no further improvement is observed. Differences in the data sets or theoretical predictions lead to differences in the resulting parameterisation.

In the full QCD fit, the uncertainties in the individual PDFs and in the extracted non-PDF parameters are estimated similarly to the approach of HERAPDF [21, 79], which accounts for the fit, model, and parameterisation uncertainties as follows.

**Fit uncertainties** originate from the uncertainties in the used measurements and are obtained by using the Hessian method [83] implying the tolerance criterion $\Delta\chi^2 = 1$, which corresponds to the 68% confidence level (CL). Alternatively, the fit uncertainties are estimated by using the MC method [84, 85], where MC replicas are created by randomly fluctuating the cross section values in the data within their statistical and systematic uncertainties. For each fluctuation, the fit is performed and the central values for the fitted parameters and their uncertainties are estimated using the mean and the root mean square values over the replicas.

**Parameterisation uncertainty** is estimated by extending the functional forms of all PDFs with additional parameters $D$ and $E$, which are added, independently, one at a time. The resulting uncertainty is constructed as an envelope, built from the maximal differences between the PDFs (or non-PDF parameters) resulting from all the parameterisation variations and the results of the central fit.

**Model uncertainties** arise from the variations in the values assumed for the heavy quark masses $m_b$ and $m_c$ with $4.25 \leq m_b \leq 4.75\,\text{GeV}$, $1.41 \leq m_c \leq 1.53\,\text{GeV}$, and the value of $Q^2_{\min}$ imposed on the HERA data, which is varied in the interval $5.0 \leq Q^2_{\min} \leq 10.0\,\text{GeV}^2$. The strangeness fraction is varied within $0.32 \leq f_s \leq 0.48$, and the starting scale within $1.7 \leq Q^2_0 \leq 2.1\,\text{GeV}^2$. In addition, the theoretical uncertainty in the QCD predictions due to missing higher order corrections (scale uncertainty) is considered as a part of the model uncertainty. The renormalisation and factorisation scales are varied in the theoretical predictions by a factor of 2 up and down independently, avoiding cases with $\mu_f/\mu_r = 4^{\pm 1}$ and the fit is repeated for every variation. Maximum deviation from the central result is included as the scale uncertainty. The individual contributions of all model variations are added in quadrature into a single model uncertainty.

The total PDF uncertainty is obtained by adding in quadrature the fit and the model uncertainties, while the parameterisation uncertainties are added linearly.

The QCD analysis is performed in few steps. First, the impact of the CMS data on global PDF set CT14 [57] is investigated by using the profiling technique [86–89], as implemented in xFITTER. The available implementation does not allow for a simultaneous profiling of the PDF and non-PDF parameters such as $\alpha_S(m_Z)$, $m_t^{pole}$ or $c_1$. Therefore, those parameters are profiled individually. Next, the HERA DIS and CMS jet data are used in a full QCD fit in SM at NNLO, where the PDFs and the value of $\alpha_S(m_Z)$ are determined simultaneously. Further, the full QCD fit in SMEFT at NLO is performed using the HERA data and the CMS measurements of inclusive jet and $t\bar{t}$ production at $\sqrt{s} = 13$ TeV, where the PDFs, $\alpha_S(m_Z)$, $m_t^{pole}$, and $c_1$ are obtained at the same time. The individual steps of the QCD interpretation are described in detail in the following.

## 6.4   Results of profiling analysis

The impact of new data on the available PDFs is assessed in a profiling analysis [86–89]. Here, the PDF profiling is performed at NLO or at NNLO, using the CT14 PDF sets [57] derived at NLO or NNLO, respectively. These PDF sets do not include the CMS $t\bar{t}$ measurements. The theoretical prediction for the triple-differential $t\bar{t}$ cross section corresponding to the CMS measurement [22] is available only at NLO.

In the PDF profiling, the strong coupling is fixed to the central value of the CT14 PDF set, $\alpha_S(m_Z) = 0.118$. Once the $t\bar{t}$ cross sections are used, the $m_t^{pole}$ is set to 170.5 GeV, corresponding to the result of Ref. [22]. The results of the PDF profiling using the present inclusive jet cross section are shown in Fig. 9 (Fig. 10) at NLO (NNLO). According to the sensitivity of the data, the uncertainties in the PDFs are significantly improved by using the CMS jet measurement in the full $x$ range for the gluon and at medium $x$ for the sea quark distributions, whereas the valence distributions remain unchanged.

In addition to profiling the PDFs, the impact of the inclusive jet measurements on the extraction of the strong coupling constant is investigated. For this purpose, the $\alpha_S$-series of the CT14 PDFs at NLO and NNLO is used, where the value of $\alpha_S(m_Z)$ was varied from 0.1110 to 0.1220. Note that any possible $\alpha_S(m_Z)$ dependence of the $k$-factors could not be accounted for. The individual profiling is performed for each of the PDF members in the $\alpha_S$ series and the resulting $\chi^2$ is shown in Fig. 11 for both NLO and NNLO. The optimal value of $\alpha_S(m_Z)$ and its uncertainty is obtained by a parabolic fit as presented in Fig. 11. The impact of the scale uncertainty on the result is investigated by varying $\mu_r$ and $\mu_f$ in the theoretical predictions for the jet cross section. The $\chi^2$ scan is performed for each scale choice individually. The values obtained for the strong coupling are $\alpha_S(m_Z) = 0.1170 \pm 0.0018$ (PDF) $\pm 0.0035$ (scale) at NLO and $\alpha_S(m_Z) = 0.1130 \pm 0.0016$ (PDF) $\pm 0.0014$ (scale) at NNLO. The NLO result is in good agreement with the world average [90].

The profiling analysis is repeated by using the triple-differential CMS $t\bar{t}$ cross section of Ref. [22] together with the inclusive jet cross section. Consistent with the available theoretical prediction for the $t\bar{t}$ measurements, this analysis is performed at NLO. The results are shown in Fig. 12, where the uncertainty in the profiled gluon distribution is presented in comparison to that of the original CT14 PDF. The reduction of the uncertainty in the gluon distribution at high $x$ is stronger than in the case when only the CMS inclusive jet cross section is used. This is expected from the additional sensitivity of the $t\bar{t}$ production to the gluon distribution at high $x$. Also the $\alpha_S(m_Z)$ scan is shown in Fig. 12, now using both CMS data sets. The resulting NLO value of the strong coupling is $\alpha_S(m_Z) = 0.1154 \pm 0.0009$ (PDF) $\pm 0.0015$ (scale), consistent with the result of Ref. [22]. The additional sensitivity of the $t\bar{t}$ production to the strong coupling becomes visible in the reduced PDF uncertainties. The profiled pole mass of the top quark results in
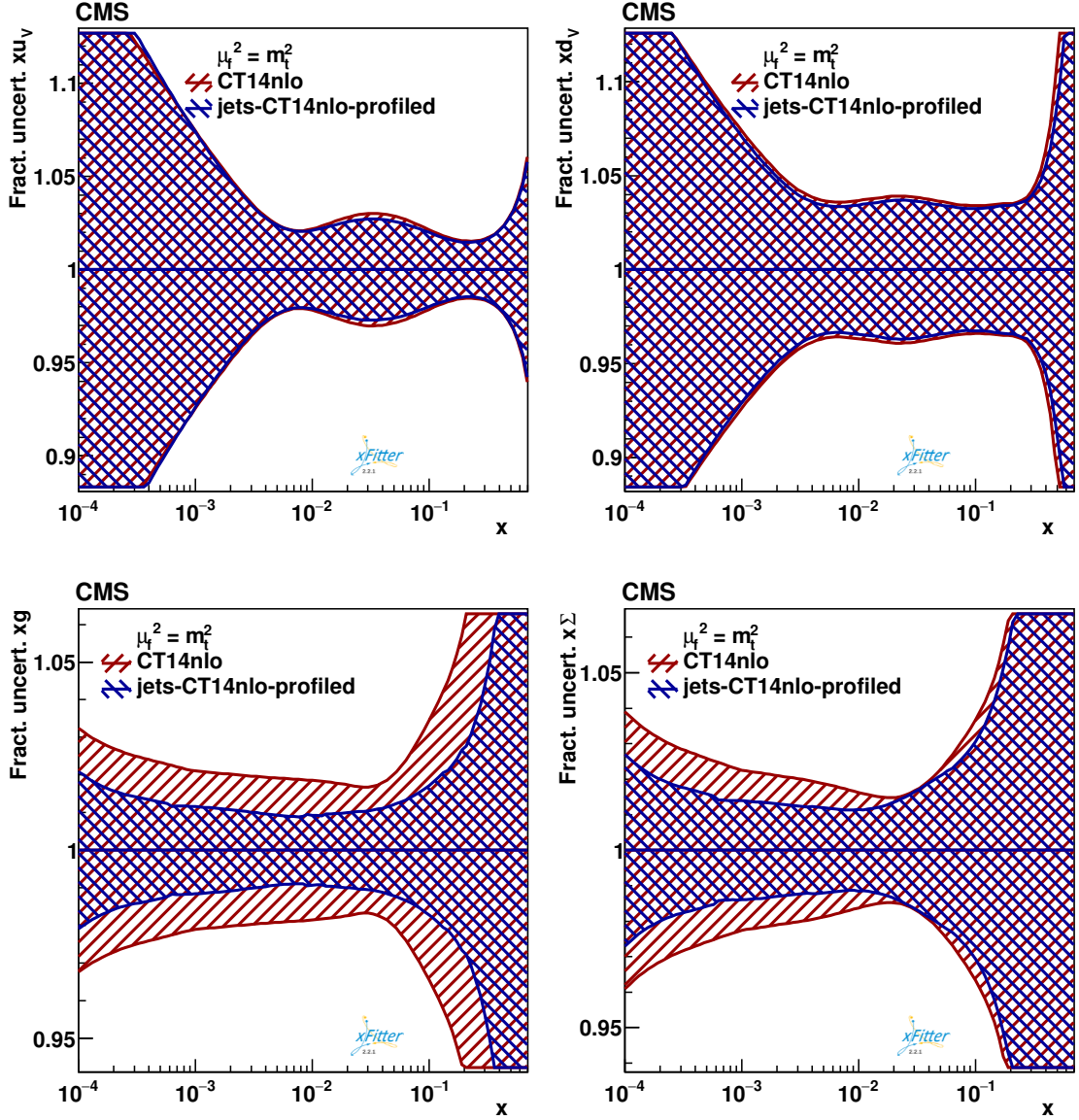
Figure 9: Fractional uncertainties in the u-valence (upper left), d-valence (upper right), gluon (lower left), and the sea quark (lower right) distributions, shown as a function of $x$ for the scale $\mu_{\mathrm{f}} = m_{\mathrm{t}}$. The profiling is performed using CT14nlo PDF at NLO, by using CMS inclusive jet cross section at $\sqrt{s} = 13\,\mathrm{TeV}$, implying the theoretical prediction for these data at NLO+NLL. The original uncertainty is shown in red, while the profiled result is shown in blue.
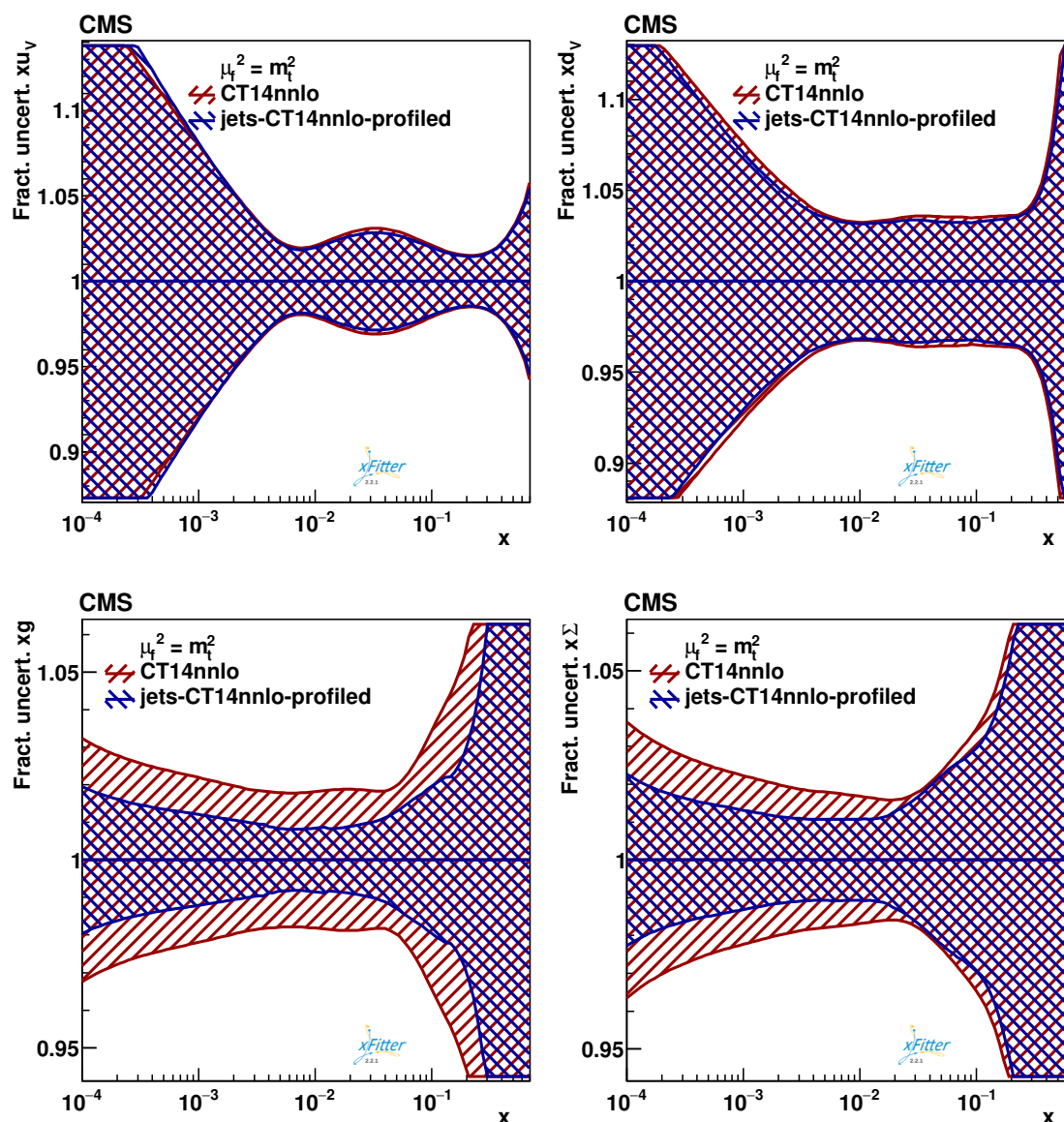
Figure 10: Fractional uncertainties in the u-valence (upper left), d-valence (upper right), gluon (lower left), and the sea quark (lower right) distributions, shown as functions of $x$ for the scale $\mu_f = m_t$. The profiling is performed using CT14nnlo PDF at NNLO, by using the CMS inclusive jet cross section at $\sqrt{s} = 13$ TeV, implying the theoretical prediction for these data at NNLO. The original uncertainty is shown in red, while the profiled result is shown in blue.

$m_t^{\text{pole}} = 170.3 \pm 0.5\,(\text{PDF}) + 0.2\,(\text{scale})\,\text{GeV}$, consistent with the value obtained in Ref. [22].

Furthermore, the profiling analysis is repeated assuming the SMEFT prediction for the inclusive jet production cross section. While the results of the profiled PDFs remain unchanged with respect to the SM results described above, the Wilson coefficient $c_1$ is profiled, assuming the value of the scale of the new interaction $\Lambda = 10\,\text{TeV}$, and the results are summarised in the Fig. 13.
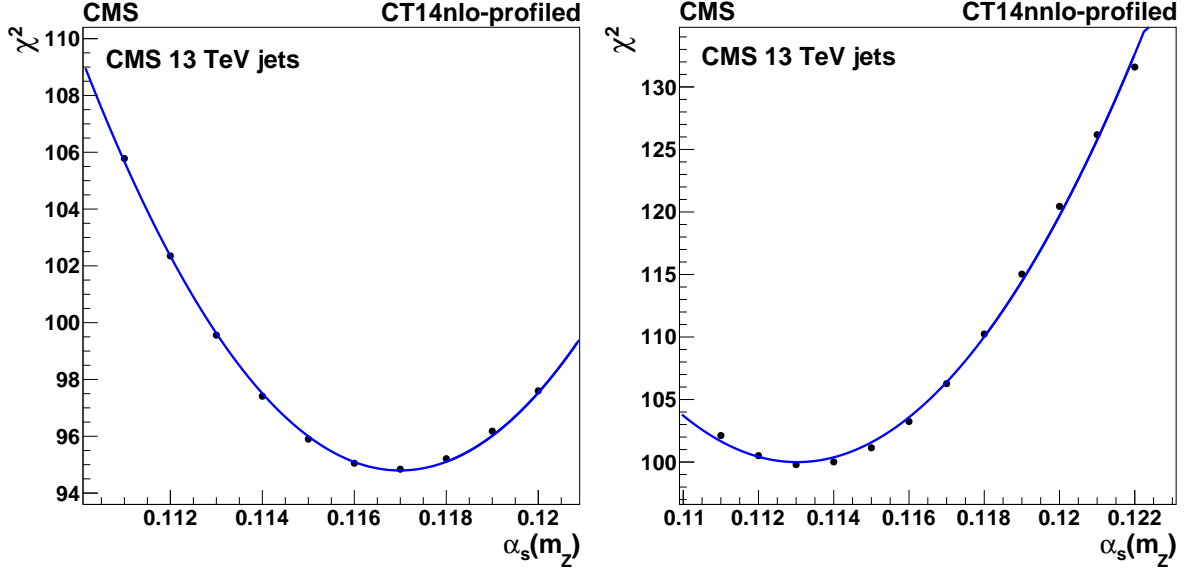


Figure 11: The $\chi^2$ obtained in profiling of CT14 PDF $\alpha_S(m_Z)$ series using the CMS inclusive jet cross section at $\sqrt{s} = 13\,\text{TeV}$ at NLO (left) and NNLO (right).
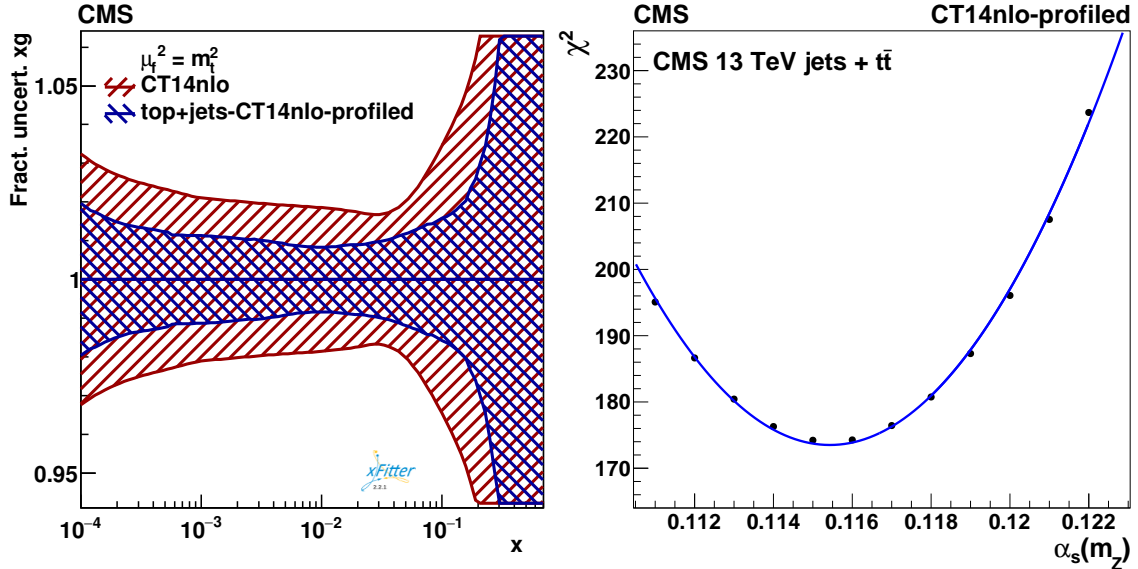


Figure 12: Fractional uncertainty in the gluon distribution (left), shown as a function of $x$ for the scale $\mu_f = m_t$. The profiling is performed using CT14nlo PDF at NLO, by using the CMS inclusive jet and the triple-differential $t\bar{t}$ cross sections at $\sqrt{s} = 13\,\text{TeV}$. The original (profiled) uncertainty is shown in red (blue). The $\chi^2$ (right) obtained in profiling of CT14 PDF $\alpha_S(m_Z)$ series using the same data as in (left).
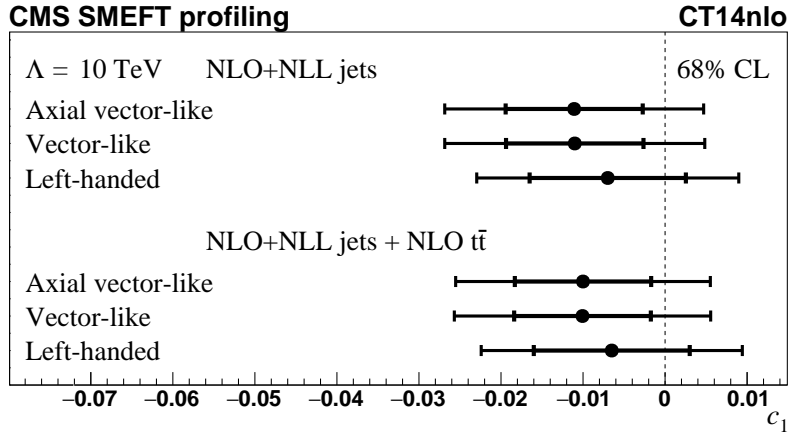
Figure 13: The profiled Wilson coefficient $c_1$ for the contact interaction models, assuming the left-handed, vector-like, and axial vector-like scenarios, as obtained in the profiling analysis using NLO+NLL calculation for the jet production and the CT14nlo PDF set. The value of $\Lambda = 10\,\text{TeV}$ is assumed. The results are obtained using the CMS measurements of inclusive jet cross section and of normalised triple-differential $t\bar{t}$ cross section at $\sqrt{s} = 13\,\text{TeV}$. The inner error bar shows the PDF uncertainty at 68% CL, while the outer error bar represents the total uncertainty, obtained from the PDF and scale uncertainties, added in quadrature.

The resulting values of $c_1$ are consistent with zero within uncertainties for all investigated CI models, demonstrating a good description of the data by the SM. Since the SMEFT computation is applied only to the inclusive jet production cross section, the $c_1$ results are independent of the inclusion of $t\bar{t}$ data. Once the relevant calculations for these data become available, a more global SMEFT interpretation would become possible.

## 6.5  Results of the full QCD fit in SM at NNLO

The present measurement of the inclusive jet production cross section is used together with the inclusive DIS cross section of HERA in a full QCD analysis at NNLO. The PDF parameterisation at the starting scale, resulting from the scan as described in Section 6.3 reads:

$$xg(x) = A_g x^{B_g} (1 - x)^{C_g} (1 + D_g x + E_g x^2),  \tag{11}$$

$$xu_v(x) = A_{u_v} x^{B_{u_v}} (1 - x)^{C_{u_v}} (1 + E_{u_v} x^2),  \tag{12}$$

$$xd_v(x) = A_{d_v} x^{B_{d_v}} (1 - x)^{C_{d_v}},  \tag{13}$$

$$x\overline{U}(x) = A_{\overline{U}} x^{B_{\overline{U}}} (1 - x)^{C_{\overline{U}}} (1 + D_{\overline{U}} x),  \tag{14}$$

$$x\overline{D}(x) = A_{\overline{D}} x^{B_{\overline{D}}} (1 - x)^{C_{\overline{D}}} (1 + E_{\overline{D}} x^2).  \tag{15}$$

The resulting PDFs are shown in Fig. 14, illustrating the contributions from the fit, model and the parameterisation uncertainties. The value of $\alpha_S(m_Z)$ is obtained simultaneously with the PDFs and corresponds to

$$\alpha_S(m_Z) = 0.1170 \pm 0.0014 \,(\text{fit}) \pm 0.0007 \,(\text{model}) \pm 0.0008 \,(\text{scale}) \pm 0.0001 \,(\text{param.}),  \tag{16}$$

which agrees with the previous extractions of the strong coupling constant at NNLO at hadron colliders [91, 92], of which it has best precision, to date.

The impact of the present CMS jet data in a full QCD fit (HERA+CMS fit) is demonstrated by comparing of the resulting PDFs with an alternative fit, where only the HERA data is used (HERA-only fit). Since the inclusive DIS data have much lower sensitivity to the value of $\alpha_S(m_Z)$, it is fixed in the HERA-only fit to the result of the HERA+CMS fit. The comparison of the resulting PDFs is presented in Fig. 15. The uncertainty is significantly reduced once the CMS jet measurements are included.

The global and partial $\chi^2$ values for each data set, for HERA-only and HERA+CMS fits, are listed in Table 5, where the $\chi^2$ values illustrate a general agreement among all the data sets. The somewhat high $\chi^2/N_{\text{dof}}$ values for the combined DIS data are very similar to those observed in Ref. [21], where they are investigated in detail.
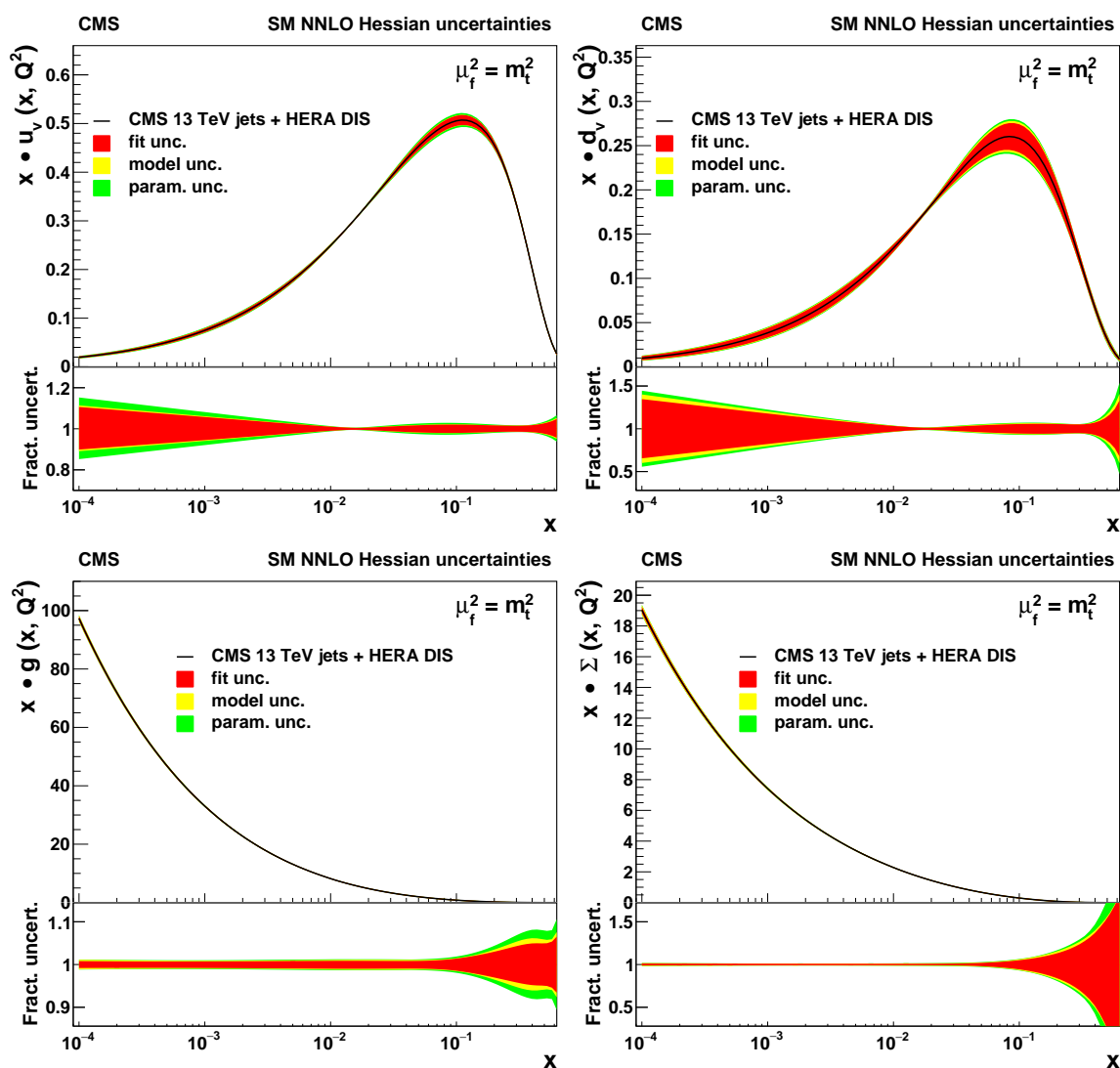
Figure 14: The u-valence (upper left), d-valence (upper right), gluon (lower left), and sea quark (lower right) distributions, shown as a function of $x$ at the scale $\mu_{\mathrm{f}} = m_t^2$, resulting from the NNLO fit using HERA DIS together with the CMS inclusive jet cross section at $\sqrt{s} = 13\,\mathrm{TeV}$. Contributions of fit, model, and parameterisation uncertainties for each PDF are shown. In the lower panels, the relative uncertainty contributions are presented.
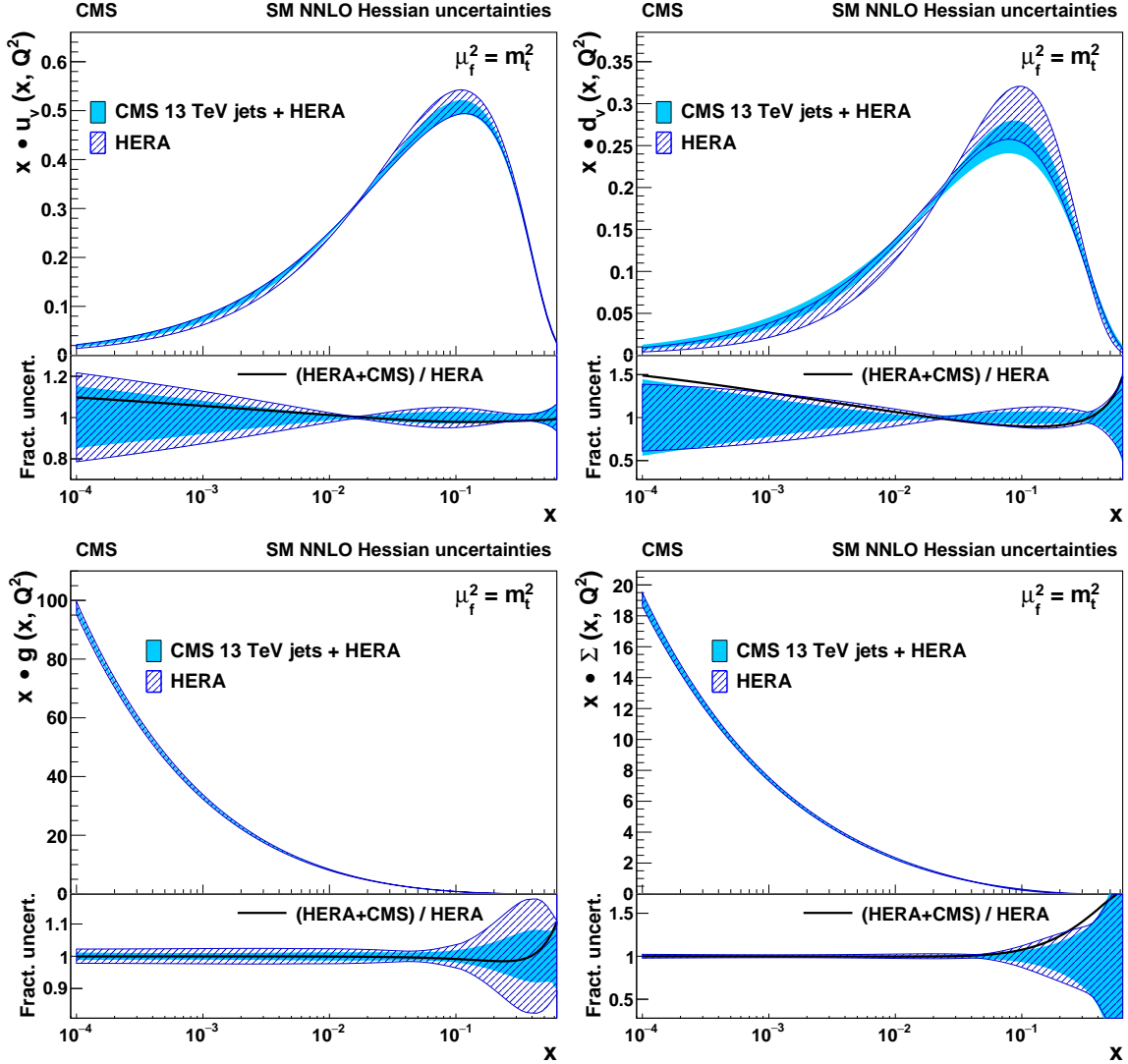
Figure 15: The u-valence (upper left), d-valence (upper right), gluon (lower left), and sea quark (lower right) distributions, shown as a function of $x$ at the scale $\mu_f = m_t^2$. The filled (hatched) band represents the results of the NNLO fit using HERA DIS and the CMS inclusive jet cross section at $\sqrt{s} = 13\,\text{TeV}$ (using the HERA DIS data only). The PDFs are shown with their total uncertainty. In the lower panels, the comparison of the relative PDF uncertainties is shown for each distribution. The dashed line corresponds to the ratio of the central PDF values of the two variants of the fit.

Table 5: Partial $\chi^2$ per number of data points $N_{dp}$ and the global $\chi^2$ per degree of freedom, $N_{dof}$, as obtained in the QCD analysis at NNLO of HERA+CMS jet data and HERA-only data. In the DIS data, the proton beam energy is given as $E_p$ and the electron energy is 27.5 GeV.

| Data sets | | HERA-only Partial $\chi^2/N_{dp}$ | HERA+CMS Partial $\chi^2/N_{dp}$ |
|---|---|---|---|
| HERA I+II neutral current | $e^+p$, $E_p = 920$ GeV | 378/332 | 375/332 |
| HERA I+II neutral current | $e^+p$, $E_p = 820$ GeV | 60/63 | 60/63 |
| HERA I+II neutral current | $e^+p$, $E_p = 575$ GeV | 201/234 | 201/234 |
| HERA I+II neutral current | $e^+p$, $E_p = 460$ GeV | 208/187 | 209/187 |
| HERA I+II neutral current | $e^-p$, $E_p = 920$ GeV | 223/159 | 227/159 |
| HERA I+II charged current | $e^+p$, $E_p = 920$ GeV | 46/39 | 46/39 |
| HERA I+II charged current | $e^-p$, $E_p = 920$ GeV | 55/42 | 56/42 |
| CMS inclusive jets 13 TeV | $0.0 < |y| < 0.5$ | — | 13/22 |
| | $0.5 < |y| < 1.0$ | — | 31/21 |
| | $1.0 < |y| < 1.5$ | — | 18/19 |
| | $1.5 < |y| < 2.0$ | — | 14/16 |
| Correlated $\chi^2$ | | 66 | 83 |
| Global $\chi^2/N_{dof}$ | | 1231/1043 | 1321/1118 |

## 6.6   Results of the SMEFT fit at NLO

To illustrate the possibility of simultaneous extraction of the SM parameters as PDFs, $\alpha_S(m_Z)$, and $m_t^{pole}$, together with the constraints on the physics beyond the SM, the present CMS measurements of the inclusive jet cross section, the triple-differential normalised CMS $t\bar{t}$ cross section at 13 TeV, and the HERA DIS cross sections are used in a SMEFT fit. Here, the SM prediction for the inclusive jet cross section is modified to account for CI as described in Section 6.2. The parameterisation is reinvestigated, as explained in Section 6.3, and results in

$$xg(x) = A_g x^{B_g} (1 - x)^{C_g} (1 + E_g x^2), \tag{17}$$

$$xu_v(x) = A_{u_v} x^{B_{u_v}} (1 - x)^{C_{u_v}} (1 + D_{u_v} x + E_{u_v} x^2), \tag{18}$$

$$xd_v(x) = A_{d_v} x^{B_{d_v}} (1 - x)^{C_{d_v}} (1 + D_{d_v} x), \tag{19}$$

$$x\overline{U}(x) = A_{\overline{U}} x^{B_{\overline{U}}} (1 - x)^{C_{\overline{U}}}, \tag{20}$$

$$x\overline{D}(x) = A_{\overline{D}} x^{B_{\overline{D}}} (1 - x)^{C_{\overline{D}}}. \tag{21}$$

First, the analysis is performed in the standard model. Then, alternatively, the SMEFT fit is done. Both SM and SMEFT fits are performed at NLO to be consistent with the order of the theoretical prediction for the $t\bar{t}$ data and for the CI corrections to the SM Lagrangian, although the SM prediction for the inclusive jet cross section is available at NNLO. The partial and global $\chi^2$ values for the SM and SMEFT fits are listed in Table 6. The fits with all CI models and various $\Lambda$ values resulted in very similar $\chi^2$ values.

The PDFs resulting from SM NLO fit are presented in Fig. 16 demonstrating the contributions of the fit, model, and parameterisation uncertainties. The NLO values of $\alpha_S(m_Z)$ and of $m_t^{pole}$ are determined simultaneously with the PDFs as $\alpha_S(m_Z) = 0.1188 \pm 0.0017\,(\text{fit}) \pm 0.0004\,(\text{model}) \pm 0.0025\,(\text{scale}) \pm 0.0001\,(\text{param.})$, and $m_t^{pole} = 170.4 \pm 0.6\,(\text{fit}) \pm 0.1\,(\text{model}) \pm 0.1\,(\text{scale}) \pm 0.1\,(\text{param.})$ GeV. These are consistent with earlier CMS results [11] and Ref. [22], respectively. The uncertainty in the value of $\alpha_S(m_Z)$ is dominated by the scale variation, which is significantly larger than in the NNLO result of Eq. (16).

In the SMEFT fit, the Wilson coefficient $c_1$ is introduced as a new free parameter, assuming different values for the scale of the new interaction $\Lambda = 5, 10, 13, 20,$ and 50 TeV. In all SMEFT fits, the $\chi^2$ is reduced by about 10, with just the addition of $c_1$ as an additional free parameter. Independent of the value of $\Lambda$, the strong coupling constant and the top quark mass in these SMEFT fits result to $\alpha_S(m_Z) = 0.1187 \pm 0.0016\,(\text{fit}) \pm 0.0005\,(\text{model}) \pm 0.0023\,(\text{scale}) \pm 0.0018\,(\text{param.})$, and $m_t^{pole} = 170.4 \pm 0.6\,(\text{fit}) \pm 0.1\,(\text{model}) \pm 0.1\,(\text{scale}) \pm 0.2\,(\text{param.})$ GeV. These values agree well with those obtained in the SM fit, and have larger parameterisation uncertainties because of increased flexibility in the SMEFT fit. The PDFs resulting from the SMEFT fits at different values of $\Lambda$ and for different CI models agree with each other and with the PDFs in the SM fit. In Fig. 17 the PDFs, which are obtained in the SM fit or in the SMEFT fit using the left-handed CI model, are compared. The PDFs are shown only with their fit uncertainty obtained by using the Hessian method.

To account for possible non-Gaussian tails, the PDF uncertainties are alternatively obtained by using the MC method, based on 800 replicas. The Hessian and the MC uncertainties in the SMEFT fit are shown in Fig. 18. The uncertainties obtained by using the MC method are larger at high $x$, which might suggest non-Gaussian tails in the PDF uncertainties. However this is not reflected in the uncertainty in $c_1$ coefficients; the respective uncertainties obtained by Hessian or MC methods agree well.

Table 6: Partial $\chi^2$ per number of data points $N_{dp}$ and the global $\chi^2$ per degree of freedom, $N_{dof}$, as obtained in the QCD analysis of HERA DIS data and the CMS measurements of inclusive jet production and the normalised triple-differential $t\bar{t}$ production at $\sqrt{s} = 13\,\text{TeV}$, obtained in SM and SMEFT analyses.

| Data sets | | SM fit Partial $\chi^2 / N_{dp}$ | SMEFT fit Partial $\chi^2 / N_{dp}$ |
|---|---|---|---|
| HERA I+II neutral current | $e^+p$, $E_p = 920\,\text{GeV}$ | 402/332 | 404/332 |
| HERA I+II neutral current | $e^+p$, $E_p = 820\,\text{GeV}$ | 60/63 | 60/63 |
| HERA I+II neutral current | $e^+p$, $E_p = 575\,\text{GeV}$ | 198/234 | 198/234 |
| HERA I+II neutral current | $e^+p$, $E_p = 460\,\text{GeV}$ | 208/187 | 208/187 |
| HERA I+II neutral current | $e^-p$, $E_p = 920\,\text{GeV}$ | 223/159 | 223/159 |
| HERA I+II charged current | $e^+p$, $E_p = 920\,\text{GeV}$ | 46/39 | 46/39 |
| HERA I+II charged current | $e^-p$, $E_p = 920\,\text{GeV}$ | 55/42 | 54/42 |
| CMS 13 TeV$t\bar{t}$ 3D | | 23/23 | 23/23 |
| CMS inclusive jets 13 TeV | $0.0 < |y| < 0.5$ | 13/22 | 20/22 |
| | $0.5 < |y| < 1.0$ | 28/21 | 27/21 |
| | $1.0 < |y| < 1.5$ | 13/19 | 11/19 |
| | $1.5 < |y| < 2.0$ | 33/16 | 28/16 |
| Correlated $\chi^2$ | | 121 | 115 |
| Global $\chi^2 / N_{dof}$ | | 1411/1141 | 1401/1140 |
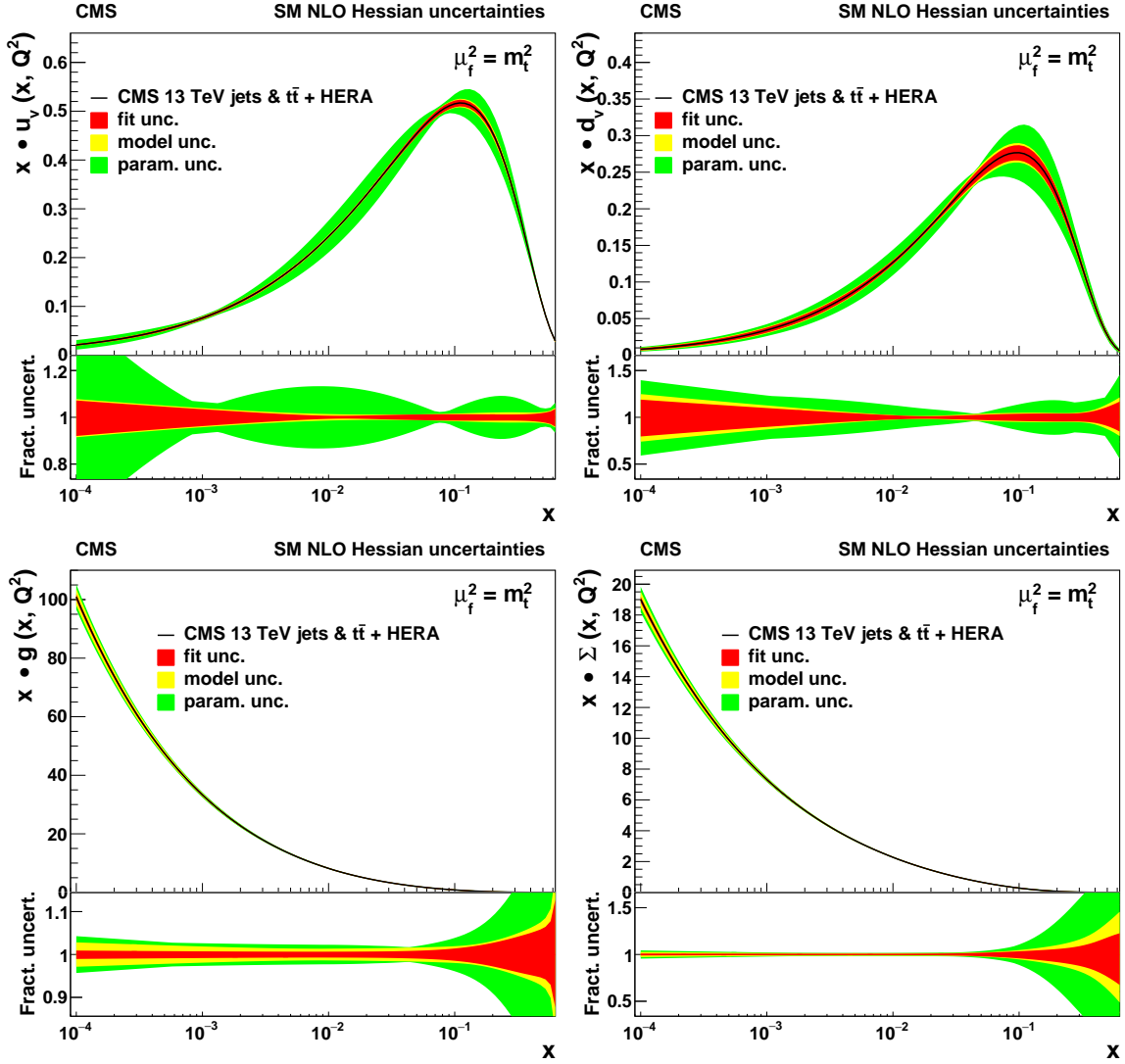
Figure 16: The u-valence (upper left), d-valence (upper right), gluon (lower left), and sea quark (lower right) distributions, shown as functions of $x$ at the scale $\mu_f = m_t^2$, resulting from the SM fit using HERA DIS together with the CMS inclusive jet cross section and the normalised triple-differential cross section of $t\bar{t}$ production at $\sqrt{s} = 13\,\text{TeV}$. Contributions of fit, model, and parameterisation uncertainties for each PDF are shown. In the lower panels, the relative uncertainty contributions are presented.
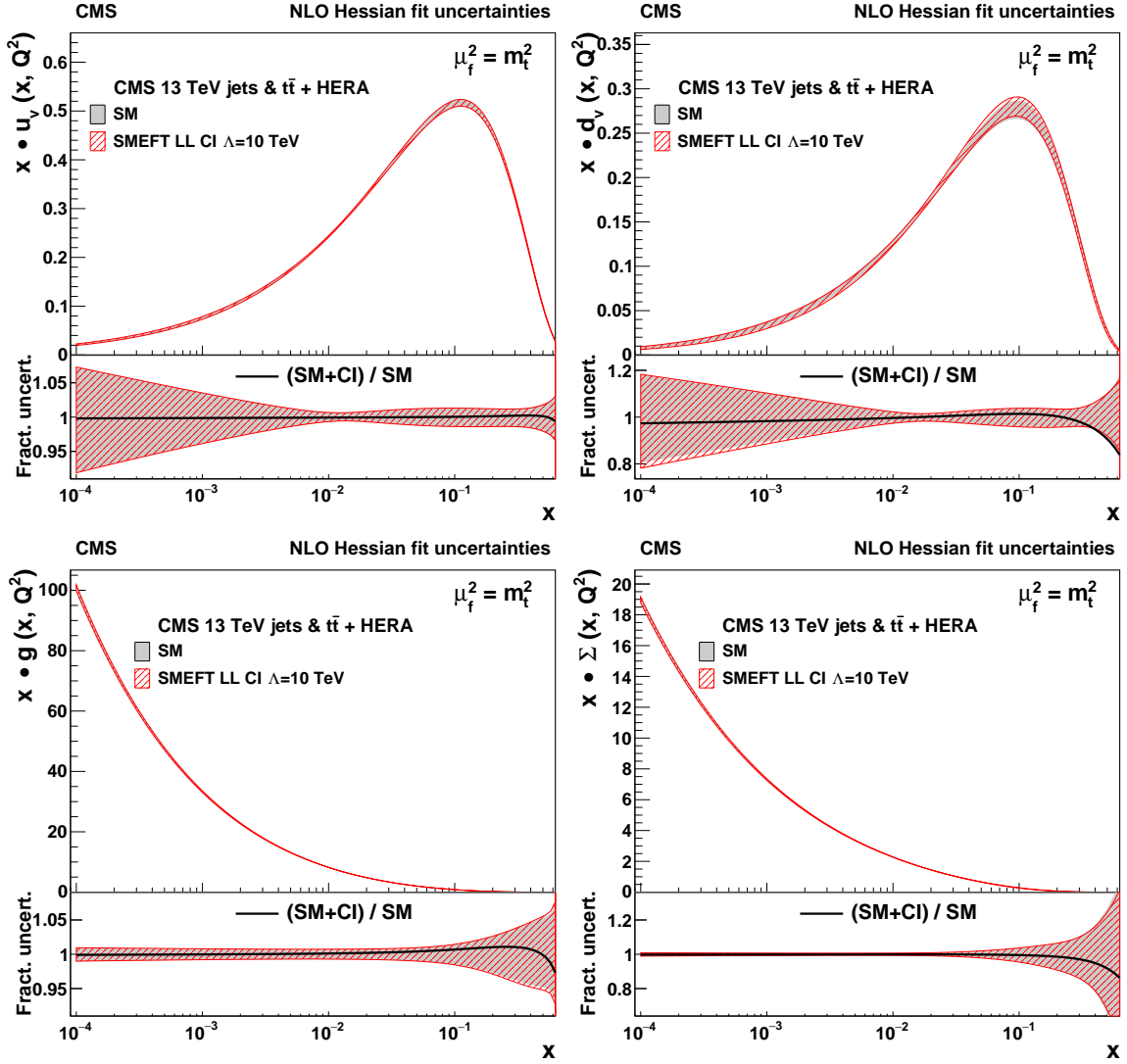
Figure 17: The u-valence (upper left), d-valence (upper right), gluon (lower left), and sea quark (lower right) distributions, shown as functions of $x$ at the scale $\mu_f^2 = m_t^2$, resulting from the fits with and without the CI terms. The SMEFT fit is performed with the left-handed CI model with $\Lambda = 10\,\text{TeV}$.
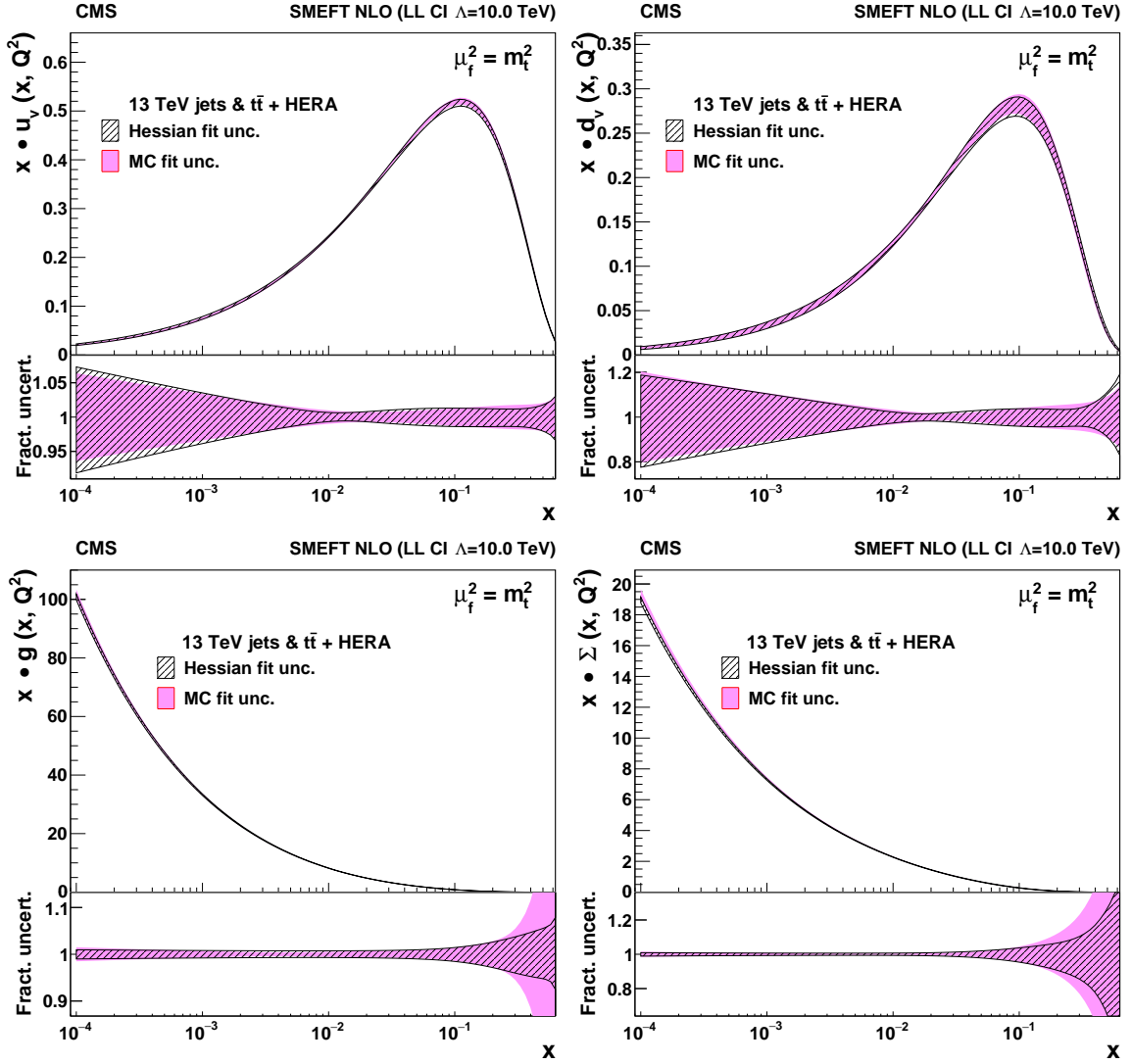
Figure 18: The u-valence (upper left), d-valence (upper right), gluon (lower left), and sea quark (lower right) distributions, shown as a function of $x$ at the scale $\mu_f^2 = m_t^2$, resulting from the SMEFT fit with the left-handed CI model with $\Lambda = 10\,\text{TeV}$. The PDFs are shown with the fit uncertainties obtained by the Hessian (solid blue) and Monte Carlo (solid red) methods.

The Wilson coefficients $c_1$ are obtained for different assumptions on the value of $\Lambda$, as listed in Table 7. All SMEFT fits lead to negative $c_1$, which would translate into a positive interference with the SM gluon exchange. However, the differences from the SM ($c_1 = 0$) are not statistically significant. The ratio $c_1/\Lambda^2$ is illustrated for $\Lambda = 50\,\text{TeV}$ in Fig. 19 and is observed to remain constant for various values of $\Lambda$.

Table 7: The values and uncertainties of the fitted Wilson coefficients $c_1$ for various scales $\Lambda$. The fit uncertainties are obtained by using the Hessian method.

| Scale | CI model | $c_1$ | Fit | Model | Scale | Param. |
|---|---|---|---|---|---|---|
| | Left-handed | $-0.017$ | 0.0047 | 0.0001 | 0.004 | 0.002 |
| $\Lambda = 5\,\text{TeV}$ | Vector-like | $-0.009$ | 0.0026 | 0.0001 | 0.002 | 0.001 |
| | Axial vector-like | $-0.009$ | 0.0025 | 0.0001 | 0.002 | 0.001 |
| | Left-handed | $-0.068$ | 0.019 | 0.003 | 0.016 | 0.009 |
| $\Lambda = 10\,\text{TeV}$ | Vector-like | $-0.037$ | 0.011 | 0.002 | 0.008 | 0.006 |
| | Axial vector-like | $-0.036$ | 0.011 | 0.003 | 0.008 | 0.005 |
| | Left-handed | $-0.116$ | 0.033 | 0.006 | 0.026 | 0.015 |
| $\Lambda = 13\,\text{TeV}$ | Vector-like | $-0.063$ | 0.018 | 0.004 | 0.015 | 0.008 |
| | Axial vector-like | $-0.062$ | 0.018 | 0.003 | 0.014 | 0.008 |
| | Left-handed | $-0.28$ | 0.08 | 0.01 | 0.06 | 0.04 |
| $\Lambda = 20\,\text{TeV}$ | Vector-like | $-0.15$ | 0.04 | 0.01 | 0.04 | 0.02 |
| | Axial vector-like | $-0.15$ | 0.04 | 0.01 | 0.04 | 0.02 |
| | Left-handed | $-1.8$ | 0.53 | 0.08 | 0.42 | 0.23 |
| $\Lambda = 50\,\text{TeV}$ | Vector-like | $-1.0$ | 0.28 | 0.05 | 0.23 | 0.13 |
| | Axial vector-like | $-1.0$ | 0.29 | 0.04 | 0.23 | 0.13 |
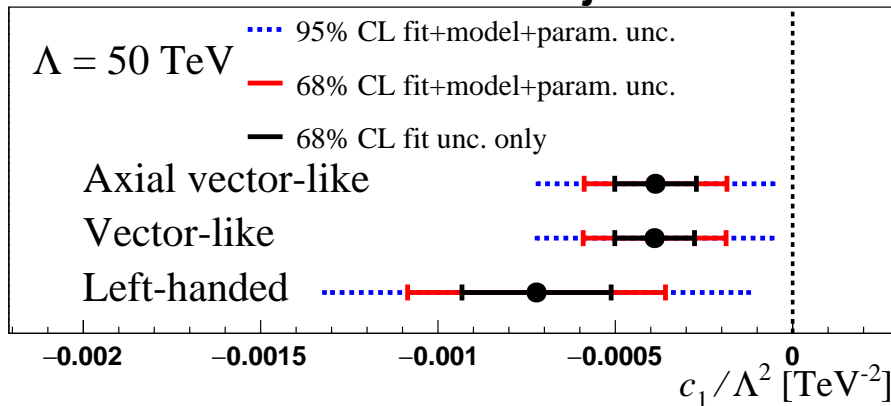


Figure 19: The Wilson coefficients $c_1$ obtained in the SMEFT analysis at NLO, divided by $\Lambda^2$, for $\Lambda = 50\,\text{TeV}$. The solid (dashed) lines represent the total uncertainty at 68 (95)% CL. The inner (outer) error bars show the fit (total) uncertainty at 68% CL.

Conventional searches for CI fix the values of Wilson coefficient to +1 (-1) for a destructive (constructive) interference with the SM gluon exchange, and impose exclusion limits on the

scale $\Lambda$ [90]. The results obtained in the present analysis that indicate negative Wilson coefficients, with $|c_1|$ close to 1 for $\Lambda = 50\,\text{TeV}$, can be translated into a 95% CL exclusion limit for the left-handed model with constructive interference, corresponding to $\Lambda > 24\,\text{TeV}$. The most stringent comparable result is obtained in the analysis of dijet cross section at $\sqrt{s} = 13\,\text{TeV}$ by the ATLAS Collaboration [93], in which the 95% CL exclusion limits for purely left-handed CI of 22 TeV for constructive interference, and of 30 TeV for destructive interference are obtained.

As already observed in the results of profiling, the results of the full fit show agreement between the measurements and the SM prediction. Since the parameterisation and the PDF uncertainties differ in the profiling analysis and in the full fit, a direct quantitative comparison of these results is not possible. The advantage of the full fit with respect to the profiling is in the properly considered, and therefore mitigated, correlations between the QCD parameters and the PDFs. The full SMEFT fit assures that the possible BSM effects are not absorbed in the PDFs and in turn, into the SM prediction, which is the basis for the search for new physics.

# 7  Summary

In this paper, the measurement of the double-differential inclusive jet cross sections in proton-proton collisions at $\sqrt{s} = 13\,\text{TeV}$ is presented as a function of the jet transverse momentum $p_T$ and the jet rapidity $|y|$ for jets reconstructed using the anti-$k_T$ clustering algorithm with a distance parameter $R$ of 0.4 and 0.7. The phase space covers jet $p_T$ from 97 GeV up to 3.1 TeV and jet rapidity up to $|y| = 2.0$. The measured jet cross sections are compared with predictions of perturbative quantum chromodynamics (pQCD) at next-to-next-to-leading order (NNLO) and next-to-leading order (NLO) with the next-to-leading-logarithmic (NLL) resummation correction, using various sets of parton distribution functions (PDFs). A strong impact of the measurement on determination of the parton distributions is observed, expressed by significant differences among the theoretical predictions using different PDF sets, and by large corresponding uncertainties.

To investigate the impact of the measurements on the PDFs and the strong coupling constant $\alpha_S$, a QCD analysis is performed, where the jet production cross section with $R = 0.7$ is used together with the HERA measurements of deep inelastic scattering. Significant improvement of the accuracy of the PDFs by using the present measurement in the QCD analysis is demonstrated in a profiling analysis using the CT14 PDF set and in the full PDF fit.

The value of the strong coupling constant at the Z boson mass is extracted in a QCD analysis at NNLO using the inclusive jet cross sections in proton-proton collisions for the first time, and results in $\alpha_S(m_Z) = 0.1170 \pm 0.0014\,\text{(fit)} \pm 0.0007\,\text{(model)} \pm 0.0008\,\text{(scale)} \pm 0.0001\,\text{(parametrisation)}$.

The QCD analysis is also performed at NLO, where the CMS measurement of the normalised triple-differential top quark-antiquark production cross section at $\sqrt{s} = 13\,\text{TeV}$ is used in addition. In this analysis, the PDFs, the values of the strong coupling constant, and of the top quark pole mass $m_t^{\text{pole}}$ are extracted simultaneously with $\alpha_S(m_Z) = 0.1188 \pm 0.0017\,\text{(fit)} \pm 0.0004\,\text{(model)} \pm 0.0025\,\text{(scale)} \pm 0.0001\,\text{(parameterisation)}$, dominated by the scale uncertainty, and $m_t^{\text{pole}} = 170.4 \pm 0.6\,\text{(fit)} \pm 0.1\,\text{(model)} \pm 0.1\,\text{(scale)} \pm 0.1\,\text{(parameterisation)}\,\text{GeV}$. The resulting values of $\alpha_S(m_Z)$ agree with the world average and the previous CMS results using the jet measurements. The value of $m_t^{\text{pole}}$ agrees well with the result of the previous CMS analysis using the triple-differential cross section of the top quark-antiquark pair production. Although the inclusive jet production is not directly sensitive to $m_t^{\text{pole}}$, the resulting value is improved by the additional constraint on the gluon distribution and on $\alpha_S(m_Z)$ provided by the jet measure-

ments.

Furthermore, an alternative QCD analysis is performed with the same data, where the standard model Lagrangian is modified by the introduction of effective terms related to 4-quark contact interactions. In the analysis, the Wilson coefficients for the contact interactions are extracted for different values assumed for the scale $\Lambda$ of the new interaction. The results are translated into a 95% confidence level exclusion limit for the left-handed model with constructive interference, corresponding to $\Lambda > 24\,\text{TeV}$. These results are compatible with the standard model and the previous limits obtained at the LHC using jet production. The advantage of the present approach is the simultaneous extraction of PDFs, thereby mitigating possible bias in the interpretation of the measurements in terms of physics beyond the standard model.

Tabulated results are provided in the HEPData record for this analysis [94].

## Acknowledgments

# References

[1] ATLAS Collaboration, "Measurement of inclusive jet and dijet cross sections in proton-proton collisions at 7 TeV centre-of-mass energy with the ATLAS detector", *Eur. Phys. J. C* **71** (2011) 1512, `doi:10.1140/epjc/s10052-010-1512-2`, `arXiv:1009.5908`.

[2] ATLAS Collaboration, "Measurement of inclusive jet and dijet production in pp collisions at $\sqrt{s} = 7$ TeV using the ATLAS detector", *Phys. Rev. D* **86** (2012) 014022, `doi:10.1103/PhysRevD.86.014022`, `arXiv:1112.6297`.

[3] CMS Collaboration, "Measurement of the inclusive jet cross section in pp collisions at $\sqrt{s} = 7$ TeV", *Phys. Rev. Lett.* **107** (2011) 132001, `doi:10.1103/PhysRevLett.107.132001`, `arXiv:1106.0208`.

[4] CMS Collaboration, "Measurement of the double-differential inclusive jet cross section in proton-proton collisions at $\sqrt{s} = 13$ TeV", *Eur. Phys. J. C* **76** (2016) 451, `doi:10.1140/epjc/s10052-016-4286-3`, `arXiv:1605.04436`.

[5] ATLAS Collaboration, "Measurement of the inclusive jet cross section in pp collisions at $\sqrt{s} = 2.76$ TeV and comparison to the inclusive jet cross section at $\sqrt{s} = 7$ TeV using the ATLAS detector", *Eur. Phys. J. C* **73** (2013) 2509, `doi:10.1140/epjc/s10052-013-2509-4`, `arXiv:1304.4739`.

[6] CMS Collaboration, "Measurement of the inclusive jet cross section in pp collisions at $\sqrt{s} = 2.76$ TeV", *Eur. Phys. J. C* **76** (2016) 265, `doi:10.1140/epjc/s10052-016-4083-z`, `arXiv:1512.06212`.

[7] ATLAS Collaboration, "Measurement of the inclusive jet cross-section in proton-proton collisions at $\sqrt{s} = 7$ TeV using $4.5$ fb$^{-1}$ of data with the ATLAS detector", *JHEP* **02** (2015) 153, `doi:10.1007/JHEP02(2015)153`, `arXiv:1410.8857`. [Erratum: `doi:10.1007/JHEP09(2015)141`].

[8] CMS Collaboration, "Measurements of differential jet cross sections in proton-proton collisions at $\sqrt{s} = 7$ TeV with the CMS detector", *Phys. Rev. D* **87** (2013) 112002, `doi:10.1103/PhysRevD.87.112002`, `arXiv:1212.6660`. [Erratum: `doi:10.1103/JHEP09(2015)141`].

[9] CMS Collaboration, "Measurement of the ratio of inclusive jet cross sections using the anti-$k_T$ algorithm with radius parameters $R = 0.5$ and 0.7 in pp collisions at $\sqrt{s} = 7$ TeV", *Phys. Rev. D* **90** (2014) 072006, `doi:10.1103/PhysRevD.90.072006`, `arXiv:1406.0324`.

[10] ATLAS Collaboration, "Measurement of the inclusive jet cross-sections in proton-proton collisions at $\sqrt{s} = 8$ TeV with the ATLAS detector", *JHEP* **09** (2017) 020, `doi:10.1007/JHEP09(2017)020`, `arXiv:1706.03192`.

[11] CMS Collaboration, "Measurement and QCD analysis of double-differential inclusive jet cross sections in pp collisions at $\sqrt{s} = 8$ TeV and cross section ratios to 2.76 and 7 TeV", *JHEP* **03** (2017) 156, `doi:10.1007/JHEP03(2017)156`, `arXiv:1609.05331`.

[12] ATLAS Collaboration, "Measurement of inclusive jet and dijet cross-sections in proton-proton collisions at $\sqrt{s} = 13$ TeV with the ATLAS detector", *JHEP* **05** (2018) 195, `doi:10.1007/JHEP05(2018)195`, `arXiv:1711.02692`.

[13] X. Liu, S.-O. Moch, and F. Ringer, "Phenomenology of single-inclusive jet production with jet radius and threshold resummation", *Phys. Rev. D* **97** (2018) 056026, `doi:10.1103/PhysRevD.97.056026`, `arXiv:1801.07284`.

[14] J. Currie, E. W. N. Glover, and J. Pires, "Next-to-next-to leading order QCD predictions for single jet inclusive production at the LHC", *Phys. Rev. Lett.* **118** (2017) 072002, `doi:10.1103/PhysRevLett.118.072002`, `arXiv:1611.01460`.

[15] J. Currie et al., "Infrared sensitivity of single jet inclusive production at hadron colliders", *JHEP* **10** (2018) 155, `doi:10.1007/JHEP10(2018)155`, `arXiv:1807.03692`.

[16] CMS Collaboration, "Constraints on parton distribution functions and extraction of the strong coupling constant from the inclusive jet cross section in pp collisions at $\sqrt{s} = 7$ TeV", *Eur. Phys. J. C* **75** (2015) 288, `doi:10.1140/epjc/s10052-015-3499-1`, `arXiv:1410.6765`.

[17] M. Cacciari, G. P. Salam, and G. Soyez, "The anti-$k_T$ jet clustering algorithm", *JHEP* **04** (2008) 063, `doi:10.1088/1126-6708/2008/04/063`, `arXiv:0802.1189`.

[18] M. Cacciari, G. P. Salam, and G. Soyez, "FASTJET user manual", *Eur. Phys. J. C* **72** (2012) 1896, `doi:10.1140/epjc/s10052-012-1896-2`, `arXiv:1111.6097`.

[19] M. Dasgupta, L. Magnea, and G. P. Salam, "Non-perturbative QCD effects in jets at hadron colliders", *JHEP* **02** (2008) 055, `doi:10.1088/1126-6708/2008/02/055`, `arXiv:0712.3014`.

[20] CMS Collaboration, "Dependence of inclusive jet production on the anti-$k_T$ distance parameter in pp collisions at $\sqrt{s} = 13$ TeV", *JHEP* **12** (2020) 082, `doi:10.1007/JHEP12(2020)082`, `arXiv:2005.05159`.

[21] H1 and ZEUS Collaborations, "Combination of measurements of inclusive deep inelastic $e^{\pm}p$ scattering cross sections and QCD analysis of HERA data", *Eur. Phys. J. C* **75** (2015) 580, `doi:10.1140/epjc/s10052-015-3710-4`, `arXiv:1506.06042`.

[22] CMS Collaboration, "Measurement of $t\bar{t}$ normalised multi-differential cross sections in pp collisions at $\sqrt{s} = 13$ TeV, and simultaneous determination of the strong coupling strength, top quark pole mass, and parton distribution functions", *Eur. Phys. J. C* **80** (2020) 658, `doi:10.1140/epjc/s10052-020-7917-7`, `arXiv:1904.05237`.

[23] J. Gao, C. S. Li, and C. P. Yuan, "NLO QCD corrections to dijet production via quark contact interactions", *JHEP* **07** (2012) 037, `doi:10.1007/JHEP07(2012)037`, `arXiv:1204.4773`.

[24] J. Gao, "CIJET: A program for computation of jet cross sections induced by quark contact interactions at hadron colliders", *Comput. Phys. Commun.* **184** (2013) 2362, `doi:10.1016/j.cpc.2013.05.019`, `arXiv:1301.7263`.

[25] CMS Collaboration, "Search for contact interactions using the inclusive jet $p_T$ spectrum in pp collisions at $\sqrt{s} = 7$ TeV", *Phys. Rev. D* **87** (2013) 052017, `doi:10.1103/PhysRevD.87.052017`, `arXiv:1301.5023`.

[26] CMS Collaboration, "Search for quark compositeness in dijet angular distributions from pp collisions at $\sqrt{s} = 7$ TeV", *JHEP* **05** (2012) 055, `doi:10.1007/JHEP05(2012)055`, `arXiv:1202.5535`.

[27] CMS Collaboration, "Search for quark contact interactions and extra spatial dimensions using dijet angular distributions in proton-proton collisions at $\sqrt{s} = 8$ TeV", *Phys. Lett. B* **746** (2015) 79, `doi:10.1016/j.physletb.2015.04.042`, `arXiv:1411.2646`.

[28] CMS Collaboration, "Search for new physics with dijet angular distributions in proton-proton collisions at $\sqrt{s} = 13$ TeV", *JHEP* **07** (2017) 013, `doi:10.1007/JHEP07(2017)013`, `arXiv:1703.09986`.

[29] CMS Collaboration, "Particle-flow reconstruction and global event description with the CMS detector", *JINST* **12** (2017) P10003, `doi:10.1088/1748-0221/12/10/P10003`, `arXiv:1706.04965`.

[30] CMS Collaboration, "Jet energy scale and resolution in the CMS experiment in pp collisions at 8 TeV", *JINST* **12** (2017) P02014, `doi:10.1088/1748-0221/12/02/P02014`, `arXiv:1607.03663`.

[31] CMS Collaboration, "Jet algorithms performance in 13 TeV data", CMS Physics Analysis Summary CMS-PAS-JME-16-003, 2017.

[32] CMS Collaboration, "Performance of missing transverse momentum reconstruction in proton-proton collisions at $\sqrt{s} = 13$ TeV using the CMS detector", *JINST* **14** (2019) P07004, `doi:10.1088/1748-0221/14/07/P07004`, `arXiv:1903.06078`.

[33] CMS Collaboration, "The CMS trigger system", *JINST* **12** (2017) P01020, `doi:10.1088/1748-0221/12/01/P01020`, `arXiv:1609.02366`.

[34] CMS Collaboration, "Performance of the CMS level-1 trigger in proton-proton collisions at $\sqrt{s} = 13$ TeV", *JINST* **15** (2020) P10017, `doi:10.1088/1748-0221/15/10/P10017`, `arXiv:2006.10165`.

[35] CMS Collaboration, "The CMS experiment at the CERN LHC", *JINST* **3** (2008) S08004, `doi:10.1088/1748-0221/3/08/S08004`.

[36] CMS Collaboration, "Precision luminosity measurement in proton-proton collisions at $\sqrt{s} = 13$ TeV in 2015 and 2016 at CMS", *Eur. Phys. J. C* **81** (2021) 800, `doi:10.1140/epjc/s10052-021-09538-2`, `arXiv:2104.01927`.

[37] GEANT4 Collaboration, "GEANT4—a simulation toolkit", *Nucl. Instrum. Meth. A* **506** (2003) 250, `doi:10.1016/S0168-9002(03)01368-8`.

[38] T. Sjöstrand et al., "An introduction to PYTHIA 8.2", *Comput. Phys. Commun.* **191** (2015) 159, `doi:10.1016/j.cpc.2015.01.024`, `arXiv:1410.3012`.

[39] R. D. Ball et al., "Parton distributions with LHC data", *Nucl. Phys. B* **867** (2013) 244, `doi:10.1016/j.nuclphysb.2012.10.003`, `arXiv:1207.1303`.

[40] CMS Collaboration, "Event generator tunes obtained from underlying event and multiparton scattering measurements", *Eur. Phys. J. C* **76** (2016) 155, `doi:10.1140/epjc/s10052-016-3988-x`, `arXiv:1512.00815`.

[41] J. Alwall et al., "MADGRAPH 5: going beyond", *JHEP* **06** (2011) 128, `doi:10.1007/JHEP06(2011)128`, `arXiv:1106.0522`.

[42] J. Alwall et al., "The automated computation of tree-level and next-to-leading order differential cross sections, and their matching to parton shower simulations", *JHEP* **07** (2014) 079, `doi:10.1007/JHEP07(2014)079`, `arXiv:1405.0301`.

[43] M. Bahr et al., "HERWIG++ physics and manual", *Eur. Phys. J. C* **58** (2008) 639, `doi:10.1140/epjc/s10052-008-0798-9`, `arXiv:0803.0883`.

[44] J. Pumplin et al., "New generation of parton distributions with uncertainties from global QCD analysis", *JHEP* **07** (2002) 012, `doi:10.1088/1126-6708/2002/07/012`, `arXiv:hep-ph/0201195`.

[45] P. L. S. Connor and R. Žlebčík, "Step: a tool to perform tests of smoothness on differential distributions based on Chebyshev polynomials of the first kind", 2021. `arXiv:2111.09968`. Submitted to SciPost Physics.

[46] M. Oreglia, "A study of the reactions $\psi\prime \rightarrow \gamma\gamma J/\psi$". PhD thesis, Stanford University, 1980. SLAC Report SLAC-R-236.

[47] J. E. Gaiser, "Charmonium spectroscopy from radiative decays of the J/$\psi$ and $\psi\prime$". PhD thesis, Stanford University, 1983. SLAC Report SLAC-R-255.

[48] M. Cacciari and G. P. Salam, "Pileup subtraction using jet areas", *Phys. Lett. B* **659** (2008) 119, `doi:10.1016/j.physletb.2007.09.077`, `arXiv:0707.1378`.

[49] S. Schmitt, "TUNFOLD, an algorithm for correcting migration effects in high energy physics", *JINST* **7** (2012) T10003, `doi:10.1088/1748-0221/7/10/t10003`, `arXiv:1205.6201`.

[50] Z. Nagy, "Three jet cross-sections in hadron-hadron collisions at next-to-leading order", *Phys. Rev. Lett.* **88** (2002) 122003, `doi:10.1103/PhysRevLett.88.122003`, `arXiv:hep-ph/0110315`.

[51] Z. Nagy, "Next-to-leading order calculation of three jet observables in hadron-hadron collision", *Phys. Rev. D* **68** (2003) 094002, `doi:10.1103/PhysRevD.68.094002`, `arXiv:hep-ph/0307268`.

[52] T. Gehrmann et al., "Jet cross sections and transverse momentum distributions with NNLOJET", *PoS* **RADCOR2017** (2018) 074, `doi:10.22323/1.290.0074`, `arXiv:1801.06415`.

[53] fastNLO Collaboration, D. Britzger, K. Rabbertz, F. Stober, and M. Wobisch, "New features in version 2 of the FASTNLO project", in *20th International Workshop on Deep-Inelastic Scattering and Related Subjects*, p. 217. 2012. `arXiv:1208.3641`. `doi:10.3204/DESY-PROC-2012-02/165`.

[54] M. Cacciari et al., "Single-jet inclusive cross section and its definition", *Phys. Rev. D* **100** (2019) 114015, `doi:10.1103/PhysRevD.100.114015`, `arXiv:1906.11850`.

[55] M. Dasgupta, F. A. Dreyer, G. P. Salam, and G. Soyez, "Inclusive jet spectrum for small-radius jets", *JHEP* **06** (2016) 057, `doi:10.1007/JHEP06(2016)057`, `arXiv:1602.01110`.

[56] J. Bellm et al., "Jet cross sections at the LHC and the quest for higher precision", *Eur. Phys. J. C* **80** (2020) 93, `doi:10.1140/epjc/s10052-019-7574-x`, `arXiv:1903.12563`.

[57] S. Dulat et al., "New parton distribution functions from a global analysis of quantum chromodynamics", *Phys. Rev. D* **93** (2016) 033006, `doi:10.1103/PhysRevD.93.033006`, `arXiv:1506.07443`.

[58] NNPDF Collaboration, "Parton distributions from high-precision collider data", *Eur. Phys. J. C* **77** (2017) 663, `doi:10.1140/epjc/s10052-017-5199-5`, `arXiv:1706.00428`.

[59] L. A. Harland-Lang, A. D. Martin, P. Motylinski, and R. S. Thorne, "Parton distributions in the LHC era: MMHT 2014 PDFs", *Eur. Phys. J. C* **75** (2015) 204, `doi:10.1140/epjc/s10052-015-3397-6`, `arXiv:1412.3989`.

[60] S. Alekhin, J. Blümlein, S. Moch, and R. Placakyte, "Parton distribution functions, $\alpha_S$, and heavy-quark masses for LHC run II", *Phys. Rev. D* **96** (2017) 014011, `doi:10.1103/PhysRevD.96.014011`, `arXiv:1701.05838`.

[61] J. Gao et al., "MEKS: a program for computation of inclusive jet cross sections at hadron colliders", *Comput. Phys. Commun.* **184** (2013) 1626, `doi:10.1016/j.cpc.2013.01.022`, `arXiv:1207.0513`.

[62] S. Dittmaier, A. Huss, and C. Speckner, "Weak radiative corrections to dijet production at hadron colliders", *JHEP* **11** (2012) 095, `doi:10.1007/JHEP11(2012)095`, `arXiv:1210.0438`.

[63] J. M. Campbell and R. K. Ellis, "An update on vector boson pair production at hadron colliders", *Phys. Rev. D* **60** (1999) 113006, `doi:10.1103/PhysRevD.60.113006`, `arXiv:hep-ph/9905386`.

[64] J. M. Campbell, R. K. Ellis, and W. T. Giele, "A multi-threaded version of MCFM", *Eur. Phys. J. C* **75** (2015) 246, `doi:10.1140/epjc/s10052-015-3461-2`, `arXiv:1503.06182`.

[65] J. M. Campbell, R. K. Ellis, and C. Williams, "Vector boson pair production at the LHC", *JHEP* **07** (2011) 018, `doi:10.1007/JHEP07(2011)018`, `arXiv:1105.0020`.

[66] CMS Collaboration, "Extraction and validation of a new set of CMS PYTHIA 8 tunes from underlying-event measurements", *Eur. Phys. J. C* **80** (2020) 4, `doi:10.1140/epjc/s10052-019-7499-4`, `arXiv:1903.12179`.

[67] S. Alekhin et al., "HERAFitter, open source QCD fit project", *Eur. Phys. J. C* **75** (2015) 304, `doi:10.1140/epjc/s10052-015-3480-z`, `arXiv:1410.4412`.

[68] V. Bertone, M. Botje, D. Britzger et al., "xFITTER 2.0.0: An open source QCD fit framework", *PoS* **DIS2017** (2018) 203, `doi:10.22323/1.297.0203`, `arXiv:1709.01151`.

[69] xFitter Developers' Team. `https://www.xfitter.org/xFitter/`.

[70] V. N. Gribov and L. N. Lipatov, "Deep inelastic ep scattering in perturbation theory", *Sov. J. Nucl. Phys.* **15** (1972) 438.

[71] G. Altarelli and G. Parisi, "Asymptotic freedom in parton language", *Nucl. Phys. B* **126** (1977) 298, `doi:10.1016/0550-3213(77)90384-4`.

[72] G. Curci, W. Furmanski, and R. Petronzio, "Evolution of parton densities beyond leading order: The non-singlet case", *Nucl. Phys. B* **175** (1980) 27, `doi:10.1016/0550-3213(80)90003-6`.

[73] W. Furmanski and R. Petronzio, "Singlet parton densities beyond leading order", *Phys. Lett. B* **97** (1980) 437, `doi:10.1016/0370-2693(80)90636-X`.

[74] S. Moch, J. A. M. Vermaseren, and A. Vogt, "The three-loop splitting functions in QCD: The nonsinglet case", *Nucl. Phys. B* **688** (2004) 101, `doi:10.1016/j.nuclphysb.2004.03.030`, `arXiv:hep-ph/0403192`.

[75] A. Vogt, S. Moch, and J. A. M. Vermaseren, "The three-loop splitting functions in QCD: The singlet case", *Nucl. Phys. B* **691** (2004) 129, `doi:10.1016/j.nuclphysb.2004.04.024`, `arXiv:hep-ph/0404111`.

[76] M. Botje, "QCDNUM: Fast QCD evolution and convolution", *Comput. Phys. Commun.* **182** (2011) 490, `doi:10.1016/j.cpc.2010.10.020`, `arXiv:1005.1481`.

[77] E. Eichten, K. D. Lane, and M. E. Peskin, "New tests for quark and lepton substructure", *Phys. Rev. Lett.* **50** (1983) 811, `doi:10.1103/PhysRevLett.50.811`.

[78] P. Langacker, "The physics of heavy Z′ gauge bosons", *Rev. Mod. Phys.* **81** (2009) 1199, `doi:10.1103/RevModPhys.81.1199`, `arXiv:0801.1345`.

[79] H1 and ZEUS Collaborations, "Combined measurement and QCD analysis of the inclusive e$^{\pm}$p scattering cross sections at HERA", *JHEP* **01** (2010) 109, `doi:10.1007/JHEP01(2010)109`, `arXiv:0911.0884`.

[80] R. S. Thorne and R. G. Roberts, "An ordered analysis of heavy flavor production in deep inelastic scattering", *Phys. Rev. D* **57** (1998) 6871, `doi:10.1103/PhysRevD.57.6871`, `arXiv:hep-ph/9709442`.

[81] R. S. Thorne, "A variable-flavor number scheme for NNLO", *Phys. Rev. D* **73** (2006) 054019, `doi:10.1103/PhysRevD.73.054019`, `arXiv:hep-ph/0601245`.

[82] R. S. Thorne, "Effect of changes of variable flavor number scheme on parton distribution functions and predicted cross sections", *Phys. Rev. D* **86** (2012) 074017, `doi:10.1103/PhysRevD.86.074017`, `arXiv:1201.6180`.

[83] J. Pumplin et al., "Uncertainties of predictions from parton distribution functions. II. The Hessian method", *Phys. Rev. D* **65** (2001) 014013, `doi:10.1103/PhysRevD.65.014013`, `arXiv:hep-ph/0101032`.

[84] W. T. Giele and S. Keller, "Implications of hadron collider observables on parton distribution function uncertainties", *Phys. Rev. D* **58** (1998) 094023, `doi:10.1103/PhysRevD.58.094023`, `arXiv:hep-ph/9803393`.

[85] W. T. Giele, S. A. Keller, and D. A. Kosower, "Parton distribution function uncertainties", 2001. `arXiv:hep-ph/0104052`.

[86] H. Paukkunen and P. Zurita, "PDF reweighting in the Hessian matrix approach", *JHEP* **12** (2014) 100, `doi:10.1007/JHEP12(2014)100`, `arXiv:1402.6623`.

[87] C. Schmidt, J. Pumplin, C. P. Yuan, and P. Yuan, "Updating and optimizing error parton distribution function sets in the Hessian approach", *Phys. Rev. D* **98** (2018) 094005, `doi:10.1103/PhysRevD.98.094005`, `arXiv:1806.07950`.

[88] HERAFitter developers' Team, "QCD analysis of W- and Z-boson production at Tevatron", *Eur. Phys. J. C* **75** (2015) 458, `doi:10.1140/ec/s10052-015-3655-7`, `arXiv:1503.05221`.

[89] R. Abdul Khalek et al., "Towards ultimate parton distributions at the high-luminosity LHC", *Eur. Phys. J. C* **78** (2018) 962, `doi:10.1140/epjc/s10052-018-6448-y`, `arXiv:1810.03639`.

[90] Particle Data Group, P. A. Zyla et al., "Review of particle physics", *Prog. Theor. Exp. Phys.* **2020** (2020) 083C01, `doi:10.1093/ptep/ptaa104`.

[91] H1 Collaboration, "Determination of the strong coupling constant $\alpha_S(m_Z)$ in next-to-next-to-leading order QCD using H1 jet cross section measurements", *Eur. Phys. J. C* **77** (2017) 791, `doi:10.1140/epjc/s10052-017-5314-7`, `arXiv:1709.07251`.

[92] CMS Collaboration, "Measurement of the $t\bar{t}$ production cross section, the top quark mass, and the strong coupling constant using dilepton events in pp collisions at $\sqrt{s} = 13\,\text{TeV}$", *Eur. Phys. J. C* **79** (2019) 368, `doi:10.1140/epjc/s10052-019-6863-8`, `arXiv:1812.10505`.

[93] ATLAS Collaboration, "Search for new phenomena in dijet events using 37 fb$^{-1}$ of pp collision data collected at $\sqrt{s} = 13\,\text{TeV}$ with the ATLAS detector", *Phys. Rev. D* **96** (2017) 052004, `doi:10.1103/PhysRevD.96.052004`, `arXiv:1703.09127`.

[94] HEPData record for this analysis, 2021. `doi:10.17182/hepdata.115022`.

[95] D. Britzger et al., "NNLO interpolation grids for jet production at the LHC", 2022. `arXiv:2207.13735`.

[96] X. Chen et al., "NNLO QCD corrections in full colour for jet production observables at the LHC", *JHEP* **09** (2022) 025, `doi:10.1007/JHEP09(2022)025`, `arXiv:2204.10173`.

# A   Supplemental material: comparison to NLO
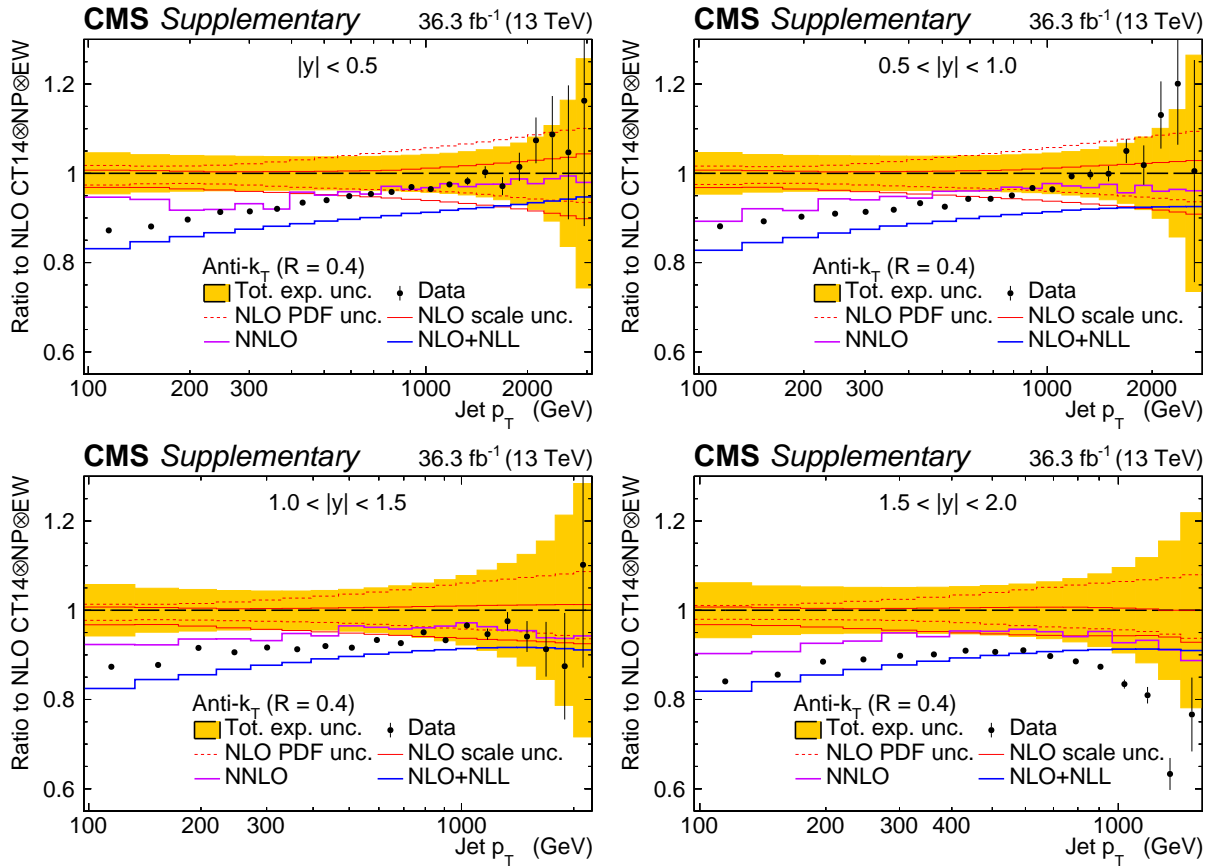


Figure A.1: Cross sections of inclusive jet production for distance parameter $R = 0.4$ as a function of transverse momentum of the individual jet in bins of absolute rapidity $|y|$, compared to the theoretical predictions at NLO, NLO+NLL, and NNLO. All results are normalised to the prediction at NLO. The measurement (solid symbols) is presented with the statistical uncertainties (vertical error bars), while the systematic uncertainty is represented by a yellow filled band, centered at 1. The NLO (black dashed line) and NLO+NLL (blue solid line) predictions are obtained using CT14nlo PDF. The PDF (dotted red line) and scale (solid red line) uncertainties are shown for the NLO prediction. The NNLO calculation (purple solid line) is obtained using CT14nnlo PDF.
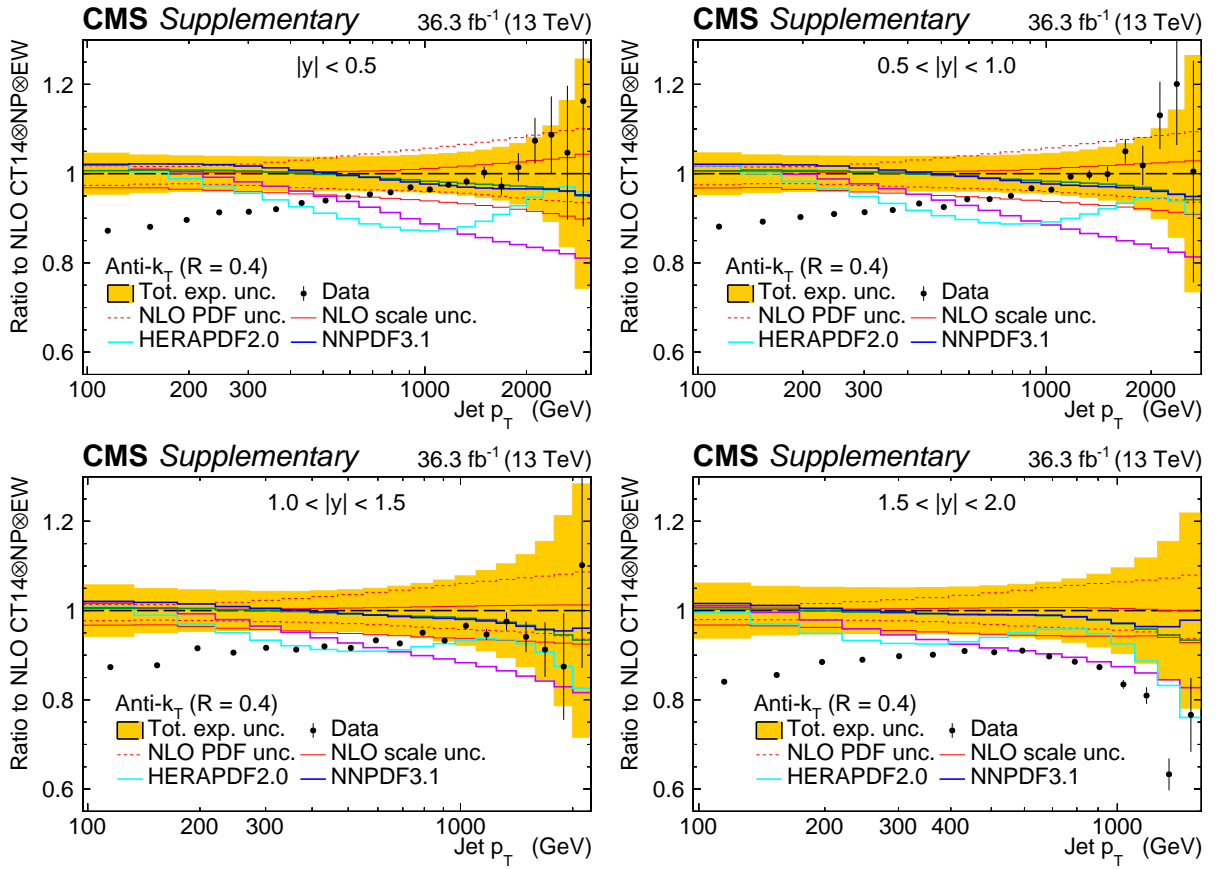
Figure A.2: Cross sections of inclusive jet production for distance parameter $R = 0.4$ as a function of transverse momentum of the individual jet in bins of absolute rapidity $|y|$, compared to the theoretical predictions at NLO using different PDFs (lines of different colors). All results are normalised to the prediction at NLO obtained using CT14nlo PDF (black dashed line). The measurement (solid symbols) is presented with the statistical uncertainties (vertical error bars), while the systematic uncertainty is represented by a yellow filled band, centered at 1.
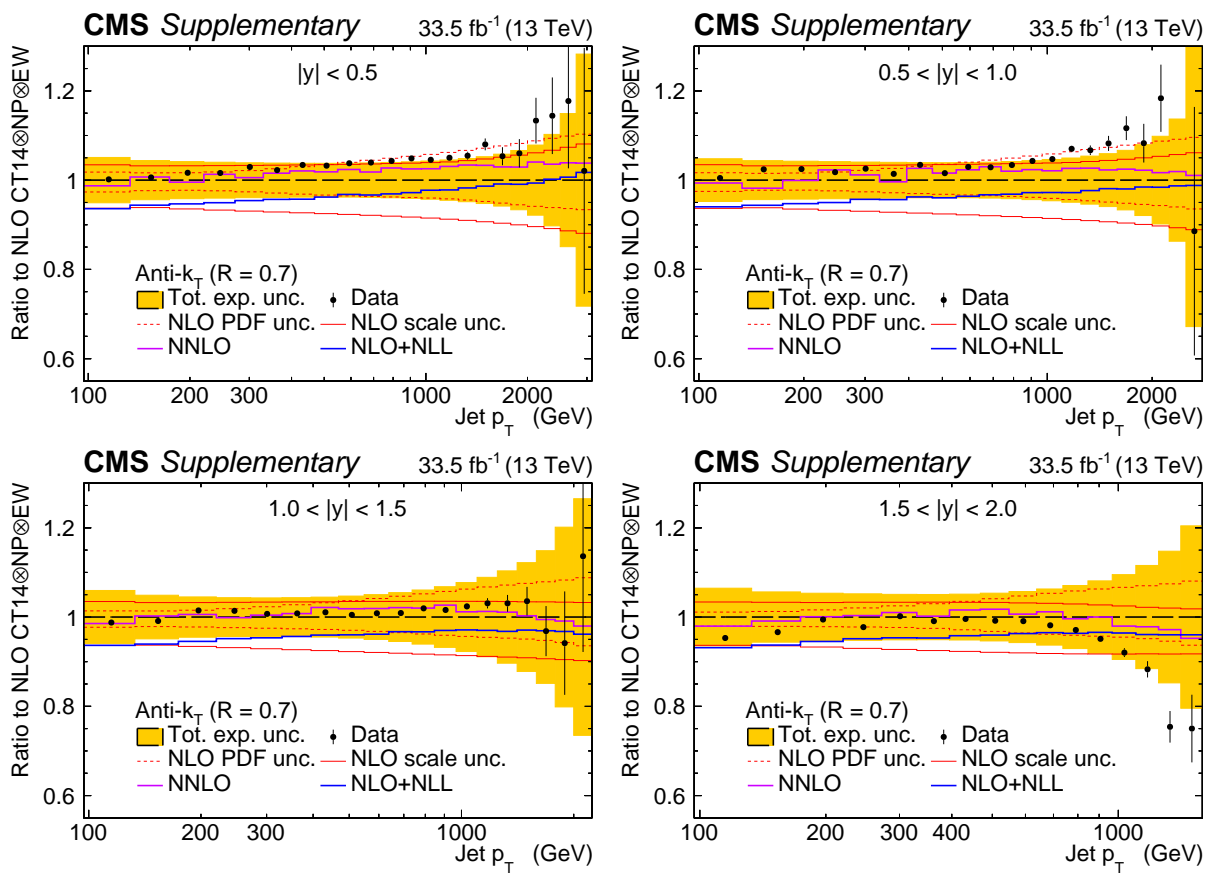
Figure A.3: Same as Fig. A.1 for the distance parameter $R = 0.7$.
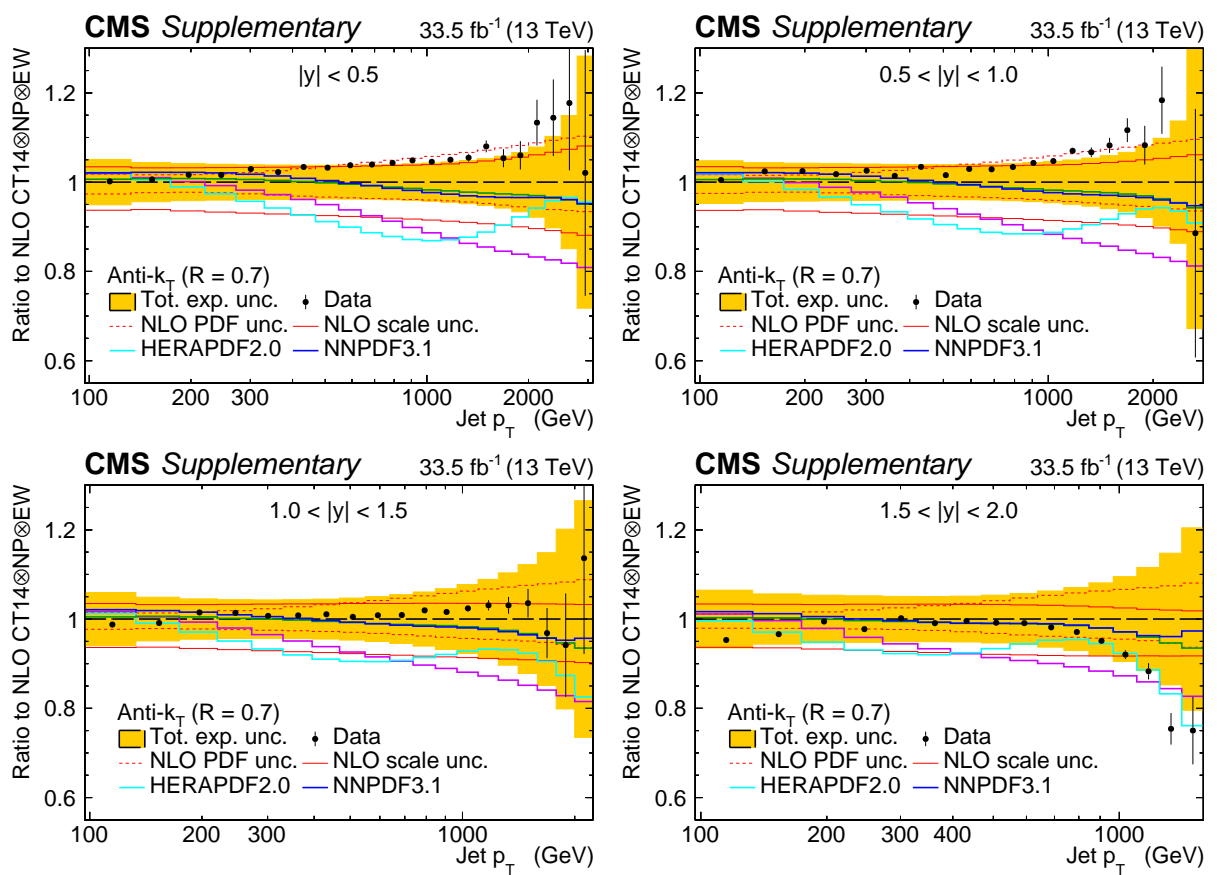
Figure A.4: Same as Fig. A.2 for the distance parameter $R = 0.7$.

# B Addendum: QCD analysis at NNLO using NNLO interpolation grids

The QCD analysis at NNLO is repeated by using the NNLO interpolation grids for the double-differential inclusive jet cross section [95], which were released after the journal publication of the original analysis. The NNLOJET calculation used to derive these grids is based on the leading-colour and leading-flavour-number approximation and does not include the most recent subleading colour contributions. However, these contributions were reported in Ref. [96] to be very small in inclusive jet production, in particular for a jet size of $R = 0.7$. The grids also contain an estimate of the numerical integration uncertainty of around 1% or less. To account for point-to-point fluctuations, this uncertainty, after consultation with the authors of NNLO-JET, has been increased by a factor of two; however, its impact in the fit is negligible. A comparison of the measurement with predictions using various PDFs is shown in Fig. B.1. Although the PDF parametrisation remains identical, higher precision in PDF and QCD parameters is expected by using NNLO grids consistently in the QCD analysis. These new results supersede those obtained by using the $k$-factor technique.
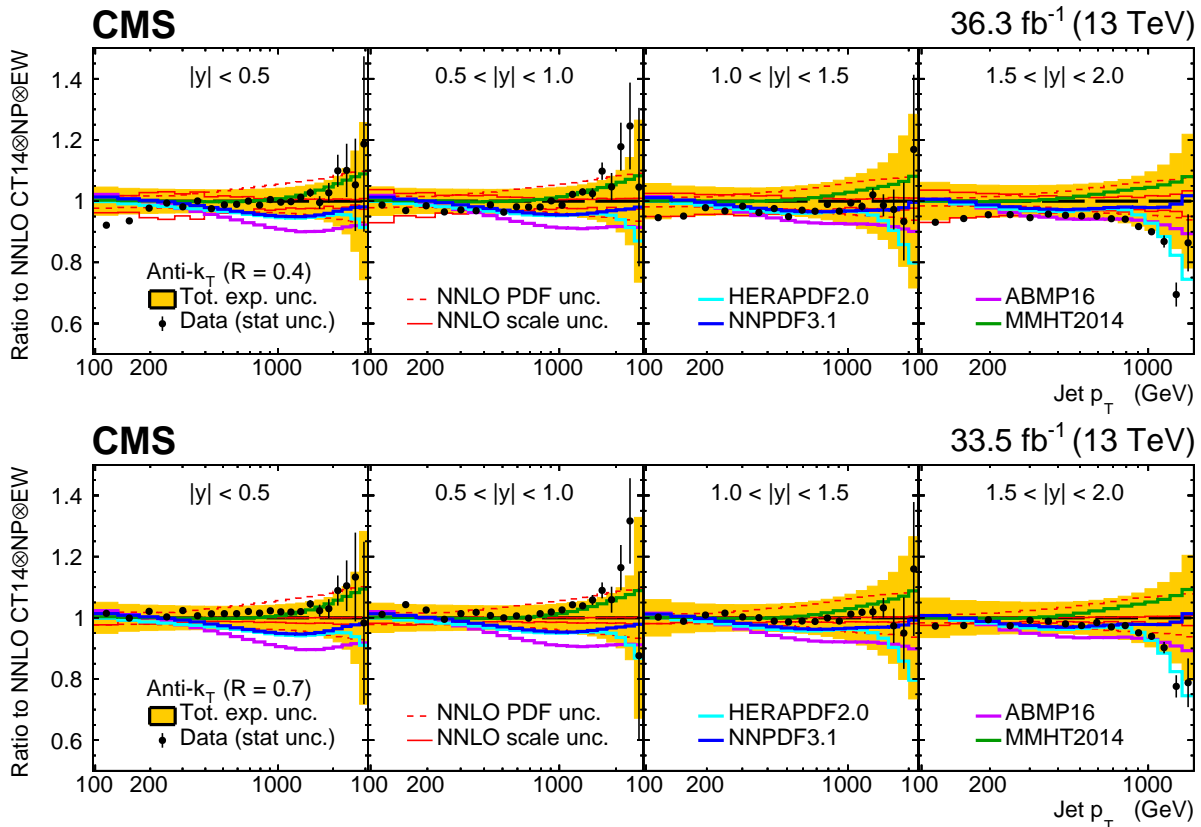


Figure B.1: The double-differential cross section of inclusive jet production, as a function of $p_T$ and $|y|$, for jets clustered using the anti-$k_T$ algorithm with $R = 0.4$ (upper panel) and $R = 0.7$ (lower panel), presented as ratios to the QCD predictions. The data points are shown by filled circles, with statistical uncertainties shown by vertical error bars, while the total experimental uncertainty is centred at one and is presented by the orange band. The data are divided by the NNLO prediction corrected for NP and EW effects, using CT14nnlo PDF and choosing jet $p_T$ as renormalisation and factorisation scale. NNLO predictions obtained with alternative PDF sets are displayed in different colours as a ratio to the central prediction using CT14nnlo.

The PDFs from the QCD analysis at NNLO of the CMS inclusive jet production and HERA

DIS cross sections are shown in Fig. B.2, illustrating the contributions of the fit, model, and parametrisation uncertainties.
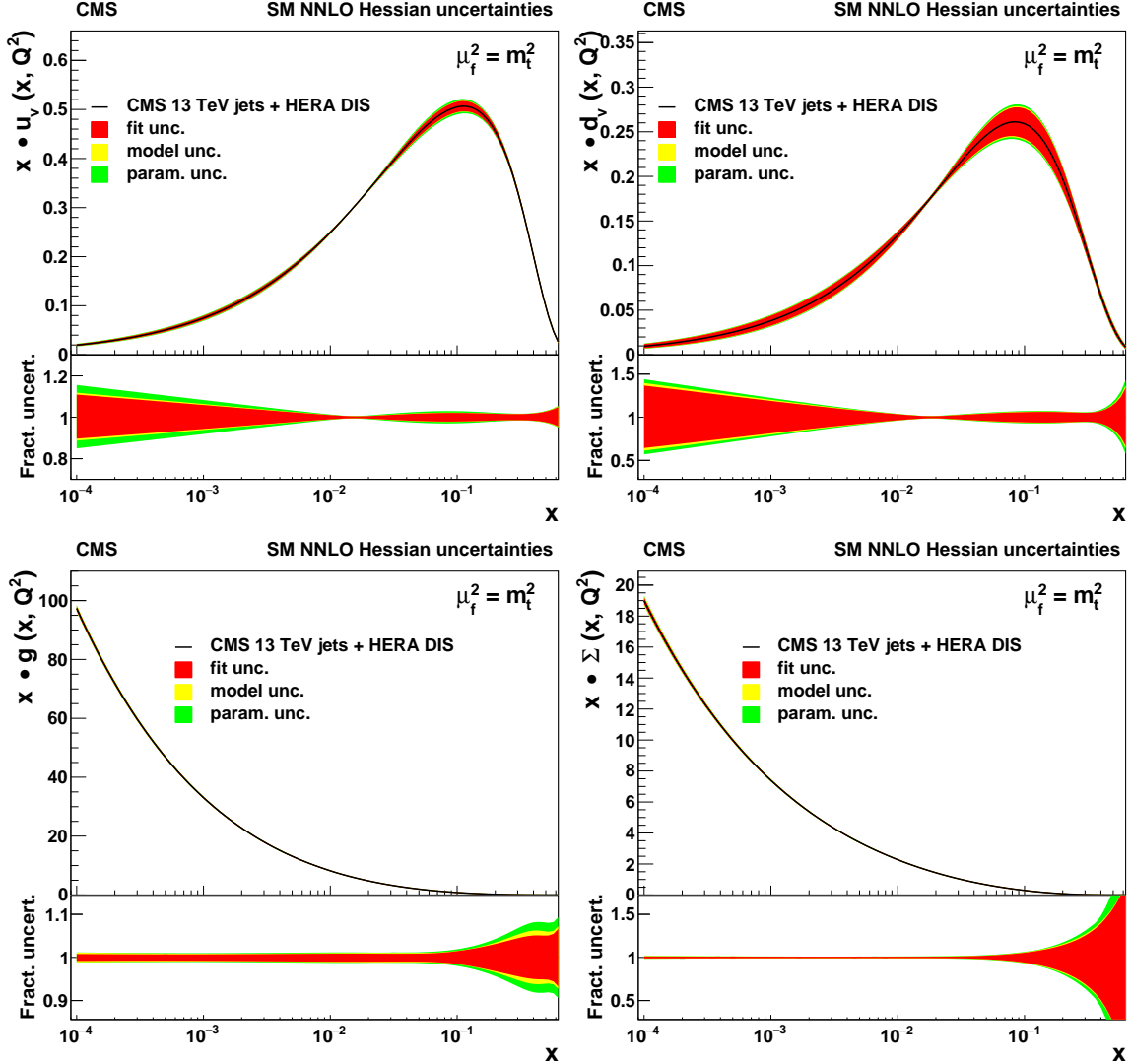


Figure B.2: The u-valence (upper left), d-valence (upper right), gluon (lower left), and sea quark (lower right) distributions shown as a function of $x$ at the scale $\mu_f = m_t$, resulting from the NNLO fit using HERA DIS data together with the CMS inclusive jet cross section at $\sqrt{s} = 13$ TeV. The prediction for the inclusive jet cross section is obtained using NNLO interpolation grids. Contributions of the fit, model, and parametrisation uncertainties for each PDF are shown. In the lower panels, the relative uncertainty contributions are presented.

The value of the strong coupling constant $\alpha_S(m_Z)$ is extracted simultaneously with the PDFs and corresponds to $\alpha_S(m_Z) = 0.1166 \pm 0.0014\,\text{(fit)} \pm 0.0007\,\text{(model)} \pm 0.0004\,\text{(scale)} \pm 0.0001\,\text{(param.)}$, showing improved precision with respect to the NNLO result obtained using the $k$-factor technique. The global and partial $\chi^2$ values for each data set in the NNLO fits using the interpolation grids are listed in Table B.1, where the $\chi^2$ values illustrate a general agreement among all the data sets.

The impact of the CMS jet data in the QCD analysis (HERA+CMS fit) at NNLO is illustrated in Fig. B.3, where the result is compared with the alternative fit using only the HERA DIS data (HERA-only fit).

Table B.1: Partial $\chi^2$ per number of data points, $N_{\text{dp}}$, and the global $\chi^2$ per degree of freedom, $N_{\text{dof}}$, as obtained in the QCD analysis at NNLO of HERA+CMS jet data, using NNLO interpolation grids for the 13 TeV inclusive jet cross section. In the DIS data, the proton beam energy is given as $E_{\text{p}}$ and the electron energy is 27.5 GeV.

| Data sets | | HERA+CMS Partial $\chi^2/N_{\text{dp}}$ |
|---|---|---|
| HERA I+II neutral current | $e^+p$, $E_{\text{p}} = 920\,\text{GeV}$ | 376/332 |
| HERA I+II neutral current | $e^+p$, $E_{\text{p}} = 820\,\text{GeV}$ | 60/63 |
| HERA I+II neutral current | $e^+p$, $E_{\text{p}} = 575\,\text{GeV}$ | 202/234 |
| HERA I+II neutral current | $e^+p$, $E_{\text{p}} = 460\,\text{GeV}$ | 209/187 |
| HERA I+II neutral current | $e^-p$, $E_{\text{p}} = 920\,\text{GeV}$ | 227/159 |
| HERA I+II charged current | $e^+p$, $E_{\text{p}} = 920\,\text{GeV}$ | 46/39 |
| HERA I+II charged current | $e^-p$, $E_{\text{p}} = 920\,\text{GeV}$ | 56/42 |
| CMS inclusive jets 13 TeV | $0.0 < |y| < 0.5$ | 8.6/22 |
| | $0.5 < |y| < 1.0$ | 23/21 |
| | $1.0 < |y| < 1.5$ | 13/19 |
| | $1.5 < |y| < 2.0$ | 14/16 |
| Correlated $\chi^2$ | | 81 |
| Global $\chi^2/N_{\text{dof}}$ | | 1302/1118 |
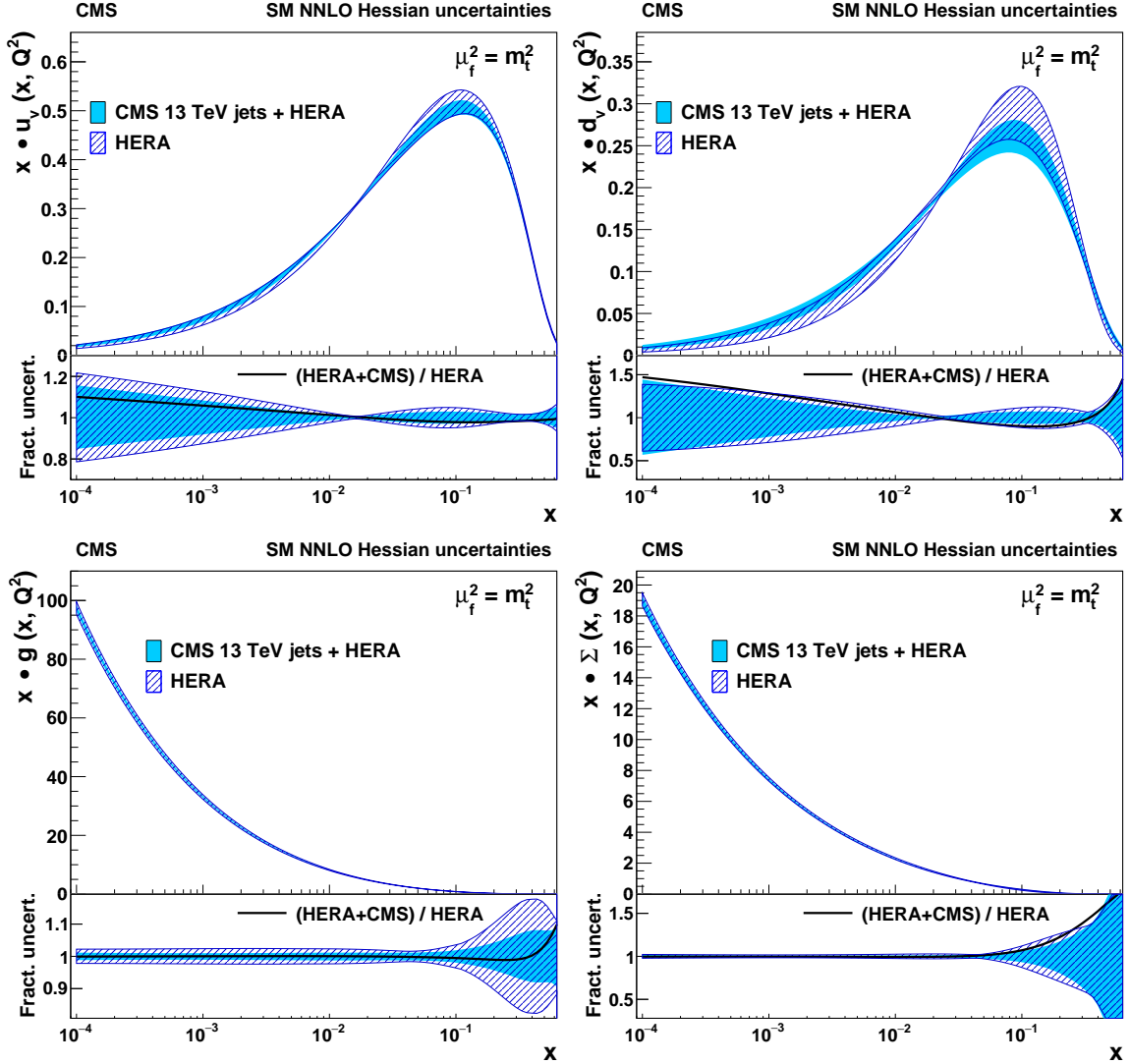
Figure B.3: The u-valence (upper left), d-valence (upper right), gluon (lower left), and sea quark (lower right) distributions shown as a function of $x$ at the scale $\mu_f = m_t$. The filled (hatched) band represents the results of the NNLO fit using HERA DIS and the CMS inclusive jet cross section at $\sqrt{s} = 13\,\text{TeV}$ (using the HERA DIS data only). The PDFs are shown with their total uncertainty. The prediction for the inclusive jet cross section is obtained using NNLO interpolation grids. In the lower panels, the comparison of the relative PDF uncertainties is shown for each distribution. The line corresponds to the ratio of the central PDF values of the two variants of the fit.

# C   The CMS Collaboration

**Yerevan Physics Institute, Yerevan, Armenia**
A. Tumasyan

**Institut für Hochenergiephysik, Vienna, Austria**
W. Adam, J.W. Andrejkovic, T. Bergauer, S. Chatterjee, K. Damanakis, M. Dragicevic, A. Escalante Del Valle, R. Frühwirth[1], M. Jeitler[1], N. Krammer, L. Lechner, D. Liko, I. Mikulec, P. Paulitsch, F.M. Pitters, J. Schieck[1], R. Schöfbeck, D. Schwarz, S. Templ, W. Waltenberger, C.-E. Wulz[1]

**Institute for Nuclear Problems, Minsk, Belarus**
V. Chekhovsky, A. Litomin, V. Makarenko

**Universiteit Antwerpen, Antwerpen, Belgium**
M.R. Darwish[2], E.A. De Wolf, T. Janssen, T. Kello[3], A. Lelek, H. Rejeb Sfar, P. Van Mechelen, S. Van Putte, N. Van Remortel

**Vrije Universiteit Brussel, Brussel, Belgium**
F. Blekman, E.S. Bols, J. D'Hondt, M. Delcourt, H. El Faham, S. Lowette, S. Moortgat, A. Morton, D. Müller, A.R. Sahasransu, S. Tavernier, W. Van Doninck

**Université Libre de Bruxelles, Bruxelles, Belgium**
D. Beghin, B. Bilin, B. Clerbaux, G. De Lentdecker, L. Favart, A. Grebenyuk, A.K. Kalsi, K. Lee, M. Mahdavikhorrami, I. Makarenko, L. Moureaux, L. Pétré, A. Popov, N. Postiau, E. Starling, L. Thomas, M. Vanden Bemden, C. Vander Velde, P. Vanlaer

**Ghent University, Ghent, Belgium**
T. Cornelis, D. Dobur, J. Knolle, L. Lambrecht, G. Mestdach, M. Niedziela, C. Roskas, A. Samalan, K. Skovpen, M. Tytgat, B. Vermassen, L. Wezenbeek

**Université Catholique de Louvain, Louvain-la-Neuve, Belgium**
A. Benecke, A. Bethani, G. Bruno, F. Bury, C. Caputo, P. David, C. Delaere, I.S. Donertas, A. Giammanco, K. Jaffel, Sa. Jain, V. Lemaitre, K. Mondal, J. Prisciandaro, A. Taliercio, M. Teklishyn, T.T. Tran, P. Vischia, S. Wertz

**Centro Brasileiro de Pesquisas Fisicas, Rio de Janeiro, Brazil**
G.A. Alves, C. Hensel, A. Moraes

**Universidade do Estado do Rio de Janeiro, Rio de Janeiro, Brazil**
W.L. Aldá Júnior, M. Alves Gallo Pereira, M. Barroso Ferreira Filho, H. Brandao Malbouisson, W. Carvalho, J. Chinellato[4], E.M. Da Costa, G.G. Da Silveira[5], D. De Jesus Damiao, S. Fonseca De Souza, C. Mora Herrera, K. Mota Amarilo, L. Mundim, H. Nogima, P. Rebello Teles, A. Santoro, S.M. Silva Do Amaral, A. Sznajder, M. Thiel, F. Torres Da Silva De Araujo[6], A. Vilela Pereira

**Universidade Estadual Paulista (a), Universidade Federal do ABC (b), São Paulo, Brazil**
C.A. Bernardes[5], L. Calligaris, T.R. Fernandez Perez Tomei, E.M. Gregores, D.S. Lemos, P.G. Mercadante, S.F. Novaes, Sandra S. Padula

**Institute for Nuclear Research and Nuclear Energy, Bulgarian Academy of Sciences, Sofia, Bulgaria**
A. Aleksandrov, G. Antchev, R. Hadjiiska, P. Iaydjiev, M. Misheva, M. Rodozov, M. Shopova, G. Sultanov

**University of Sofia, Sofia, Bulgaria**
A. Dimitrov, T. Ivanov, L. Litov (iD), B. Pavlov, P. Petkov, A. Petrov

**Beihang University, Beijing, China**
T. Cheng (iD), T. Javaid[7], M. Mittal, L. Yuan

**Department of Physics, Tsinghua University, Beijing, China**
M. Ahmad (iD), G. Bauer, C. Dozen[8] (iD), Z. Hu (iD), J. Martins[9] (iD), Y. Wang, K. Yi[10,11]

**Institute of High Energy Physics, Beijing, China**
E. Chapon (iD), G.M. Chen[7] (iD), H.S. Chen[7] (iD), M. Chen (iD), F. Iemmi, A. Kapoor (iD), D. Leggat, H. Liao, Z.-A. Liu[7] (iD), V. Milosevic (iD), F. Monti (iD), R. Sharma (iD), J. Tao (iD), J. Thomas-Wilsker, J. Wang (iD), H. Zhang (iD), J. Zhao (iD)

**State Key Laboratory of Nuclear Physics and Technology, Peking University, Beijing, China**
A. Agapitos, Y. An, Y. Ban, C. Chen, A. Levin (iD), Q. Li (iD), X. Lyu, Y. Mao, S.J. Qian, D. Wang (iD), Q. Wang (iD), J. Xiao

**Sun Yat-Sen University, Guangzhou, China**
M. Lu, Z. You (iD)

**Institute of Modern Physics and Key Laboratory of Nuclear Physics and Ion-beam Application (MOE) - Fudan University, Shanghai, China**
X. Gao[3], H. Okawa (iD), Y. Zhang (iD)

**Zhejiang University, Hangzhou, China, Zhejiang, China**
Z. Lin (iD), M. Xiao (iD)

**Universidad de Los Andes, Bogota, Colombia**
C. Avila (iD), A. Cabrera (iD), C. Florez (iD), J. Fraga

**Universidad de Antioquia, Medellin, Colombia**
J. Mejia Guisao, F. Ramirez, J.D. Ruiz Alvarez (iD), C.A. Salazar González (iD)

**University of Split, Faculty of Electrical Engineering, Mechanical Engineering and Naval Architecture, Split, Croatia**
D. Giljanovic, N. Godinovic (iD), D. Lelas (iD), I. Puljak (iD)

**University of Split, Faculty of Science, Split, Croatia**
Z. Antunovic, M. Kovac, T. Sculac (iD)

**Institute Rudjer Boskovic, Zagreb, Croatia**
V. Brigljevic (iD), D. Ferencek (iD), D. Majumder (iD), M. Roguljic, A. Starodumov[12] (iD), T. Susa (iD)

**University of Cyprus, Nicosia, Cyprus**
A. Attikis (iD), K. Christoforou, E. Erodotou, A. Ioannou, G. Kole (iD), M. Kolosova, S. Konstantinou, J. Mousa (iD), C. Nicolaou, F. Ptochos (iD), P.A. Razis, H. Rykaczewski, H. Saka (iD)

**Charles University, Prague, Czech Republic**
M. Finger[13], M. Finger Jr.[13] (iD), A. Kveton

**Escuela Politecnica Nacional, Quito, Ecuador**
E. Ayala

**Universidad San Francisco de Quito, Quito, Ecuador**
E. Carrera Jarrin (iD)

**Academy of Scientific Research and Technology of the Arab Republic of Egypt, Egyp-**

**tian Network of High Energy Physics, Cairo, Egypt**
Y. Assran[14,15], A. Ellithi Kamel[16]

**Center for High Energy Physics (CHEP-FU), Fayoum University, El-Fayoum, Egypt**
M.A. Mahmoud, Y. Mohammed

**National Institute of Chemical Physics and Biophysics, Tallinn, Estonia**
S. Bhowmik, R.K. Dewanjee, K. Ehataht, M. Kadastik, S. Nandan, C. Nielsen, J. Pata, M. Raidal, L. Tani, C. Veelken

**Department of Physics, University of Helsinki, Helsinki, Finland**
P. Eerola, L. Forthomme, H. Kirschenmann, K. Osterberg, M. Voutilainen

**Helsinki Institute of Physics, Helsinki, Finland**
S. Bharthuar, E. Brücken, F. Garcia, J. Havukainen, M.S. Kim, R. Kinnunen, T. Lampén, K. Lassila-Perini, S. Lehti, T. Lindén, M. Lotti, L. Martikainen, M. Myllymäki, J. Ott, H. Siikonen, E. Tuominen, J. Tuominiemi

**Lappeenranta University of Technology, Lappeenranta, Finland**
P. Luukka, H. Petrow, T. Tuuva

**IRFU, CEA, Université Paris-Saclay, Gif-sur-Yvette, France**
C. Amendola, M. Besancon, F. Couderc, M. Dejardin, D. Denegri, J.L. Faure, F. Ferri, S. Ganjour, P. Gras, G. Hamel de Monchenault, P. Jarry, B. Lenzi, E. Locci, J. Malcles, J. Rander, A. Rosowsky, M.Ö. Sahin, A. Savoy-Navarro[17], M. Titov, G.B. Yu

**Laboratoire Leprince-Ringuet, CNRS/IN2P3, Ecole Polytechnique, Institut Polytechnique de Paris, Palaiseau, France**
S. Ahuja, F. Beaudette, M. Bonanomi, A. Buchot Perraguin, P. Busson, A. Cappati, C. Charlot, O. Davignon, B. Diab, G. Falmagne, S. Ghosh, R. Granier de Cassagnac, A. Hakimi, I. Kucher, J. Motta, M. Nguyen, C. Ochando, P. Paganini, J. Rembser, R. Salerno, U. Sarkar, J.B. Sauvan, Y. Sirois, A. Tarabini, A. Zabi, A. Zghiche

**Université de Strasbourg, CNRS, IPHC UMR 7178, Strasbourg, France**
J.-L. Agram[18], J. Andrea, D. Apparu, D. Bloch, G. Bourgatte, J.-M. Brom, E.C. Chabert, C. Collard, D. Darej, J.-C. Fontaine[18], U. Goerlach, C. Grimault, A.-C. Le Bihan, E. Nibigira, P. Van Hove

**Institut de Physique des 2 Infinis de Lyon (IP2I ), Villeurbanne, France**
E. Asilar, S. Beauceron, C. Bernet, G. Boudoul, C. Camen, A. Carle, N. Chanon, D. Contardo, P. Depasse, H. El Mamouni, J. Fay, S. Gascon, M. Gouzevitch, B. Ille, I.B. Laktineh, H. Lattaud, A. Lesauvage, M. Lethuillier, L. Mirabito, S. Perries, K. Shchablo, V. Sordini, L. Torterotot, G. Touquet, M. Vander Donckt, S. Viret

**Georgian Technical University, Tbilisi, Georgia**
I. Lomidze, T. Toriashvili[19], Z. Tsamalaidze[13]

**RWTH Aachen University, I. Physikalisches Institut, Aachen, Germany**
V. Botta, L. Feld, K. Klein, M. Lipinski, D. Meuser, A. Pauls, N. Röwert, J. Schulz, M. Teroerde

**RWTH Aachen University, III. Physikalisches Institut A, Aachen, Germany**
A. Dodonova, D. Eliseev, M. Erdmann, P. Fackeldey, B. Fischer, S. Ghosh, T. Hebbeker, K. Hoepfner, F. Ivone, L. Mastrolorenzo, M. Merschmeyer, A. Meyer, G. Mocellin, S. Mondal, S. Mukherjee, D. Noll, A. Novak, T. Pook, A. Pozdnyakov,

Y. Rath, H. Reithler, J. Roemer, A. Schmidt (iD), S.C. Schuler, A. Sharma (iD), L. Vigilante, S. Wiedenbeck, S. Zaleski

**RWTH Aachen University, III. Physikalisches Institut B, Aachen, Germany**
C. Dziwok, G. Flügge, W. Haj Ahmad[20] (iD), O. Hlushchenko, T. Kress, A. Nowack (iD), C. Pistone, O. Pooth, D. Roy (iD), H. Sert (iD), A. Stahl[21] (iD), T. Ziemons (iD), A. Zotz

**Deutsches Elektronen-Synchrotron, Hamburg, Germany**
H. Aarup Petersen, M. Aldaya Martin, P. Asmuss, S. Baxter, M. Bayatmakou, O. Behnke, A. Bermúdez Martínez, S. Bhattacharya, A.A. Bin Anuar (iD), K. Borras[22], D. Brunner, A. Campbell (iD), A. Cardini (iD), C. Cheng, F. Colombina, S. Consuegra Rodríguez (iD), G. Correia Silva, V. Danilov, M. De Silva, L. Didukh, G. Eckerlin, D. Eckstein, E. Eren, L.I. Estevez Banos (iD), O. Filatov (iD), E. Gallo[23], J. Gao, A. Geiser, A. Giraldi, A. Grohsjean (iD), M. Guthoff, A. Jafari[24] (iD), N.Z. Jomhari (iD), H. Jung (iD), A. Kasem[22] (iD), M. Kasemann (iD), H. Kaveh (iD), C. Kleinwort (iD), D. Krücker (iD), W. Lange, J. Lidrych (iD), K. Lipka, W. Lohmann[25], T. Mäkelä, R. Mankel, I.-A. Melzer-Pellmann (iD), M. Mendizabal Morentin, J. Metwally, A.B. Meyer (iD), M. Meyer (iD), J. Mnich (iD), A. Mussgiller, Y. Otarid, D. Pérez Adán (iD), D. Pitzl, A. Raspereza, B. Ribeiro Lopes, J. Rübenach, A. Saggio (iD), A. Saibel (iD), M. Savitskyi (iD), M. Scham[26], V. Scheurer, S. Schnake, P. Schütze, C. Schwanenberger[23] (iD), M. Shchedrolosiev, R.E. Sosa Ricardo (iD), D. Stafford, N. Tonon (iD), M. Van De Klundert (iD), R. Walsh, D. Walter, Y. Wen (iD), K. Wichmann, L. Wiens, C. Wissing, S. Wuchterl (iD), R. Zlebcik (iD)

**University of Hamburg, Hamburg, Germany**
R. Aggleton, S. Albrecht (iD), S. Bein (iD), L. Benato (iD), P. Connor (iD), K. De Leo (iD), M. Eich, F. Feindt, A. Fröhlich, C. Garbers (iD), E. Garutti (iD), P. Gunnellini, M. Hajheidari, J. Haller (iD), A. Hinzmann (iD), G. Kasieczka, R. Klanner (iD), R. Kogler (iD), T. Kramer, V. Kutzner, J. Lange (iD), T. Lange (iD), A. Lobanov (iD), A. Malara (iD), A. Nigamova, K.J. Pena Rodriguez, O. Rieger, P. Schleper, M. Schröder (iD), J. Schwandt (iD), J. Sonneveld (iD), H. Stadie, G. Steinbrück, A. Tews, I. Zoi (iD)

**Karlsruher Institut fuer Technologie, Karlsruhe, Germany**
J. Bechtel (iD), S. Brommer, M. Burkart, E. Butz (iD), R. Caspart (iD), T. Chwalek, W. De Boer[+], A. Dierlamm, A. Droll, K. El Morabit, N. Faltermann (iD), M. Giffels, J.o. Gosewisch, A. Gottmann, F. Hartmann[21] (iD), C. Heidecker, U. Husemann (iD), P. Keicher, R. Koppenhöfer, S. Maier, M. Metzler, S. Mitra (iD), Th. Müller, M. Neukum, A. Nürnberg, G. Quast (iD), K. Rabbertz (iD), J. Rauser, D. Savoiu (iD), M. Schnepf, D. Seith, I. Shvetsov, H.J. Simonis, R. Ulrich (iD), J. Van Der Linden, R.F. Von Cube, M. Wassmer, M. Weber (iD), S. Wieland, R. Wolf (iD), S. Wozniewski, S. Wunsch

**Institute of Nuclear and Particle Physics (INPP), NCSR Demokritos, Aghia Paraskevi, Greece**
G. Anagnostou, G. Daskalakis, T. Geralis (iD), A. Kyriakis, D. Loukas, A. Stakia (iD)

**National and Kapodistrian University of Athens, Athens, Greece**
M. Diamantopoulou, D. Karasavvas, G. Karathanasis, P. Kontaxakis (iD), C.K. Koraka, A. Manousakis-Katsikakis, A. Panagiotou, I. Papavergou, N. Saoulidou (iD), K. Theofilatos (iD), E. Tziaferi (iD), K. Vellidis, E. Vourliotis

**National Technical University of Athens, Athens, Greece**
G. Bakas, K. Kousouris (iD), I. Papakrivopoulos, G. Tsipolitis, A. Zacharopoulou

**University of Ioánnina, Ioánnina, Greece**
K. Adamidis, I. Bestintzanos, I. Evangelou (iD), C. Foudas, P. Gianneios, P. Katsoulis, P. Kokkas,

N. Manthos, I. Papadopoulos (iD), J. Strologas (iD)

**MTA-ELTE Lendület CMS Particle and Nuclear Physics Group, Eötvös Loránd University, Budapest, Hungary**
M. Csanad (iD), K. Farkas, M.M.A. Gadallah[27] (iD), S. Lökös[28] (iD), P. Major, K. Mandal (iD), A. Mehta (iD), G. Pasztor (iD), A.J. Rádl, O. Surányi, G.I. Veres (iD)

**Wigner Research Centre for Physics, Budapest, Hungary**
M. Bartók[29] (iD), G. Bencze, C. Hajdu (iD), D. Horvath[30] (iD), F. Sikler (iD), V. Veszpremi (iD)

**Institute of Nuclear Research ATOMKI, Debrecen, Hungary**
S. Czellar, J. Karancsi[29] (iD), J. Molnar, Z. Szillasi, D. Teyssier

**Institute of Physics, University of Debrecen, Debrecen, Hungary**
P. Raics, Z.L. Trocsanyi[31] (iD), B. Ujvari

**Karoly Robert Campus, MATE Institute of Technology, Gyongyos, Hungary**
T. Csorgo[32] (iD), F. Nemes[32], T. Novak

**Indian Institute of Science (IISc), Bangalore, India**
S. Choudhury, J.R. Komaragiri (iD), D. Kumar, L. Panwar (iD), P.C. Tiwari (iD)

**National Institute of Science Education and Research, HBNI, Bhubaneswar, India**
S. Bahinipati[33] (iD), C. Kar (iD), P. Mal, T. Mishra (iD), V.K. Muraleedharan Nair Bindhu[34], A. Nayak[34] (iD), P. Saha, N. Sur (iD), S.K. Swain, D. Vats[34]

**Panjab University, Chandigarh, India**
S. Bansal (iD), S.B. Beri, V. Bhatnagar (iD), G. Chaudhary (iD), S. Chauhan (iD), N. Dhingra[35] (iD), R. Gupta, A. Kaur, M. Kaur (iD), S. Kaur, P. Kumari (iD), M. Meena, K. Sandeep (iD), J.B. Singh (iD), A.K. Virdi (iD)

**University of Delhi, Delhi, India**
A. Ahmed, A. Bhardwaj (iD), B.C. Choudhary (iD), M. Gola, S. Keshri (iD), A. Kumar (iD), M. Naimuddin (iD), P. Priyanka (iD), K. Ranjan, A. Shah (iD)

**Saha Institute of Nuclear Physics, HBNI, Kolkata, India**
M. Bharti[36], R. Bhattacharya, S. Bhattacharya (iD), D. Bhowmik, S. Dutta, S. Dutta, B. Gomber[37] (iD), M. Maity[38], P. Palit (iD), P.K. Rout (iD), G. Saha, B. Sahu (iD), S. Sarkar, M. Sharan, B. Singh[36], S. Thakur[36]

**Indian Institute of Technology Madras, Madras, India**
P.K. Behera (iD), S.C. Behera, P. Kalbhor (iD), A. Muhammad, R. Pradhan, P.R. Pujahari, A. Sharma (iD), A.K. Sikdar

**Bhabha Atomic Research Centre, Mumbai, India**
D. Dutta (iD), V. Jha, V. Kumar (iD), D.K. Mishra, K. Naskar[39], P.K. Netrakanti, L.M. Pant, P. Shukla (iD)

**Tata Institute of Fundamental Research-A, Mumbai, India**
T. Aziz, S. Dugad, M. Kumar

**Tata Institute of Fundamental Research-B, Mumbai, India**
S. Banerjee (iD), R. Chudasama, M. Guchait, S. Karmakar, S. Kumar, G. Majumder, K. Mazumdar, S. Mukherjee (iD)

**Indian Institute of Science Education and Research (IISER), Pune, India**
K. Alpana, S. Dube (iD), B. Kansal, A. Laha, S. Pandey (iD), A. Rane (iD), A. Rastogi (iD), S. Sharma (iD)

**Isfahan University of Technology, Isfahan, Iran**
H. Bakhshiansohi[40] (iD), E. Khazaie, M. Zeinali[41]

**Institute for Research in Fundamental Sciences (IPM), Tehran, Iran**
S. Chenarani[42], S.M. Etesami (iD), M. Khakzad (iD), M. Mohammadi Najafabadi (iD)

**University College Dublin, Dublin, Ireland**
M. Grunewald (iD)

**INFN Sezione di Bari [a], Bari, Italy, Università di Bari [b], Bari, Italy, Politecnico di Bari [c], Bari, Italy**
M. Abbrescia[a,b] (iD), R. Aly[a,b,43] (iD), C. Aruta[a,b], A. Colaleo[a] (iD), D. Creanza[a,c] (iD), N. De Filippis[a,c] (iD), M. De Palma[a,b] (iD), A. Di Florio[a,b], A. Di Pilato[a,b] (iD), W. Elmetenawee[a,b] (iD), L. Fiore[a] (iD), A. Gelmi[a,b] (iD), M. Gul[a] (iD), G. Iaselli[a,c] (iD), M. Ince[a,b] (iD), S. Lezki[a,b] (iD), G. Maggi[a,c] (iD), M. Maggi[a] (iD), I. Margjeka[a,b], V. Mastrapasqua[a,b] (iD), S. My[a,b] (iD), S. Nuzzo[a,b] (iD), A. Pellecchia[a,b], A. Pompili[a,b] (iD), G. Pugliese[a,c] (iD), D. Ramos[a], A. Ranieri[a] (iD), G. Selvaggi[a,b] (iD), L. Silvestris[a] (iD), F.M. Simone[a,b] (iD), R. Venditti[a], P. Verwilligen[a] (iD)

**INFN Sezione di Bologna [a], Bologna, Italy, Università di Bologna [b], Bologna, Italy**
G. Abbiendi[a] (iD), C. Battilana[a,b] (iD), D. Bonacorsi[a,b] (iD), L. Borgonovi[a], L. Brigliadori[a], R. Campanini[a,b] (iD), P. Capiluppi[a,b] (iD), A. Castro[a,b] (iD), F.R. Cavallo[a] (iD), M. Cuffiani[a,b] (iD), G.M. Dallavalle[a] (iD), T. Diotalevi[a,b] (iD), F. Fabbri[a] (iD), A. Fanfani[a,b] (iD), P. Giacomelli[a] (iD), L. Giommi[a,b] (iD), C. Grandi[a] (iD), L. Guiducci[a,b], S. Lo Meo[a,44], L. Lunerti[a,b], S. Marcellini[a] (iD), G. Masetti[a] (iD), F.L. Navarria[a,b] (iD), A. Perrotta[a] (iD), F. Primavera[a,b] (iD), A.M. Rossi[a,b] (iD), T. Rovelli[a,b] (iD), G.P. Siroli[a,b] (iD)

**INFN Sezione di Catania [a], Catania, Italy, Università di Catania [b], Catania, Italy**
S. Albergo[a,b,45] (iD), S. Costa[a,b,45] (iD), A. Di Mattia[a] (iD), R. Potenza[a,b], A. Tricomi[a,b,45] (iD), C. Tuve[a,b] (iD)

**INFN Sezione di Firenze [a], Firenze, Italy, Università di Firenze [b], Firenze, Italy**
G. Barbagli[a] (iD), A. Cassese[a] (iD), R. Ceccarelli[a,b], V. Ciulli[a,b] (iD), C. Civinini[a] (iD), R. D'Alessandro[a,b] (iD), E. Focardi[a,b] (iD), G. Latino[a,b] (iD), P. Lenzi[a,b] (iD), M. Lizzo[a,b], M. Meschini[a] (iD), S. Paoletti[a] (iD), R. Seidita[a,b], G. Sguazzoni[a] (iD), L. Viliani[a] (iD)

**INFN Laboratori Nazionali di Frascati, Frascati, Italy**
L. Benussi (iD), S. Bianco (iD), D. Piccolo (iD)

**INFN Sezione di Genova [a], Genova, Italy, Università di Genova [b], Genova, Italy**
M. Bozzo[a,b] (iD), F. Ferro[a] (iD), R. Mulargia[a,b], E. Robutti[a] (iD), S. Tosi[a,b] (iD)

**INFN Sezione di Milano-Bicocca [a], Milano, Italy, Università di Milano-Bicocca [b], Milano, Italy**
A. Benaglia[a] (iD), G. Boldrini (iD), F. Brivio[a,b], F. Cetorelli[a,b], F. De Guio[a,b] (iD), M.E. Dinardo[a,b] (iD), P. Dini[a] (iD), S. Gennai[a] (iD), A. Ghezzi[a,b] (iD), P. Govoni[a,b] (iD), L. Guzzi[a,b] (iD), M.T. Lucchini[a,b] (iD), M. Malberti[a], S. Malvezzi[a] (iD), A. Massironi[a] (iD), D. Menasce[a] (iD), L. Moroni[a] (iD), M. Paganoni[a,b] (iD), D. Pedrini[a] (iD), B.S. Pinolini, S. Ragazzi[a,b] (iD), N. Redaelli[a] (iD), T. Tabarelli de Fatis[a,b] (iD), D. Valsecchi[a,b,21] (iD), D. Zuolo[a,b] (iD)

**INFN Sezione di Napoli [a], Napoli, Italy, Università di Napoli 'Federico II' [b], Napoli, Italy, Università della Basilicata [c], Potenza, Italy, Università G. Marconi [d], Roma, Italy**
S. Buontempo[a] (iD), F. Carnevali[a,b], N. Cavallo[a,c] (iD), A. De Iorio[a,b] (iD), F. Fabozzi[a,c] (iD), A.O.M. Iorio[a,b] (iD), L. Lista[a,b] (iD), S. Meola[a,d,21] (iD), P. Paolucci[a,21] (iD), B. Rossi[a] (iD), C. Sciacca[a,b] (iD)

**INFN Sezione di Padova [a], Padova, Italy, Università di Padova [b], Padova, Italy, Università**

di Trento [c], Trento, Italy

P. Azzi[a] , N. Bacchetta[a] , D. Bisello[a,b] , P. Bortignon[a] , A. Bragagnolo[a,b] , R. Carlin[a,b] , P. Checchia[a] , T. Dorigo[a] , U. Dosselli[a] , F. Gasparini[a,b] , U. Gasparini[a,b] , G. Grosso, S.Y. Hoh[a,b] , L. Layer[a,46], E. Lusiani , M. Margoni[a,b] , A.T. Meneguzzo[a,b] , J. Pazzini[a,b] , P. Ronchese[a,b] , R. Rossin[a,b], F. Simonetto[a,b] , G. Strong[a] , M. Tosi[a,b] , H. Yarar[a,b], M. Zanetti[a,b] , P. Zotto[a,b] , A. Zucchetta[a,b] , G. Zumerle[a,b] 

**INFN Sezione di Pavia [a], Pavia, Italy, Università di Pavia [b], Pavia, Italy**

C. Aime'[a,b], A. Braghieri[a] , S. Calzaferri[a,b], D. Fiorina[a,b] , P. Montagna[a,b], S.P. Ratti[a,b], V. Re[a] , C. Riccardi[a,b] , P. Salvini[a] , I. Vai[a] , P. Vitulo[a,b] 

**INFN Sezione di Perugia [a], Perugia, Italy, Università di Perugia [b], Perugia, Italy**

P. Asenov[a,47] , G.M. Bilei[a] , D. Ciangottini[a,b] , L. Fanò[a,b] , P. Lariccia[a,b], M. Magherini[b], G. Mantovani[a,b], V. Mariani[a,b], M. Menichelli[a] , F. Moscatelli[a,47] , A. Piccinelli[a,b] , M. Presilla[a,b] , A. Rossi[a,b] , A. Santocchia[a,b] , D. Spiga[a] , T. Tedeschi[a,b] 

**INFN Sezione di Pisa [a], Pisa, Italy, Università di Pisa [b], Pisa, Italy, Scuola Normale Superiore di Pisa [c], Pisa, Italy, Università di Siena [d], Siena, Italy**

P. Azzurri[a] , G. Bagliesi[a] , V. Bertacchi[a,c] , L. Bianchini[a] , T. Boccali[a] , E. Bossini[a,b] , R. Castaldi[a] , M.A. Ciocci[a,b] , V. D'Amante[a,d] , R. Dell'Orso[a] , M.R. Di Domenico[a,d] , S. Donato[a] , A. Giassi[a] , F. Ligabue[a,c] , E. Manca[a,c] , G. Mandorli[a,c] , D. Matos Figueiredo, A. Messineo[a,b] , F. Palla[a] , S. Parolia[a,b], G. Ramirez-Sanchez[a,c], A. Rizzi[a,b] , G. Rolandi[a,c] , S. Roy Chowdhury[a,c], A. Scribano[a], N. Shafiei[a,b] , P. Spagnolo[a] , R. Tenchini[a] , G. Tonelli[a,b] , N. Turini[a,d] , A. Venturi[a] , P.G. Verdini[a] 

**INFN Sezione di Roma [a], Rome, Italy, Sapienza Università di Roma [b], Rome, Italy**

P. Barria[a] , M. Campana[a,b], F. Cavallari[a] , D. Del Re[a,b] , E. Di Marco[a] , M. Diemoz[a] , E. Longo[a,b] , P. Meridiani[a] , G. Organtini[a,b] , F. Pandolfi[a], R. Paramatti[a,b] , C. Quaranta[a,b], S. Rahatlou[a,b] , C. Rovelli[a] , F. Santanastasio[a,b] , L. Soffi[a] , R. Tramontano[a,b]

**INFN Sezione di Torino [a], Torino, Italy, Università di Torino [b], Torino, Italy, Università del Piemonte Orientale [c], Novara, Italy**

N. Amapane[a,b] , R. Arcidiacono[a,c] , S. Argiro[a,b] , M. Arneodo[a,c] , N. Bartosik[a] , R. Bellan[a,b] , A. Bellora[a,b] , J. Berenguer Antequera[a,b] , C. Biino[a] , N. Cartiglia[a] , S. Cometti[a] , M. Costa[a,b] , R. Covarelli[a,b] , N. Demaria[a] , B. Kiani[a,b] , F. Legger[a] , C. Mariotti[a] , S. Maselli[a] , E. Migliore[a,b] , E. Monteil[a,b] , M. Monteno[a] , M.M. Obertino[a,b] , G. Ortona[a] , L. Pacher[a,b] , N. Pastrone[a] , M. Pelliccioni[a] , G.L. Pinna Angioni[a,b], M. Ruspa[a,c] , K. Shchelina[a] , F. Siviero[a,b] , V. Sola[a] , A. Solano[a,b] , D. Soldi[a,b] , A. Staiano[a] , M. Tornago[a,b], D. Trocino[a] , A. Vagnerini[a,b]

**INFN Sezione di Trieste [a], Trieste, Italy, Università di Trieste [b], Trieste, Italy**

S. Belforte[a] , V. Candelise[a,b] , M. Casarsa[a] , F. Cossutti[a] , A. Da Rold[a,b] , G. Della Ricca[a,b] , G. Sorrentino[a,b], F. Vazzoler[a,b] 

**Kyungpook National University, Daegu, Korea**

S. Dogra , C. Huh , B. Kim, D.H. Kim , G.N. Kim , J. Kim, J. Lee, S.W. Lee , C.S. Moon , Y.D. Oh , S.I. Pak, B.C. Radburn-Smith, S. Sekmen , Y.C. Yang

**Chonnam National University, Institute for Universe and Elementary Particles, Kwangju, Korea**

H. Kim , D.H. Moon

**Hanyang University, Seoul, Korea**
B. Francois ⓘD, T.J. Kim ⓘD, J. Park ⓘD

**Korea University, Seoul, Korea**
S. Cho, S. Choi ⓘD, Y. Go, B. Hong ⓘD, K. Lee, K.S. Lee ⓘD, J. Lim, J. Park, S.K. Park, J. Yoo

**Kyung Hee University, Department of Physics, Seoul, Republic of Korea, Seoul, Korea**
J. Goh ⓘD, A. Gurtu

**Sejong University, Seoul, Korea**
H.S. Kim ⓘD, Y. Kim

**Seoul National University, Seoul, Korea**
J. Almond, J.H. Bhyun, J. Choi, S. Jeon, J. Kim, J.S. Kim, S. Ko, H. Kwon, H. Lee ⓘD, S. Lee, B.H. Oh, M. Oh ⓘD, S.B. Oh, H. Seo ⓘD, U.K. Yang, I. Yoon ⓘD

**University of Seoul, Seoul, Korea**
W. Jang, D.Y. Kang, Y. Kang, S. Kim, B. Ko, J.S.H. Lee ⓘD, Y. Lee, J.A. Merlin, I.C. Park, Y. Roh, M.S. Ryu, D. Song, I.J. Watson ⓘD, S. Yang

**Yonsei University, Department of Physics, Seoul, Korea**
S. Ha, H.D. Yoo

**Sungkyunkwan University, Suwon, Korea**
M. Choi, H. Lee, Y. Lee, I. Yu ⓘD

**College of Engineering and Technology, American University of the Middle East (AUM), Egaila, Kuwait, Dasman, Kuwait**
T. Beyrouthy, Y. Maghrbi

**Riga Technical University, Riga, Latvia**
K. Dreimanis ⓘD, V. Veckalns[48] ⓘD

**Vilnius University, Vilnius, Lithuania**
M. Ambrozas, A. Carvalho Antunes De Oliveira ⓘD, A. Juodagalvis ⓘD, A. Rinkevicius ⓘD, G. Tamulaitis ⓘD

**National Centre for Particle Physics, Universiti Malaya, Kuala Lumpur, Malaysia**
N. Bin Norjoharuddeen ⓘD, W.A.T. Wan Abdullah, M.N. Yusli, Z. Zolkapli

**Universidad de Sonora (UNISON), Hermosillo, Mexico**
J.F. Benitez ⓘD, A. Castaneda Hernandez ⓘD, M. León Coello, J.A. Murillo Quijada ⓘD, A. Sehrawat, L. Valencia Palomo ⓘD

**Centro de Investigacion y de Estudios Avanzados del IPN, Mexico City, Mexico**
G. Ayala, H. Castilla-Valdez, E. De La Cruz-Burelo ⓘD, I. Heredia-De La Cruz[49] ⓘD, R. Lopez-Fernandez, C.A. Mondragon Herrera, D.A. Perez Navarro, A. Sánchez Hernández ⓘD

**Universidad Iberoamericana, Mexico City, Mexico**
S. Carrillo Moreno, C. Oropeza Barrera ⓘD, F. Vazquez Valencia

**Benemerita Universidad Autonoma de Puebla, Puebla, Mexico**
I. Pedraza, H.A. Salazar Ibarguen, C. Uribe Estrada

**University of Montenegro, Podgorica, Montenegro**
J. Mijuskovic[50], N. Raicevic

**University of Auckland, Auckland, New Zealand**

D. Krofcheck [ID]

**University of Canterbury, Christchurch, New Zealand**
P.H. Butler [ID]

**National Centre for Physics, Quaid-I-Azam University, Islamabad, Pakistan**
A. Ahmad, M.I. Asghar, A. Awais, M.I.M. Awan, H.R. Hoorani, W.A. Khan, M.A. Shah, M. Shoaib [ID], M. Waqas [ID]

**AGH University of Science and Technology Faculty of Computer Science, Electronics and Telecommunications, Krakow, Poland**
V. Avati, L. Grzanka, M. Malawski

**National Centre for Nuclear Research, Swierk, Poland**
H. Bialkowska, M. Bluj [ID], B. Boimska [ID], M. Górski, M. Kazana, M. Szleper [ID], P. Zalewski

**Institute of Experimental Physics, Faculty of Physics, University of Warsaw, Warsaw, Poland**
K. Bunkowski, K. Doroba, A. Kalinowski [ID], M. Konecki [ID], J. Krolikowski [ID]

**Laboratório de Instrumentação e Física Experimental de Partículas, Lisboa, Portugal**
M. Araujo, P. Bargassa [ID], D. Bastos, A. Boletti [ID], P. Faccioli [ID], M. Gallinaro [ID], J. Hollar [ID], N. Leonardo [ID], T. Niknejad, M. Pisano, J. Seixas [ID], O. Toldaiev [ID], J. Varela [ID]

**Joint Institute for Nuclear Research, Dubna, Russia**
S. Afanasiev, D. Budkouski, I. Golutvin, I. Gorbunov [ID], V. Karjavine, V. Korenkov [ID], A. Lanev, A. Malakhov, V. Matveev[51,52], V. Palichik, V. Perelygin, M. Savina, D. Seitova, V. Shalaev, S. Shmatov, S. Shulha, V. Smirnov, O. Teryaev, N. Voytishin, B.S. Yuldashev[53], A. Zarubin, I. Zhizhin

**Petersburg Nuclear Physics Institute, Gatchina (St. Petersburg), Russia**
G. Gavrilov [ID], V. Golovtcov, Y. Ivanov, V. Kim[54] [ID], E. Kuznetsova[55], V. Murzin, V. Oreshkin, I. Smirnov, D. Sosnov [ID], V. Sulimov, L. Uvarov, S. Volkov, A. Vorobyev

**Institute for Nuclear Research, Moscow, Russia**
Yu. Andreev [ID], A. Dermenev, S. Gninenko [ID], N. Golubev, A. Karneyeu [ID], D. Kirpichnikov [ID], M. Kirsanov, N. Krasnikov, A. Pashenkov, G. Pivovarov [ID], A. Toropin

**Institute for Theoretical and Experimental Physics named by A.I. Alikhanov of NRC 'Kurchatov Institute', Moscow, Russia**
V. Epshteyn, V. Gavrilov, N. Lychkovskaya, A. Nikitenko[56], V. Popov, A. Stepennov, M. Toms, E. Vlasov [ID], A. Zhokin

**Moscow Institute of Physics and Technology, Moscow, Russia**
T. Aushev

**National Research Nuclear University 'Moscow Engineering Physics Institute' (MEPhI), Moscow, Russia**
M. Chadeeva[57] [ID], A. Oskin, P. Parygin, E. Popova, V. Rusinov, D. Selivanova

**P.N. Lebedev Physical Institute, Moscow, Russia**
V. Andreev, M. Azarkin, I. Dremin [ID], M. Kirakosyan, A. Terkulov

**Skobeltsyn Institute of Nuclear Physics, Lomonosov Moscow State University, Moscow, Russia**
A. Belyaev, E. Boos [ID], M. Dubinin[58] [ID], L. Dudko [ID], A. Ershov, V. Klyukhin [ID], O. Kodolova [ID], I. Lokhtin [ID], O. Lukina, S. Obraztsov, S. Petrushanko, V. Savrin, A. Snigirev [ID]

**Novosibirsk State University (NSU), Novosibirsk, Russia**

V. Blinov[59], T. Dimova[59], L. Kardapoltsev[59], A. Kozyrev[59], I. Ovtin[59], O. Radchenko[59], Y. Skovpen[59] (iD)

**Institute for High Energy Physics of National Research Centre 'Kurchatov Institute', Protvino, Russia**

I. Azhgirey (iD), I. Bayshev, D. Elumakhov, V. Kachanov, D. Konstantinov (iD), P. Mandrik (iD), V. Petrov, R. Ryutin, S. Slabospitskii (iD), A. Sobol, S. Troshin (iD), N. Tyurin, A. Uzunian, A. Volkov

**National Research Tomsk Polytechnic University, Tomsk, Russia**

A. Babaev, V. Okhotnikov

**Tomsk State University, Tomsk, Russia**

V. Borshch, V. Ivanchenko (iD), E. Tcherniaev (iD)

**University of Belgrade: Faculty of Physics and VINCA Institute of Nuclear Sciences, Belgrade, Serbia**

P. Adzic[60] (iD), M. Dordevic (iD), P. Milenovic (iD), J. Milosevic (iD)

**Centro de Investigaciones Energéticas Medioambientales y Tecnológicas (CIEMAT), Madrid, Spain**

M. Aguilar-Benitez, J. Alcaraz Maestre (iD), A. Álvarez Fernández, I. Bachiller, M. Barrio Luna, Cristina F. Bedoya (iD), C.A. Carrillo Montoya (iD), M. Cepeda (iD), M. Cerrada, N. Colino (iD), B. De La Cruz, A. Delgado Peris (iD), J.P. Fernández Ramos (iD), J. Flix (iD), M.C. Fouz (iD), O. Gonzalez Lopez (iD), S. Goy Lopez (iD), J.M. Hernandez (iD), M.I. Josa (iD), J. León Holgado (iD), D. Moran, Á. Navarro Tobar (iD), C. Perez Dengra, A. Pérez-Calero Yzquierdo (iD), J. Puerta Pelayo (iD), I. Redondo (iD), L. Romero, S. Sánchez Navas, L. Urda Gómez (iD), C. Willmott

**Universidad Autónoma de Madrid, Madrid, Spain**

J.F. de Trocóniz, R. Reyes-Almanza (iD)

**Universidad de Oviedo, Instituto Universitario de Ciencias y Tecnologías Espaciales de Asturias (ICTEA), Oviedo, Spain**

B. Alvarez Gonzalez (iD), J. Cuevas (iD), C. Erice (iD), J. Fernandez Menendez (iD), S. Folgueras (iD), I. Gonzalez Caballero (iD), J.R. González Fernández, E. Palencia Cortezon (iD), C. Ramón Álvarez, V. Rodríguez Bouza (iD), A. Soto Rodríguez, A. Trapote, N. Trevisani (iD), C. Vico Villalba

**Instituto de Física de Cantabria (IFCA), CSIC-Universidad de Cantabria, Santander, Spain**

J.A. Brochero Cifuentes (iD), I.J. Cabrillo, A. Calderon (iD), J. Duarte Campderros (iD), M. Fernandez (iD), C. Fernandez Madrazo (iD), P.J. Fernández Manteca (iD), A. García Alonso, G. Gomez, C. Martinez Rivero, P. Martinez Ruiz del Arbol (iD), F. Matorras (iD), P. Matorras Cuevas (iD), J. Piedra Gomez (iD), C. Prieels, T. Rodrigo (iD), A. Ruiz-Jimeno (iD), L. Scodellaro (iD), I. Vila, J.M. Vizan Garcia (iD)

**University of Colombo, Colombo, Sri Lanka**

M.K. Jayananda, B. Kailasapathy[61], D.U.J. Sonnadara, D.D.C. Wickramarathna

**University of Ruhuna, Department of Physics, Matara, Sri Lanka**

W.G.D. Dharmaratna (iD), K. Liyanage, N. Perera, N. Wickramage

**CERN, European Organization for Nuclear Research, Geneva, Switzerland**

T.K. Aarrestad (iD), D. Abbaneo, J. Alimena (iD), E. Auffray, G. Auzinger, J. Baechler, P. Baillon[†], D. Barney (iD), J. Bendavid, M. Bianco (iD), A. Bocci (iD), T. Camporesi, M. Capeans Garrido (iD), G. Cerminara, N. Chernyavskaya (iD), S.S. Chhibra (iD), M. Cipriani (iD), L. Cristella (iD), D. d'Enterria (iD), A. Dabrowski (iD), A. David (iD), A. De Roeck (iD), M.M. Defranchis (iD), M. Deile (iD),

M. Dobson, M. Dünser (iD), N. Dupont, A. Elliott-Peisert, N. Emriskova, F. Fallavollita[62], D. Fasanella (iD), A. Florent (iD), G. Franzoni (iD), W. Funk, S. Giani, D. Gigi, K. Gill, F. Glege, L. Gouskos (iD), M. Haranko (iD), J. Hegeman (iD), V. Innocente (iD), T. James, P. Janot (iD), J. Kaspar (iD), J. Kieseler (iD), M. Komm (iD), N. Kratochwil, C. Lange (iD), S. Laurila, P. Lecoq (iD), A. Lintuluoto, K. Long (iD), C. Lourenço (iD), B. Maier, L. Malgeri (iD), S. Mallios, M. Mannelli, A.C. Marini (iD), F. Meijers, S. Mersi (iD), E. Meschi (iD), F. Moortgat (iD), M. Mulders (iD), S. Orfanelli, L. Orsini, F. Pantaleo (iD), L. Pape, E. Perez, M. Peruzzi (iD), A. Petrilli, G. Petrucciani (iD), A. Pfeiffer (iD), M. Pierini (iD), D. Piparo, M. Pitt (iD), H. Qu (iD), T. Quast, D. Rabady (iD), A. Racz, G. Reales Gutiérrez, M. Rieger (iD), M. Rovere, H. Sakulin, J. Salfeld-Nebgen (iD), S. Scarfi, C. Schäfer, C. Schwick, M. Selvaggi (iD), A. Sharma, P. Silva (iD), W. Snoeys (iD), P. Sphicas[63] (iD), S. Summers (iD), K. Tatar (iD), V.R. Tavolaro (iD), D. Treille, P. Tropea, A. Tsirou, G.P. Van Onsem (iD), J. Wanczyk[64], K.A. Wozniak, W.D. Zeuner

**Paul Scherrer Institut, Villigen, Switzerland**

L. Caminada[65] (iD), A. Ebrahimi (iD), W. Erdmann, R. Horisberger, Q. Ingram, H.C. Kaestli, D. Kotlinski, U. Langenegger, M. Missiroli[65] (iD), L. Noehte[65] (iD), T. Rohe

**ETH Zurich - Institute for Particle Physics and Astrophysics (IPA), Zurich, Switzerland**

K. Androsov[64] (iD), M. Backhaus (iD), P. Berger, A. Calandri (iD), A. De Cosa, G. Dissertori (iD), M. Dittmar, M. Donegà, C. Dorfer (iD), F. Eble, K. Gedia, F. Glessgen, T.A. Gómez Espinosa (iD), C. Grab (iD), D. Hits, W. Lustermann, A.-M. Lyon, R.A. Manzoni (iD), L. Marchese (iD), C. Martin Perez, M.T. Meinhard, F. Nessi-Tedaldi, J. Niedziela (iD), F. Pauss, V. Perovic, S. Pigazzini (iD), M.G. Ratti (iD), M. Reichmann, C. Reissel, T. Reitenspiess, B. Ristic (iD), D. Ruini, D.A. Sanz Becerra (iD), V. Stampf, J. Steggemann[64] (iD), R. Wallny (iD), D.H. Zhu

**Universität Zürich, Zurich, Switzerland**

C. Amsler[66] (iD), P. Bärtschi, C. Botta (iD), D. Brzhechko, M.F. Canelli (iD), K. Cormier, A. De Wit (iD), R. Del Burgo, J.K. Heikkilä (iD), M. Huwiler, W. Jin, A. Jofrehei (iD), B. Kilminster (iD), S. Leontsinis (iD), S.P. Liechti, A. Macchiolo (iD), P. Meiring, V.M. Mikuni (iD), U. Molinatti, I. Neutelings, A. Reimers, P. Robmann, S. Sanchez Cruz (iD), K. Schweiger (iD), M. Senger, Y. Takahashi (iD)

**National Central University, Chung-Li, Taiwan**

C. Adloff[67], C.M. Kuo, W. Lin, A. Roy (iD), T. Sarkar[38] (iD), S.S. Yu

**National Taiwan University (NTU), Taipei, Taiwan**

L. Ceard, Y. Chao, K.F. Chen (iD), P.H. Chen (iD), W.-S. Hou (iD), Y.y. Li, R.-S. Lu, E. Paganis (iD), A. Psallidas, A. Steen, H.y. Wu, E. Yazgan (iD), P.r. Yu

**Chulalongkorn University, Faculty of Science, Department of Physics, Bangkok, Thailand**

B. Asavapibhop (iD), C. Asawatangtrakuldee (iD), N. Srimanobhas (iD)

**Çukurova University, Physics Department, Science and Art Faculty, Adana, Turkey**

F. Boran (iD), S. Damarseckin[68], Z.S. Demiroglu (iD), F. Dolek (iD), I. Dumanoglu[69] (iD), E. Eskut, Y. Guler[70] (iD), E. Gurpinar Guler[70] (iD), C. Isik, O. Kara, A. Kayis Topaksu, U. Kiminsu (iD), G. Onengut, K. Ozdemir[71], A. Polatoz, A.E. Simsek (iD), B. Tali[72], U.G. Tok (iD), S. Turkcapar, I.S. Zorbakir (iD)

**Middle East Technical University, Physics Department, Ankara, Turkey**

B. Isildak[73], G. Karapinar, K. Ocalan[74] (iD), M. Yalvac[75] (iD)

**Bogazici University, Istanbul, Turkey**

B. Akgun, I.O. Atakisi (iD), E. Gülmez (iD), M. Kaya[76] (iD), O. Kaya[77], Ö. Özçelik, S. Tekten[78], E.A. Yetkin[79] (iD)

**62**

**Istanbul Technical University, Istanbul, Turkey**
A. Cakir [iD], K. Cankocak[69] [iD], Y. Komurcu, S. Sen[80] [iD]

**Istanbul University, Istanbul, Turkey**
S. Cerci[72], I. Hos[81], B. Kaynak, S. Ozkorucuklu, D. Sunar Cerci[72] [iD], C. Zorbilmez

**Institute for Scintillation Materials of National Academy of Science of Ukraine, Kharkov, Ukraine**
B. Grynyov

**National Scientific Center, Kharkov Institute of Physics and Technology, Kharkov, Ukraine**
L. Levchuk [iD]

**University of Bristol, Bristol, United Kingdom**
D. Anthony, E. Bhal [iD], S. Bologna, J.J. Brooke [iD], A. Bundock [iD], E. Clement [iD], D. Cussans [iD], H. Flacher [iD], J. Goldstein [iD], G.P. Heath, H.F. Heath [iD], L. Kreczko [iD], B. Krikler [iD], S. Paramesvaran, S. Seif El Nasr-Storey, V.J. Smith, N. Stylianou[82] [iD], K. Walkingshaw Pass, R. White

**Rutherford Appleton Laboratory, Didcot, United Kingdom**
K.W. Bell, A. Belyaev[83] [iD], C. Brew [iD], R.M. Brown, D.J.A. Cockerill, C. Cooke, K.V. Ellis, K. Harder, S. Harper, M.-L. Holmberg[84], J. Linacre [iD], K. Manolopoulos, D.M. Newbold [iD], E. Olaiya, D. Petyt, T. Reis [iD], T. Schuh, C.H. Shepherd-Themistocleous, I.R. Tomalin, T. Williams [iD]

**Imperial College, London, United Kingdom**
R. Bainbridge [iD], P. Bloch [iD], S. Bonomally, J. Borg [iD], S. Breeze, O. Buchmuller, V. Cepaitis [iD], G.S. Chahal[85] [iD], D. Colling, P. Dauncey [iD], G. Davies [iD], M. Della Negra [iD], S. Fayer, G. Fedi [iD], G. Hall [iD], M.H. Hassanshahi, G. Iles, J. Langford, L. Lyons, A.-M. Magnan, S. Malik, A. Martelli [iD], D.G. Monk, J. Nash[86] [iD], M. Pesaresi, D.M. Raymond, A. Richards, A. Rose, E. Scott [iD], C. Seez, A. Shtipliyski, A. Tapper [iD], K. Uchida, T. Virdee[21] [iD], M. Vojinovic [iD], N. Wardle [iD], S.N. Webb [iD], D. Winterbottom

**Brunel University, Uxbridge, United Kingdom**
K. Coldham, J.E. Cole [iD], A. Khan, P. Kyberd [iD], I.D. Reid [iD], L. Teodorescu, S. Zahid [iD]

**Baylor University, Waco, Texas, USA**
S. Abdullin [iD], A. Brinkerhoff [iD], B. Caraway [iD], J. Dittmann [iD], K. Hatakeyama [iD], A.R. Kanuganti, B. McMaster [iD], N. Pastika, M. Saunders [iD], S. Sawant, C. Sutantawibul, J. Wilson [iD]

**Catholic University of America, Washington, DC, USA**
R. Bartek [iD], A. Dominguez [iD], R. Uniyal [iD], A.M. Vargas Hernandez

**The University of Alabama, Tuscaloosa, Alabama, USA**
A. Buccilli [iD], S.I. Cooper [iD], D. Di Croce [iD], S.V. Gleyzer [iD], C. Henderson [iD], C.U. Perez [iD], P. Rumerio[87] [iD], C. West [iD]

**Boston University, Boston, Massachusetts, USA**
A. Akpinar [iD], A. Albert [iD], D. Arcaro [iD], C. Cosby [iD], Z. Demiragli [iD], E. Fontanesi, D. Gastler, S. May [iD], J. Rohlf [iD], K. Salyer [iD], D. Sperka, D. Spitzbart [iD], I. Suarez [iD], A. Tsatsos, S. Yuan, D. Zou

**Brown University, Providence, Rhode Island, USA**
G. Benelli [iD], B. Burkle [iD], X. Coubez[22], D. Cutts [iD], M. Hadley [iD], U. Heintz [iD], J.M. Hogan[88] [iD],

T. KWON, G. Landsberg ⬡, K.T. Lau ⬡, D. Li, M. Lukasik, J. Luo ⬡, M. Narain, N. Pervan, S. Sagir[89] ⬡, F. Simpson, E. Usai ⬡, W.Y. Wong, X. Yan ⬡, D. Yu ⬡, W. Zhang

**University of California, Davis, Davis, California, USA**
J. Bonilla ⬡, C. Brainerd ⬡, R. Breedon, M. Calderon De La Barca Sanchez, M. Chertok ⬡, J. Conway ⬡, P.T. Cox, R. Erbacher, G. Haza, F. Jensen ⬡, O. Kukral, R. Lander, M. Mulhearn ⬡, D. Pellett, B. Regnery ⬡, D. Taylor ⬡, Y. Yao ⬡, F. Zhang ⬡

**University of California, Los Angeles, California, USA**
M. Bachtis ⬡, R. Cousins ⬡, A. Datta ⬡, D. Hamilton, J. Hauser ⬡, M. Ignatenko, M.A. Iqbal, T. Lam, W.A. Nash, S. Regnard ⬡, D. Saltzberg ⬡, B. Stone, V. Valuev ⬡

**University of California, Riverside, Riverside, California, USA**
K. Burt, Y. Chen, R. Clare ⬡, J.W. Gary ⬡, M. Gordon, G. Hanson ⬡, G. Karapostoli ⬡, O.R. Long ⬡, N. Manganelli, M. Olmedo Negrete, W. Si ⬡, S. Wimpenny, Y. Zhang

**University of California, San Diego, La Jolla, California, USA**
J.G. Branson, P. Chang ⬡, S. Cittolin, S. Cooperstein ⬡, N. Deelen ⬡, D. Diaz ⬡, J. Duarte ⬡, R. Gerosa ⬡, L. Giannini ⬡, J. Guiang, R. Kansal ⬡, V. Krutelyov ⬡, R. Lee, J. Letts ⬡, M. Masciovecchio ⬡, F. Mokhtar, M. Pieri ⬡, B.V. Sathia Narayanan ⬡, V. Sharma ⬡, M. Tadel, A. Vartak ⬡, F. Würthwein, Y. Xiang ⬡, A. Yagil ⬡

**University of California, Santa Barbara - Department of Physics, Santa Barbara, California, USA**
N. Amin, C. Campagnari ⬡, M. Citron ⬡, A. Dorsett, V. Dutta ⬡, J. Incandela ⬡, M. Kilpatrick ⬡, J. Kim ⬡, B. Marsh, H. Mei, M. Oshiro, M. Quinnan ⬡, J. Richman, U. Sarica ⬡, F. Setti, J. Sheplock, D. Stuart, S. Wang ⬡

**California Institute of Technology, Pasadena, California, USA**
A. Bornheim ⬡, O. Cerri, I. Dutta ⬡, J.M. Lawhorn ⬡, N. Lu ⬡, J. Mao, H.B. Newman ⬡, T.Q. Nguyen ⬡, M. Spiropulu ⬡, J.R. Vlimant ⬡, C. Wang ⬡, S. Xie, Z. Zhang ⬡, R.Y. Zhu ⬡

**Carnegie Mellon University, Pittsburgh, Pennsylvania, USA**
J. Alison ⬡, S. An ⬡, M.B. Andrews, P. Bryant ⬡, T. Ferguson ⬡, A. Harilal, C. Liu, T. Mudholkar ⬡, M. Paulini ⬡, A. Sanchez, W. Terrill

**University of Colorado Boulder, Boulder, Colorado, USA**
J.P. Cumalat ⬡, W.T. Ford ⬡, A. Hassani, E. MacDonald, R. Patel, A. Perloff ⬡, C. Savard, K. Stenson ⬡, K.A. Ulmer ⬡, S.R. Wagner ⬡

**Cornell University, Ithaca, New York, USA**
J. Alexander ⬡, S. Bright-Thonney ⬡, X. Chen ⬡, Y. Cheng ⬡, D.J. Cranshaw ⬡, S. Hogan, J. Monroy ⬡, J.R. Patterson ⬡, D. Quach ⬡, J. Reichert ⬡, M. Reid ⬡, A. Ryd, W. Sun ⬡, J. Thom ⬡, P. Wittich ⬡, R. Zou ⬡

**Fermi National Accelerator Laboratory, Batavia, Illinois, USA**
M. Albrow ⬡, M. Alyari ⬡, G. Apollinari, A. Apresyan ⬡, A. Apyan ⬡, S. Banerjee, L.A.T. Bauerdick ⬡, D. Berry ⬡, J. Berryhill ⬡, P.C. Bhat, K. Burkett ⬡, J.N. Butler, A. Canepa, G.B. Cerati ⬡, H.W.K. Cheung ⬡, F. Chlebana, K.F. Di Petrillo ⬡, V.D. Elvira ⬡, Y. Feng, J. Freeman, Z. Gecse, L. Gray, D. Green, S. Grünendahl ⬡, O. Gutsche ⬡, R.M. Harris ⬡, R. Heller, T.C. Herwig ⬡, J. Hirschauer ⬡, B. Jayatilaka ⬡, S. Jindariani, M. Johnson, U. Joshi, T. Klijnsma ⬡, B. Klima ⬡, K.H.M. Kwok, S. Lammel ⬡, D. Lincoln ⬡, R. Lipton, T. Liu, C. Madrid, K. Maeshima, C. Mantilla ⬡, D. Mason, P. McBride ⬡, P. Merkel, S. Mrenna ⬡, S. Nahn ⬡, J. Ngadiuba ⬡, V. O'Dell, V. Papadimitriou, K. Pedro ⬡, C. Pena[58] ⬡, O. Prokofyev,

F. Ravera ⬤, A. Reinsvold Hall ⬤, L. Ristori ⬤, E. Sexton-Kennedy ⬤, N. Smith ⬤, A. Soha ⬤, W.J. Spalding ⬤, L. Spiegel, S. Stoynev ⬤, J. Strait ⬤, L. Taylor ⬤, S. Tkaczyk, N.V. Tran ⬤, L. Uplegger ⬤, E.W. Vaandering ⬤, H.A. Weber ⬤

**University of Florida, Gainesville, Florida, USA**
D. Acosta ⬤, P. Avery, D. Bourilkov ⬤, L. Cadamuro ⬤, V. Cherepanov, F. Errico ⬤, R.D. Field, D. Guerrero, B.M. Joshi ⬤, M. Kim, E. Koenig, J. Konigsberg ⬤, A. Korytov, K.H. Lo, K. Matchev ⬤, N. Menendez ⬤, G. Mitselmakher ⬤, A. Muthirakalayil Madhu, N. Rawal, D. Rosenzweig, S. Rosenzweig, J. Rotter, K. Shi ⬤, J. Sturdy ⬤, J. Wang ⬤, E. Yigitbasi ⬤, X. Zuo

**Florida State University, Tallahassee, Florida, USA**
T. Adams ⬤, A. Askew ⬤, R. Habibullah ⬤, V. Hagopian, K.F. Johnson, R. Khurana, T. Kolberg ⬤, G. Martinez, H. Prosper ⬤, C. Schiber, O. Viazlo ⬤, R. Yohay ⬤, J. Zhang

**Florida Institute of Technology, Melbourne, Florida, USA**
M.M. Baarmand ⬤, S. Butalla, T. Elkafrawy[90] ⬤, M. Hohlmann ⬤, R. Kumar Verma ⬤, D. Noonan ⬤, M. Rahmani, F. Yumiceva ⬤

**University of Illinois at Chicago (UIC), Chicago, Illinois, USA**
M.R. Adams, H. Becerril Gonzalez ⬤, R. Cavanaugh ⬤, S. Dittmer, O. Evdokimov ⬤, C.E. Gerber ⬤, D.A. Hangal ⬤, D.J. Hofman ⬤, A.H. Merrit, C. Mills ⬤, G. Oh ⬤, T. Roy, S. Rudrabhatla, M.B. Tonjes ⬤, N. Varelas ⬤, J. Viinikainen ⬤, X. Wang, Z. Wu ⬤, Z. Ye ⬤

**The University of Iowa, Iowa City, Iowa, USA**
M. Alhusseini ⬤, K. Dilsiz[91] ⬤, R.P. Gandrajula ⬤, O.K. Köseyan ⬤, J.-P. Merlo, A. Mestvirishvili[92], J. Nachtman, H. Ogul[93] ⬤, Y. Onel ⬤, A. Penzo, C. Snyder, E. Tiras[94] ⬤

**Johns Hopkins University, Baltimore, Maryland, USA**
O. Amram ⬤, B. Blumenfeld ⬤, L. Corcodilos ⬤, J. Davis, M. Eminizer ⬤, A.V. Gritsan ⬤, S. Kyriacou, P. Maksimovic ⬤, J. Roskes ⬤, M. Swartz, T.Á. Vámi ⬤

**The University of Kansas, Lawrence, Kansas, USA**
A. Abreu, J. Anguiano, C. Baldenegro Barrera ⬤, P. Baringer ⬤, A. Bean ⬤, A. Bylinkin ⬤, Z. Flowers, T. Isidori, S. Khalil ⬤, J. King, G. Krintiras ⬤, A. Kropivnitskaya ⬤, M. Lazarovits, C. Le Mahieu, C. Lindsey, J. Marquez, N. Minafra ⬤, M. Murray ⬤, M. Nickel, C. Rogan ⬤, C. Royon, R. Salvatico ⬤, S. Sanders, E. Schmitz, C. Smith ⬤, J.D. Tapia Takaki ⬤, Q. Wang ⬤, Z. Warner, J. Williams ⬤, G. Wilson ⬤

**Kansas State University, Manhattan, Kansas, USA**
S. Duric, A. Ivanov ⬤, K. Kaadze ⬤, D. Kim, Y. Maravin ⬤, T. Mitchell, A. Modak, K. Nam

**Lawrence Livermore National Laboratory, Livermore, California, USA**
F. Rebassoo, D. Wright

**University of Maryland, College Park, Maryland, USA**
E. Adams, A. Baden, O. Baron, A. Belloni ⬤, S.C. Eno ⬤, N.J. Hadley ⬤, S. Jabeen ⬤, R.G. Kellogg, T. Koeth, A.C. Mignerey, S. Nabili, C. Palmer ⬤, M. Seidel ⬤, A. Skuja ⬤, L. Wang, K. Wong ⬤

**Massachusetts Institute of Technology, Cambridge, Massachusetts, USA**
D. Abercrombie, G. Andreassi, R. Bi, W. Busza ⬤, I.A. Cali, Y. Chen ⬤, M. D'Alfonso ⬤, J. Eysermans, C. Freer ⬤, G. Gomez Ceballos, M. Goncharov, P. Harris, M. Hu, M. Klute ⬤, D. Kovalskyi ⬤, J. Krupa, Y.-J. Lee ⬤, C. Mironov ⬤, C. Paus ⬤, D. Rankin ⬤, C. Roland ⬤, G. Roland, Z. Shi ⬤, G.S.F. Stephans ⬤, J. Wang, Z. Wang ⬤, B. Wyslouch ⬤

**University of Minnesota, Minneapolis, Minnesota, USA**

R.M. Chatterjee, A. Evans, J. Hiltbrand, Sh. Jain, M. Krohn, Y. Kubota, J. Mans, M. Revering, R. Rusack, R. Saradhy, N. Schroeder, N. Strobbe, M.A. Wadud

**University of Nebraska-Lincoln, Lincoln, Nebraska, USA**

K. Bloom, M. Bryson, S. Chauhan, D.R. Claes, C. Fangmeier, L. Finco, F. Golf, C. Joo, I. Kravchenko, M. Musich, I. Reed, J.E. Siado, G.R. Snow[+], W. Tabb, F. Yan, A.G. Zecchinelli

**State University of New York at Buffalo, Buffalo, New York, USA**

G. Agarwal, H. Bandyopadhyay, L. Hay, I. Iashvili, A. Kharchilava, C. McLean, D. Nguyen, J. Pekkanen, S. Rappoccio, A. Williams

**Northeastern University, Boston, Massachusetts, USA**

G. Alverson, E. Barberis, Y. Haddad, A. Hortiangtham, J. Li, G. Madigan, B. Marzocchi, D.M. Morse, V. Nguyen, T. Orimoto, A. Parker, L. Skinnari, A. Tishelman-Charny, T. Wamorkar, B. Wang, A. Wisecarver, D. Wood

**Northwestern University, Evanston, Illinois, USA**

S. Bhattacharya, J. Bueghly, Z. Chen, A. Gilbert, T. Gunter, K.A. Hahn, Y. Liu, N. Odell, M.H. Schmitt, M. Velasco

**University of Notre Dame, Notre Dame, Indiana, USA**

R. Band, R. Bucci, M. Cremonesi, A. Das, N. Dev, R. Goldouzian, M. Hildreth, K. Hurtado Anampa, C. Jessop, K. Lannon, J. Lawrence, N. Loukas, D. Lutton, N. Marinelli, I. Mcalister, T. McCauley, C. Mcgrady, K. Mohrman, C. Moore, Y. Musienko[51], R. Ruchti, P. Siddireddy, A. Townsend, M. Wayne, A. Wightman, M. Zarucki, L. Zygala

**The Ohio State University, Columbus, Ohio, USA**

B. Bylsma, B. Cardwell, L.S. Durkin, B. Francis, C. Hill, M. Nunez Ornelas, K. Wei, B.L. Winer, B.R. Yates

**Princeton University, Princeton, New Jersey, USA**

F.M. Addesa, B. Bonham, P. Das, G. Dezoort, P. Elmer, A. Frankenthal, B. Greenberg, N. Haubrich, S. Higginbotham, A. Kalogeropoulos, G. Kopp, S. Kwan, D. Lange, D. Marlow, K. Mei, I. Ojalvo, J. Olsen, D. Stickland, C. Tully

**University of Puerto Rico, Mayaguez, Puerto Rico, USA**

S. Malik, S. Norberg

**Purdue University, West Lafayette, Indiana, USA**

A.S. Bakshi, V.E. Barnes, R. Chawla, S. Das, L. Gutay, M. Jones, A.W. Jung, S. Karmarkar, D. Kondratyev, M. Liu, G. Negro, N. Neumeister, G. Paspalaki, S. Piperov, A. Purohit, J.F. Schulte, M. Stojanovic[17], J. Thieman, F. Wang, R. Xiao, W. Xie

**Purdue University Northwest, Hammond, Indiana, USA**

J. Dolen, N. Parashar

**Rice University, Houston, Texas, USA**

A. Baty, T. Carnahan, M. Decaro, S. Dildick, K.M. Ecklund, S. Freed, P. Gardner, F.J.M. Geurts, A. Kumar, W. Li, B.P. Padley, R. Redjimi, W. Shi, A.G. Stahl Leiton, S. Yang, L. Zhang[95], Y. Zhang

**University of Rochester, Rochester, New York, USA**

A. Bodek, P. de Barbaro, R. Demina, J.L. Dulemba, C. Fallon, T. Ferbel, M. Galanti,

A. Garcia-Bellido, O. Hindrichs, A. Khukhunaishvili, E. Ranken, R. Taus

**Rutgers, The State University of New Jersey, Piscataway, New Jersey, USA**
B. Chiarito, J.P. Chou, A. Gandrakota, Y. Gershtein, E. Halkiadakis, A. Hart, M. Heindl, O. Karacheban[25], I. Laflotte, A. Lath, R. Montalvo, K. Nash, M. Osherson, S. Salur, S. Schnetzer, S. Somalwar, R. Stone, S.A. Thayil, S. Thomas, H. Wang

**University of Tennessee, Knoxville, Tennessee, USA**
H. Acharya, A.G. Delannoy, S. Fiorendi, S. Spanier

**Texas A&M University, College Station, Texas, USA**
O. Bouhali[96], M. Dalchenko, A. Delgado, R. Eusebi, J. Gilmore, T. Huang, T. Kamon[97], H. Kim, S. Luo, S. Malhotra, R. Mueller, D. Overton, D. Rathjens, A. Safonov

**Texas Tech University, Lubbock, Texas, USA**
N. Akchurin, J. Damgov, V. Hegde, S. Kunori, K. Lamichhane, S.W. Lee, T. Mengke, S. Muthumuni, T. Peltola, I. Volobouev, Z. Wang, A. Whitbeck

**Vanderbilt University, Nashville, Tennessee, USA**
E. Appelt, S. Greene, A. Gurrola, W. Johns, A. Melo, H. Ni, K. Padeken, F. Romeo, P. Sheldon, S. Tuo, J. Velkovska

**University of Virginia, Charlottesville, Virginia, USA**
M.W. Arenton, B. Cox, G. Cummings, J. Hakala, R. Hirosky, M. Joyce, A. Ledovskoy, A. Li, C. Neu, C.E. Perez Lara, B. Tannenwald, S. White, E. Wolfe

**Wayne State University, Detroit, Michigan, USA**
N. Poudyal

**University of Wisconsin - Madison, Madison, WI, Wisconsin, USA**
K. Black, T. Bose, C. Caillol, S. Dasu, I. De Bruyn, P. Everaerts, F. Fienga, C. Galloni, H. He, M. Herndon, A. Hervé, U. Hussain, A. Lanaro, A. Loeliger, R. Loveless, J. Madhusudanan Sreekala, A. Mallampalli, A. Mohammadi, D. Pinna, A. Savin, V. Shang, V. Sharma, W.H. Smith, D. Teague, S. Trembath-Reichert, W. Vetens

†: Deceased
1: Also at TU Wien, Wien, Austria
2: Also at Institute of Basic and Applied Sciences, Faculty of Engineering, Arab Academy for Science, Technology and Maritime Transport, Alexandria, Egypt
3: Also at Université Libre de Bruxelles, Bruxelles, Belgium
4: Also at Universidade Estadual de Campinas, Campinas, Brazil
5: Also at Federal University of Rio Grande do Sul, Porto Alegre, Brazil
6: Also at The University of the State of Amazonas, Manaus, Brazil
7: Also at University of Chinese Academy of Sciences, Beijing, China
8: Also at Department of Physics, Tsinghua University, Beijing, China
9: Also at UFMS, Nova Andradina, Brazil
10: Also at Nanjing Normal University Department of Physics, Nanjing, China
11: Now at The University of Iowa, Iowa City, Iowa, USA
12: Also at Institute for Theoretical and Experimental Physics named by A.I. Alikhanov of NRC 'Kurchatov Institute', Moscow, Russia
13: Also at Joint Institute for Nuclear Research, Dubna, Russia
14: Also at Suez University, Suez, Egypt
15: Now at British University in Egypt, Cairo, Egypt
16: Now at Cairo University, Cairo, Egypt

17: Also at Purdue University, West Lafayette, Indiana, USA

18: Also at Université de Haute Alsace, Mulhouse, France

19: Also at Tbilisi State University, Tbilisi, Georgia

20: Also at Erzincan Binali Yildirim University, Erzincan, Turkey

21: Also at CERN, European Organization for Nuclear Research, Geneva, Switzerland

22: Also at RWTH Aachen University, III. Physikalisches Institut A, Aachen, Germany

23: Also at University of Hamburg, Hamburg, Germany

24: Also at Isfahan University of Technology, Isfahan, Iran

25: Also at Brandenburg University of Technology, Cottbus, Germany

26: Also at Forschungszentrum Jülich, Juelich, Germany

27: Also at Physics Department, Faculty of Science, Assiut University, Assiut, Egypt

28: Also at Karoly Robert Campus, MATE Institute of Technology, Gyongyos, Hungary

29: Also at Institute of Physics, University of Debrecen, Debrecen, Hungary

30: Also at Institute of Nuclear Research ATOMKI, Debrecen, Hungary

31: Also at MTA-ELTE Lendület CMS Particle and Nuclear Physics Group, Eötvös Loránd University, Budapest, Hungary

32: Also at Wigner Research Centre for Physics, Budapest, Hungary

33: Also at IIT Bhubaneswar, Bhubaneswar, India

34: Also at Institute of Physics, Bhubaneswar, India

35: Also at Punjab Agricultural University, Ludhiana, India

36: Also at Shoolini University, Solan, India

37: Also at University of Hyderabad, Hyderabad, India

38: Also at University of Visva-Bharati, Santiniketan, India

39: Also at Indian Institute of Technology (IIT), Mumbai, India

40: Also at Deutsches Elektronen-Synchrotron, Hamburg, Germany

41: Also at Sharif University of Technology, Tehran, Iran

42: Also at Department of Physics, University of Science and Technology of Mazandaran, Behshahr, Iran

43: Now at INFN Sezione di Bari, Università di Bari, Politecnico di Bari, Bari, Italy

44: Also at Italian National Agency for New Technologies, Energy and Sustainable Economic Development, Bologna, Italy

45: Also at Centro Siciliano di Fisica Nucleare e di Struttura Della Materia, Catania, Italy

46: Also at Università di Napoli 'Federico II', Napoli, Italy

47: Also at Consiglio Nazionale delle Ricerche - Istituto Officina dei Materiali, Perugia, Italy

48: Also at Riga Technical University, Riga, Latvia

49: Also at Consejo Nacional de Ciencia y Tecnología, Mexico City, Mexico

50: Also at IRFU, CEA, Université Paris-Saclay, Gif-sur-Yvette, France

51: Also at Institute for Nuclear Research, Moscow, Russia

52: Now at National Research Nuclear University 'Moscow Engineering Physics Institute' (MEPhI), Moscow, Russia

53: Also at Institute of Nuclear Physics of the Uzbekistan Academy of Sciences, Tashkent, Uzbekistan

54: Also at St. Petersburg Polytechnic University, St. Petersburg, Russia

55: Also at University of Florida, Gainesville, Florida, USA

56: Also at Imperial College, London, United Kingdom

57: Also at P.N. Lebedev Physical Institute, Moscow, Russia

58: Also at California Institute of Technology, Pasadena, California, USA

59: Also at Budker Institute of Nuclear Physics, Novosibirsk, Russia

60: Also at Faculty of Physics, University of Belgrade, Belgrade, Serbia

61: Also at Trincomalee Campus, Eastern University, Sri Lanka, Nilaveli, Sri Lanka
62: Also at INFN Sezione di Pavia, Università di Pavia, Pavia, Italy
63: Also at National and Kapodistrian University of Athens, Athens, Greece
64: Also at Ecole Polytechnique Fédérale Lausanne, Lausanne, Switzerland
65: Also at Universität Zürich, Zurich, Switzerland
66: Also at Stefan Meyer Institute for Subatomic Physics, Vienna, Austria
67: Also at Laboratoire d'Annecy-le-Vieux de Physique des Particules, IN2P3-CNRS, Annecy-le-Vieux, France
68: Also at Şırnak University, Sirnak, Turkey
69: Also at Near East University, Research Center of Experimental Health Science, Nicosia, Turkey
70: Also at Konya Technical University, Konya, Turkey
71: Also at Piri Reis University, Istanbul, Turkey
72: Also at Adiyaman University, Adiyaman, Turkey
73: Also at Ozyegin University, Istanbul, Turkey
74: Also at Necmettin Erbakan University, Konya, Turkey
75: Also at Bozok Universitetesi Rektörlügü, Yozgat, Turkey
76: Also at Marmara University, Istanbul, Turkey
77: Also at Milli Savunma University, Istanbul, Turkey
78: Also at Kafkas University, Kars, Turkey
79: Also at Istanbul Bilgi University, Istanbul, Turkey
80: Also at Hacettepe University, Ankara, Turkey
81: Also at Istanbul University - Cerrahpasa, Faculty of Engineering, Istanbul, Turkey
82: Also at Vrije Universiteit Brussel, Brussel, Belgium
83: Also at School of Physics and Astronomy, University of Southampton, Southampton, United Kingdom
84: Also at Rutherford Appleton Laboratory, Didcot, United Kingdom
85: Also at IPPP Durham University, Durham, United Kingdom
86: Also at Monash University, Faculty of Science, Clayton, Australia
87: Also at Università di Torino, Torino, Italy
88: Also at Bethel University, St. Paul, Minneapolis, USA
89: Also at Karamanoğlu Mehmetbey University, Karaman, Turkey
90: Also at Ain Shams University, Cairo, Egypt
91: Also at Bingol University, Bingol, Turkey
92: Also at Georgian Technical University, Tbilisi, Georgia
93: Also at Sinop University, Sinop, Turkey
94: Also at Erciyes University, Kayseri, Turkey
95: Also at Institute of Modern Physics and Key Laboratory of Nuclear Physics and Ion-beam Application (MOE) - Fudan University, Shanghai, China
96: Also at Texas A&M University at Qatar, Doha, Qatar
97: Also at Kyungpook National University, Daegu, Korea